

NASA/TP-1999-209539



# Experimental and Numerical Optimization of a High-Lift System To Improve Low-Speed Performance, Stability, and Control of an Arrow-Wing Supersonic Transport

*David E. Hahne  
Langley Research Center, Hampton, Virginia*

*Louis J. Glaab  
Lockheed Engineering & Sciences Company, Hampton, Virginia*

---

December 1999

## The NASA STI Program Office . . . in Profile

Since its founding, NASA has been dedicated to the advancement of aeronautics and space science. The NASA Scientific and Technical Information (STI) Program Office plays a key part in helping NASA maintain this important role.

The NASA STI Program Office is operated by Langley Research Center, the lead center for NASA's scientific and technical information. The NASA STI Program Office provides access to the NASA STI Database, the largest collection of aeronautical and space science STI in the world. The Program Office is also NASA's institutional mechanism for disseminating the results of its research and development activities. These results are published by NASA in the NASA STI Report Series, which includes the following report types:

- **TECHNICAL PUBLICATION.** Reports of completed research or a major significant phase of research that present the results of NASA programs and include extensive data or theoretical analysis. Includes compilations of significant scientific and technical data and information deemed to be of continuing reference value. NASA counterpart of peer-reviewed formal professional papers, but having less stringent limitations on manuscript length and extent of graphic presentations.
- **TECHNICAL MEMORANDUM.** Scientific and technical findings that are preliminary or of specialized interest, e.g., quick release reports, working papers, and bibliographies that contain minimal annotation. Does not contain extensive analysis.
- **CONTRACTOR REPORT.** Scientific and technical findings by NASA-sponsored contractors and grantees.

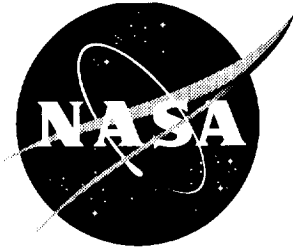
- **CONFERENCE PUBLICATION.** Collected papers from scientific and technical conferences, symposia, seminars, or other meetings sponsored or co-sponsored by NASA.
- **SPECIAL PUBLICATION.** Scientific, technical, or historical information from NASA programs, projects, and missions, often concerned with subjects having substantial public interest.
- **TECHNICAL TRANSLATION.** English-language translations of foreign scientific and technical material pertinent to NASA's mission.

Specialized services that complement the STI Program Office's diverse offerings include creating custom thesauri, building customized databases, organizing and publishing research results . . . even providing videos.

For more information about the NASA STI Program Office, see the following:

- Access the NASA STI Program Home Page at <http://www.sti.nasa.gov>
- Email your question via the Internet to [help@sti.nasa.gov](mailto:help@sti.nasa.gov)
- Fax your question to the NASA STI Help Desk at (301) 621-0134
- Telephone the NASA STI Help Desk at (301) 621-0390
- Write to:  
NASA STI Help Desk  
NASA Center for AeroSpace Information  
7121 Standard Drive  
Hanover, MD 21076-1320

NASA/TP-1999-209539



# Experimental and Numerical Optimization of a High-Lift System To Improve Low-Speed Performance, Stability, and Control of an Arrow-Wing Supersonic Transport

*David E. Hahne  
Langley Research Center, Hampton, Virginia*

*Louis J. Glaab  
Lockheed Martin Engineering & Sciences Company, Hampton, Virginia*

National Aeronautics and  
Space Administration

Langley Research Center  
Hampton, Virginia 23681-2199

---

December 1999

---

Available from:

NASA Center for Aerospace Information (CASI)  
7121 Standard Drive  
Hanover, MD 21076-1320  
(301) 621-0390

National Technical Information Service (NTIS)  
5285 Port Royal Road  
Springfield, VA 22161-2171  
(703) 605-6000

## Summary

An investigation was performed to evaluate leading- and trailing-edge flap deflections for optimal aerodynamic performance of a High-Speed Civil Transport concept during takeoff and approach-to-landing conditions. The configuration used for this study was designed by the Douglas Aircraft Company during the Supersonic Cruise Aircraft Research program of the 1970's. A 0.1-scale model of this configuration was tested with both the original leading-edge flap system and a new leading-edge flap system which was designed with modern computational flow analysis and optimization tools. Leading- and trailing-edge flap deflections, which optimized aerodynamic performance, were generated for the original and modified leading-edge flap systems with the computational flow analysis and optimization tools. Although wind-tunnel data indicated dramatic improvements in untrimmed aerodynamic performance (relative to the cruise configuration) using the analytically derived leading- and trailing-edge flap deflections for both leading-edge flap systems, analysis of the aerodynamic data indicated further improvements in performance could be achieved. Various perturbations of the analytically derived leading-edge flap deflections were investigated and significant additional improvements in aerodynamic performance were achieved.

In addition to the aerodynamic performance optimization testing, stability and control data were also obtained. An evaluation of the crosswind landing capability of the aircraft configuration was conducted and revealed that insufficient lateral control existed as a result of high levels of lateral stability combined with inadequate levels of roll control. Deflection of the leading- and trailing-edge flaps improved the crosswind landing capability of the vehicle considered; however, additional improvements are still required.

## Introduction

The advantage of commercial transpacific flight with block times of 4 to 6 hours has generated renewed interest in developing a viable supersonic commercial transport. Recent studies (refs. 1 and 2) have identified the potential economic benefit of a high-speed civil transport (HSCT) resulting from continued population growth and economic expansion of the Pacific-rim countries. Significant environmental and economic constraints to HSCT operations need to be met, however, for this aircraft to become a viable commercial transport vehicle.

A major constraint on HSCT operations is the Federal Aviation Regulation (FAR) Part 36 Stage 3 noise restrictions (ref. 3), which define maximum allowable takeoff and landing noise levels, based on aircraft takeoff

weight, and are anticipated to be applied to HSCT aircraft certifications. Additionally, the projected subsonic fleet existing at the time the HSCT would enter service could be even quieter than Stage 3 levels. This could lead to problems for HSCT aircraft if they are significantly louder than their subsonic competitors and could cause restrictions to be placed on their operations. Although engine noise can be theoretically reduced to acceptable levels by using advanced suppressor technology, the resulting suppressors can add greatly to the weight and cost of the vehicle. The work of references 4 and 5, conducted as part of the High-Speed Research Program (HSRP), has shown that improved low-speed aerodynamic performance can reduce the amount of noise suppression required for an aircraft to meet Stage 3 noise restrictions. Improved low-speed aerodynamic performance can significantly reduce the complexity and weight of engine noise suppressors and reduce aircraft takeoff weight.

In addition to potential problems meeting Stage 3 noise restrictions, this class of vehicle also exhibits (1) a marked break in longitudinal stability (referred to as pitch-up), (2) excessive effective dihedral and inadequate lateral control (making crosswind landings difficult), (3) low directional stability which can result in oversized vertical tails, and (4) poor low-speed lift characteristics which require operations at high pitch attitudes. For example, because of high takeoff and approach-to-landing pitch attitudes, the Concorde requires a "visor nose" to achieve acceptable pilot visibility. The Concorde, however, pays a significant weight penalty as a result of this.

The objective of the present investigation was to address these issues and assess improvements in low-speed performance (lift-drag ratio and suction parameter), stability, and control through the use of optimized leading- and trailing-edge flap deflections. The 0.1-scale model used in this investigation was originally built and tested in the late 1970's as part of the Supersonic Cruise Aircraft Research (SCAR) program. Results of that study are contained in reference 6. To rapidly evaluate advanced leading-edge flap design methods and deflection optimization codes, this model was refitted with a new leading-edge flap system. The model was subsequently tested in the Langley 30- by 60-Foot Tunnel and evaluations, both aerodynamic performance and stability and control, were made of both the original and modified leading-edge flap systems in conjunction with wing trailing-edge flaps and an all-moving horizontal tail. The model also included 270 upper and lower surface pressure orifices. The main focus of the present study was on the evaluation of two flap systems: the original leading-edge flap system with its constant-chord flaps and a new leading-edge flap system developed by the Douglas

Aircraft Company (DAC). This new flap system, which had an inversely tapered inboard segment and a normally tapered outboard segment, was developed by using several linear design codes which were developed at the Langley Research Center. Leading-edge flap deflection schedules for both leading-edge flap systems were then developed with these new design methods and experimentally evaluated and optimized.

## Symbols

All data were initially obtained in the stability axis system. Longitudinal forces and moments in this report are presented in the stability axis system, and lateral-directional forces and moments are presented in the body axis system.

AR	aspect ratio, $\frac{b^2}{S}$
$b$	wing span, ft
$C_D$	drag coefficient, $\frac{\text{Drag}}{\bar{q}S}$
$\Delta C_D$	$= C_D - C_{D,o}$
$C_{D,\min}$	minimum drag coefficient
$C_{D,o}$	drag coefficient of equivalent symmetric configuration (without twist or camber) at zero lift
$C_L$	lift coefficient, $\frac{\text{Lift}}{\bar{q}S}$
$C_{L\alpha}$	lift-curve slope per degree
$C_l$	rolling-moment coefficient, $\frac{\text{Rolling moment}}{\bar{q}Sb}$
$\Delta C_l$	incremental rolling-moment coefficient
$C_m$	pitching-moment coefficient, $\frac{\text{Pitching moment}}{\bar{q}S\bar{c}}$
$C_n$	yawing-moment coefficient, $\frac{\text{Yawing moment}}{\bar{q}Sb}$
$\Delta C_n$	incremental yawing-moment coefficient
$C_p$	pressure coefficient, $\frac{p - p_\infty}{\bar{q}}$
$C_Y$	side-force coefficient, $\frac{\text{Side force}}{\bar{q}S}$
$\Delta C_Y$	incremental side-force coefficient
$c$	local wing chord, ft
$\bar{c}$	mean aerodynamic chord, ft
$c_f$	local flap chord, ft
$L/D$	lift-drag ratio
$p$	local static pressure, lb/ft <sup>2</sup>
$p_\infty$	free-stream pressure, lb/ft <sup>2</sup>
$\bar{q}$	free-stream dynamic pressure, lb/ft <sup>2</sup>
$S$	wing area, ft <sup>2</sup>

$S_s$	wing leading-edge suction parameter
$V_{\min\text{-app}}$	minimum-approach speed, knots
$V_{\text{app}}$	approach speed, knots
$x/c$	fraction of chordwise location as measured from wing leading edge
$y$	span ordinate, ft
$\alpha$	angle of attack, deg
$\beta$	angle of sideslip, deg
$\delta_a$	aileron deflection, positive for left roll, $\frac{\delta_{a,R} - \delta_{a,L}}{2}$ , deg
$\delta_{a,s}$	symmetric aileron deflection, positive trailing edge down, deg
$\delta_h$	horizontal tail deflection, positive trailing edge down, deg
$\delta_{le}$	leading-edge flap deflection, positive leading edge down, deg
$\delta_r$	rudder deflection, positive trailing edge left, deg
$\delta_{te}$	trailing-edge flap deflection, positive trailing edge down, deg
$\eta$	semispan location, $\frac{2y}{b}$

Stability derivatives:

$$C_{l_\beta} = \frac{\partial C_l}{\partial \beta} \quad C_{n_\beta} = \frac{\partial C_n}{\partial \beta} \quad C_{Y_\beta} = \frac{\partial C_Y}{\partial \beta}$$

Subscripts:

$L$	left
$R$	right

Abbreviations:

BL	butt line, in.
FS	fuselage station, in.
IB	inboard
LE	leading edge
mod	modification
OB	outboard
seg	leading-edge flap segment
TE	trailing edge
WL	waterline, in.

Model components:

B	body
B'	body with new forebody
H	horizontal tail
LEF1	original leading-edge flap

LEF2	modified leading-edge flap
N	nacelle
V	vertical tail
V*	vertical tail and ventral
W	wing

## Model

The model was a 0.1-scale version of a supersonic transport aircraft configuration (fig. 1). The geometric characteristics of the model are presented in table I. Details of the design of the camber and twist distributions for the original wing can be found in reference 7. The original configuration incorporated a highly swept cranked-arrow wing (leading-edge sweep of 71°IB/57°OB) with leading- and trailing-edge flaps. Installation of an alternate leading-edge flap resulted in a leading-edge sweep of 68°IB/58°OB and moved the location of the leading-edge break inboard from 63.6 percent to 60.5 percent semispan. The modified leading edge was designed such that camber and twist were nearly the same as for the original wing. Each leading-edge flap was divided into four segments inboard and two segments outboard of the crank. Leading-edge flap segments were numbered consecutively from inboard to outboard (1 through 6). The baseline leading-edge flap had a constant chord and was segmented with cuts normal to the flap hinge line. The modified flap chord was inversely tapered inboard of the crank and conventionally tapered outboard. Unlike the baseline flap, the alternate flap was segmented with streamwise cuts. In addition, the outer panel was modified to reduce the outer panel hinge-line sweep slightly. The wing trailing edge was divided into three movable surfaces: two single-slotted trailing-edge flaps and a simple aileron (the most outboard trailing-edge surface). A schematic of how the leading- and trailing-edge flaps were mechanized is shown in figure 1(b). Two removable flow-through engine nacelles were located on each wing semispan. The configuration also included a vertical tail with rudder, fixed ventral fin, and an all-moving horizontal tail. The right wing was instrumented with up to 270 pressure ports for measuring wing surface pressures. These pressure ports were distributed along five streamwise rows on both the upper and lower wing surface. The relative spanwise positions of the five rows of pressure ports are shown in figure 2. A complete listing of each pressure port location (spanwise and chordwise stations) can be found in table II.

## Tests and Corrections

Tests of the 0.1-scale model of a supersonic transport aircraft configuration were conducted in the Langley

30- by 60-Foot Tunnel at a dynamic pressure of 10 lb/ft<sup>2</sup>, which resulted in a Reynolds number per foot of  $0.595 \times 10^6$ . A photograph showing the test setup is presented as figure 3. Force, moment, and surface pressure data were obtained at angles of attack from about -4° to 25° and angles of sideslip of 0°, +5°, and -5°. Force and moment data were measured with an external balance system; pressures were measured with an electronic pressure sensing system.

During the previous tunnel entry of this configuration (ref. 6), the model was tested upright and inverted. Information from these tests was used to calculate tares that were applied to drag, pitching moment, rolling moment, and yawing moment to account for aerodynamic forces on the exposed portion of the support struts and to correct for interference effects of the struts on lift, drag, and pitching moment. The data were also corrected for tunnel blockage and flow angularity with information from this previous entry by using the method of reference 8. A buoyancy correction, determined in reference 6, was also applied to the drag data. Tests of similar configurations (refs. 9 and 10) showed jet boundary corrections to be negligible and therefore unnecessary.

## Leading-Edge Suction Parameter

Early in the High-Speed Research Program (HRSP), it was clear that virtually all wind tunnel testing conducted on HSCT configurations would be at Reynolds numbers well below full-scale values. In order to minimize the effect of Reynolds number when evaluating high-lift systems at various test conditions, the leading-edge suction parameter was chosen as a figure of merit. The suction parameter, which is basically a measure of lifting efficiency, is defined as

$$S_s = \frac{C_L \tan(C_L/C_{L_\alpha}) - \Delta C_D}{C_L \tan(C_L/C_{L_\alpha}) - (C_L^2/\pi AR)}$$

where  $\Delta C_D$  is the measured drag minus  $C_{D,o}$ , which is

$$C_{D,o} = \frac{(C_L^2)C_{D,\min}}{\pi AR}$$

This parameter can be further explained with the aid of figure 4. The lower bound  $C_{D,o} + C_L \tan(C_L/C_{L_\alpha})$ , which represents 0 percent leading-edge suction, is the theoretical drag on a symmetric wing with full leading-edge separation and no subsequent flow reattachment. The upper bound  $C_{D,o} + (C_L^2/\pi AR)$ , which represents 100 percent leading-edge suction, is the theoretical minimum induced drag. Further discussion on the employment of the leading-edge suction parameter as applied to this type of vehicle can be found in references 11 and 12.

The ultimate goal in this area of the HSRP is to achieve a value of 0.92 for  $S_j$  on HSCT-type aircraft at operationally useful lift coefficients for takeoff and approach-to-landing conditions.

## Development of Modified Planform

The development of the alternate leading edge for the DAC 2.2 configuration utilized several design codes developed at the Langley Research Center. A vortex flap design code (refs. 13 and 14), codes for designing (SWDES) and analyzing (AERO2S) attached flow flaps (ref. 15), and geometric constraints were employed by DAC to develop a leading-edge flap system that would promote attached flow at takeoff and approach-to-landing conditions and also take advantage of any vortical flow emanating from the wing leading edge. The leading-edge suction parameter, as defined in the previous section, was used as a figure of merit for the design process. Based on projected weight and desired takeoff and landing velocities, a design lift coefficient of 0.5 was chosen for design purposes.

The first step in the process was to determine a flap chord distribution. An initial chord distribution (designated flap F1) was determined by using the vortex flap design code (VFD). Figure 5(a) shows F1 and the subsequent intermediate flap geometries, as well as the final flap (LEF2) geometry, for comparison with the original leading-edge flap system. At this point in the design process, the original wing leading-edge sweep was held fixed and the flap hinge-line location was allowed to vary. Deflections for F1 were optimized by using SWDES, but when the results were analyzed this flap geometry was found not to perform any better than the analytically optimized original leading-edge flaps. The inboard chord of the F1 flap was then lengthened and the deflections reoptimized. Again, the performance was similar to the original flap.

Theorizing that a larger flap chord was needed near the leading-edge break and on the outboard panel to improve performance, flap F2 was designed by using lessons learned from past studies. At this point, structural constraints (e.g., leading-edge spar location) were not considered; however, the inboard leading edge was constrained to have a sweep of not less than  $68^\circ$  and the outboard leading-edge sweep was limited to between  $55^\circ$  and  $60^\circ$ . Optimization and analysis of this flap showed a 7-percent improvement in  $S_j$  over the original flap.

With the geometry of F2 as a guide, a second flap design cycle using VFD was performed. This time the original hinge line was held constant and the local wing leading-edge flap chord was allowed to increase; this resulted in a flap (F3) with a curved leading edge and an outboard panel sweep of  $61.5^\circ$ . The distribution of  $c_f/c$

for F3 was then used as a starting point for a series of iterations that incorporated the following structural and geometry constraints: (1)  $c_f/c$  at tip not to exceed 0.3 (structural); (2)  $c_f/c$  at leading-edge break not to exceed 0.33 (structural); (3) straight inboard leading-edge sweep greater than  $68^\circ$  (geometry); (4) outboard leading-edge sweep between  $55^\circ$  and  $60^\circ$  (geometry); and (5) minimum modifications to the existing model and flap hinge line. Final optimization of deflections by using SWDES resulted in a configuration with a straight wing leading edge that gave nearly the same performance as the unrestricted (curved leading edge) design. This final flap design was then incorporated into the existing DAC 2.2 model and designated LEF2. The distribution of leading-edge flap chord for both the original (LEF1) and modified (LEF2) configurations is shown in figure 5(b).

## Results and Discussion

### Longitudinal Characteristics of Original DAC 2.2 Planform

*Leading- and trailing-edge flap effects.* The first phase of the present investigation evaluated the improvements in performance that could be obtained with the original DAC 2.2 leading-edge flap system. Table III gives all the leading-edge flap deflections tested. The experimental optimization process used the results from SWDES and AERO2S as a starting point about which some predetermined variations in leading-edge flap deflection were tested. The results from these initial studies are presented in figures 6 and 7. Although the design  $C_L$  was 0.5, the range of lift coefficients of interest for HSCT applications in general is 0.4 to 0.8. As can be seen in figure 6, both Schedule R (the best performing leading-edge schedule from ref. 6) and the AERO2S optimized leading-edge flap deflections resulted in significant increases in the suction parameter over the range of  $C_L$  from 0.4 to 0.8 when compared with the undeflected leading edge. The AERO2S schedule, which performed just better than Schedule R, did not show the magnitude of improvement that AERO2S had predicted (AERO2S predicted  $S_j = 0.82$  at  $C_L = 0.5$ ). The effect of leading-edge flap deflection on lift and pitching moment is also shown in figure 6. As expected, leading-edge flap deflection tended to decrease the severity of the pitch-up at the higher lift coefficients and increased the angle of attack necessary to achieve a given  $C_L$ . Also presented in figure 6 are the theoretical predictions made by the AERO2S code. Although the trends in lift and pitching moment were characterized reasonably well, drag (and as a result, suction parameter) was not well predicted. This poor prediction is likely due to the fact that AERO2S models the break between leading-edge flap segments as streamwise cuts, whereas the actual model flap breaks were perpendicular to the flap hinge line.

Because it was recognized that the optimum leading-edge flap deflection would likely be some perturbation about the AERO2S schedule, a series of experimental runs was made to look at the sensitivity of the suction parameter to small changes in leading-edge flap deflection. Four variations of the leading-edge flap schedule were investigated: two proportional variations and two twist variations. The proportional variations were 90 percent and 110 percent of the AERO2S deflection angles. One of the twist variations evaluated the effect of decreasing flap deflections inboard while increasing them outboard. This evaluation resulted in the following deflection schedule: segment 1 deflected 90 percent of the AERO2S deflection; segment 2 deflected 95 percent; segments 3 and 4 unchanged; segment 5 deflected 105 percent; and segment 6 deflected 110 percent of the AERO2S deflection. The other twist variation simply reversed this schedule. As can be seen in figure 7, these variations generally had only a small impact on the lift and pitching-moment characteristics of this configuration. The twist variation with increased inboard flap deflection, however, did show an increase in the suction parameter of about 0.04 at the design  $C_L$ . Although this improvement may seem insignificant, small changes in the suction parameter can result in improvements in low-speed performance as seen in figure 8, which shows results on a similar configuration from reference 11 and illustrates the effect of leading-edge suction  $S_s$  on  $L/D$ .

The effect of trailing-edge flap deflection on the longitudinal characteristics is shown in figures 9(a) and (b) for the leading edge undeflected and the optimum leading-edge deflection, respectively. As can be seen in figure 9(a), without leading-edge flap deflection, maximum untrimmed suction parameter ( $S_s \approx 0.69$ ) at the design  $C_L$  would be achieved with  $\delta_{te}$  between  $20^\circ$  and  $30^\circ$ . With the leading-edge flaps deflected to their experimentally derived optimum settings, the suction parameter at the design  $C_L$  is maximized ( $S_s = 0.82$ ) between trailing-edge flap deflections of  $13^\circ$  and  $20^\circ$  (fig. 9(b)). Examination of the pitching-moment characteristics in figure 9(b) indicates a download on the horizontal tail would be required to trim the configuration and, as is discussed in detail later, would have a detrimental effect on overall vehicle performance.

An evaluation was also made of the use of symmetric aileron deflection for improving the performance characteristics of the outboard panel of the wing. The results shown in figure 10 indicate only a slight improvement in wing performance at the design  $C_L$ . When weighed against the reduction in roll control power associated with symmetric aileron deflection, this improvement was decided not to be large enough to warrant using the ailerons as part of the high-lift system.

**Configuration buildup and horizontal tail effectiveness.** Figure 11(a) shows the effect of the horizontal and vertical tails on the longitudinal characteristics of the cruise configuration. It is interesting to note that the addition of the horizontal tail ( $\delta_h = 0^\circ$ ) resulted in only a small change in the pitching-moment stability. The downwash from the wing is believed to result in a flow angle at the horizontal tail that is nearly constant with angle of attack. Flow surveys conducted on a similar configuration (ref. 10) substantiate this assumption. This effect also holds true when the leading- and trailing-edge flaps are deflected (fig. 11(b)). The primary effect of adding the empennage surfaces to the configuration was to increase drag. This effect shows up in figure 11 as a decrease in the suction parameter at the lower lift coefficients.

Horizontal tail effectiveness (the change in pitching moment with horizontal tail deflection) is shown with and without flap deflection in figure 12. For the cruise configuration (fig. 12(a)), horizontal tail effectiveness is linear at all angles of attack for the range of surface deflections tested. As would be expected, negative deflections (trailing edge up) significantly decrease the overall configuration untrimmed performance as indicated by the suction parameter. This reduction in performance results from an increase in overall drag. This drag increase results from an increase in angle of attack in order to achieve the desired lift coefficient and from the increased horizontal tail deflection. The increase in lift associated with positive tail deflections, however, reduces angle of attack enough to offset the increase in drag due to the increased horizontal tail deflection and results in small improvements in performance. With the leading- and trailing-edge flaps deflected, the horizontal tail effectiveness is similar to that of the cruise configuration although there is a slight reduction in effectiveness for positive deflections. The suction data show, however, that configuration performance decreases with positive deflections above  $5^\circ$  as well as negative deflections. Although the range for horizontal tail deflection from  $0^\circ$  to  $5^\circ$  produces the highest levels of suction over the entire test angle-of-attack range, it results in trimmed lift coefficients of 0.6 to about 0.7. The decrease in suction parameter at these high lift coefficients is much more than the decrease which results from using negative tail deflections to trim the configuration at  $C_L = 0.5$ .

### Longitudinal Characteristics of Modified DAC 2.2 Planform

**Leading- and trailing-edge flap effects.** An optimization of the leading-edge flap system of the modified DAC 2.2 planform was conducted and the results are

shown in figure 13. Based on the results from the original planform, three variations of the deflections developed during the theoretical design process were investigated: 95 percent of the AERO2S deflections; segment 1 deflected 110 percent, segment 2 deflected 105 percent, segments 3 and 4 unchanged, and segments 5 and 6 deflected 95 percent of the AERO2S deflections; and a deflection schedule that minimized the discontinuities between flap segments. (See table III for the flap deflections tested.) The effect of deflecting the leading-edge flap was similar to the effect seen for the original leading edge. Figure 13 shows that each of the four leading-edge flap schedules increased  $S_s$  by about 0.2 at the design  $C_L$  of 0.5 over that obtained with leading-edge flaps undeflected. A decrease in the severity of the pitch-up as well as an increase in the angle of attack needed to achieve a given  $C_L$  was also seen. A close examination of the suction parameter shows that, like the original leading edge, some improvement in the levels of suction could be achieved by experimental optimization. Once again, the theoretical predictions made by AERO2S are also presented for comparison (fig. 13). As with the original planform, predictions of lift and pitching-moment characteristics are reasonably good. Unlike the original planform, however, the performance predictions are reasonably good also. Although somewhat optimistic, the shape of both the drag and suction parameter curves match well with the experimental data. This match can be attributed to the fact that the modified planform was built to match the AERO2S model (both used streamwise breaks between flap segments).

For the modified planform, the optimum deflection schedule was the one that minimized the discontinuity between adjacent flap segments (1.45 to 0.95 AERO2S). As a result of the change in hinge-line sweep between the inboard and outboard panel, however, the gap between segments 4 and 5 was very large with the flaps deflected. In order to see the real benefit of minimizing the discontinuity between flap segments, it was recognized that this gap would need to be faired. The model was tested with a simple filler between segments 4 and 5 (table III), and the results are shown in figure 14. As can be seen, an additional increase in suction parameter (approximately 0.03) was realized by eliminating the discontinuities between flap segments. Lift characteristics show little or no impact due to filling this gap; therefore, the benefit is assumed to be derived from a reduction in drag only. Also, a change in the pitching-moment characteristics occurred which would result in a lower trimmed drag penalty.

Like the original leading edge, the untrimmed suction parameter for the modified planform without leading-edge deflections was maximized with trailing-edge flap deflections between  $20^\circ$  and  $30^\circ$  (fig. 15(a)) at

$S_s \approx 0.69$ . With leading-edge flaps deflected (fig. 15(b)), the optimum trailing-edge deflection at the design  $C_L$  is  $15^\circ$ , as was predicted by SWDES. This trailing-edge flap deflection also results in a longitudinally trimmed configuration. The use of symmetric aileron deflection was also examined for the modified planform (fig. 16) with the same result as was seen for the original wing: a slight increase in untrimmed performance, additional nose-down pitching-moment increment, and potential cross-wind problems due to reduced roll control.

In order to assess the need to deflect both the inboard and outboard leading-edge flaps, several runs were made with partial span leading-edge flap deflections. The data from these runs and runs with zero leading-edge deflection and the optimum leading-edge deflection are shown in figure 17. As can be seen at the design  $C_L$  of 0.5, the inboard flaps alone produced about half of the improvement seen for the optimum deflections. At this same lift coefficient, however, the outboard flaps alone provided very little improvement in the suction parameter. This result indicates that there is a synergistic relation between the inboard and outboard flaps (the whole is greater than the sum of the parts) and that deflection of the entire leading edge is necessary to achieve reasonable improvements in wing performance. Examination of the pitching moment in this figure also shows, as expected, that the pitch-up characteristic is alleviated by inboard flap deflection, which reduces leading-edge vortex strength.

*Configuration buildup and horizontal tail effectiveness.* There was a marked difference in the effect of the horizontal and vertical tails on the modified planform longitudinal characteristics as compared with that on the original wing. Whereas the original wing showed significant changes in the suction parameter with the addition of the horizontal and vertical tails, the modified wing showed much smaller variations (fig. 18(a)), particularly between  $C_L = 0.2$  and 0.4. The horizontal tail also had a slight stabilizing effect on pitching moment which was most pronounced at the lower lift coefficients. With the leading- and trailing-edge flaps deflected (fig. 18(b)), there was even less change in the suction parameter. The horizontal tail was again stabilizing but primarily at the lower lift coefficients.

Figure 19 shows the effect of horizontal tail deflection on the longitudinal characteristics for the modified planform with leading- and trailing-edge flaps deflected. As expected, horizontal tail effectiveness was fairly linear with surface deflection. Once again, there is a slight reduction in effectiveness for positive horizontal tail deflections with the highest levels of suction over the entire test angle-of-attack range produced with horizontal tail deflections between  $0^\circ$  and  $5^\circ$ . These deflections

trim, however, at lift coefficients of 0.7 to about 0.8. The decrease in suction parameter at these high lift coefficients, as was true for the original planform, is much more than the decrease which results from using negative tail deflections to trim the configuration at  $C_L = 0.5$ .

### Comparison of Original and Modified Planforms

The cruise and high-lift configurations for both the original and modified planforms are presented in figure 20. As can be seen, the lift and pitching-moment characteristics of the two planforms, with and without flap deflections, are similar with only slight differences in pitching moment and lift coefficient at the higher angles of attack. The suction parameter for the two cruise configurations is also similar near  $C_L = 0.4$ . Below this value of lift coefficient, the performance of the modified planform drops off significantly. The performance characteristics for the two high-lift configurations do show some interesting differences. The original planform achieves a much higher maximum level of suction than the modified planform. This occurs, however, at a lift coefficient that may be too low to be of significant benefit for the anticipated weight and operational limitations of an HSCT configuration. Note that the level of suction decreases rapidly with increasing lift coefficient. In contrast, not only is the suction peak for the modified planform much closer to the design  $C_L$ , the decrease in suction with increasing lift coefficient is less than the original planform.

In order to make an overall assessment of the design process and the improvement in technology since the SCAR program, the suction parameter for the original and modified planforms is presented in figure 21. This figure presents the percentage improvement in untrimmed  $S_s$  over the performance of Schedule R (experimentally determined) on the original planform at the design  $C_L$  of 0.5. Also shown is the improvement predicted by the AERO2S code. The predicted results use the value of suction determined by AERO2S for Schedule R as a point of reference, whereas the experimental results use the value of suction determined in the wind tunnel for Schedule R. For the original planform it was predicted that a 5.1-percent improvement in performance could be achieved simply by optimizing the leading-edge flap deflections. When this predicted set of deflections was tested, only a 2.5-percent improvement was realized. Experimental perturbations about the predicted flap setting eventually produced an 8.6-percent improvement over Schedule R. Note that these optimized flap deflections were quite different from the Schedule R settings and the predicted deflections were important as a starting point in the experimental optimization process. The improvement in performance predicted by AERO2S for the modified planform was 11.5 percent. As was true

for the original planform, the realized improvement in suction for this configuration was less than predicted (9.5 percent). Experimental optimization, including fairing the gap between the inboard and outboard leading-edge flaps, resulted in an improvement over Schedule R of 15.8 percent. The improvement obtained by experimentally optimizing the leading-edge flap deflection when compared with the AERO2S deflections was similar to that obtained during the experimental optimization of the original planform. This similarity indicates that the modifications to the planform played a significant role in the performance improvements seen during this test and illustrates the potential that can be achieved by using the newer design tools, in conjunction with wind tunnel experiments, to develop high-lift systems for HSCT configurations.

### Pressure Data

Wing surface pressure data were obtained for most of the wind tunnel experimental runs. Because of the large volume of data obtained, only data pertaining to significant points discussed in the previous sections are presented. The pressure data presented form a summary of the findings determined from the force data and further illustrate the effect of optimized leading- and trailing-edge flap deflections. Refer to figure 2 for the locations of wing surface pressure orifice rows. Angles of attack, at which surface pressure data are presented, are limited to values which produced lift coefficients just above and below the design lift coefficient of 0.5.

Wing surface pressure distributions for the original DAC 2.2 planform are shown in figure 22 with leading- and trailing-edge flaps undeflected for the angle-of-attack condition described previously. This figure illustrates the basic flow problems encountered by highly swept cranked-arrow wings. As can be seen in figures 22(a) and (b), the outboard wing upper surface is completely separated as indicated by the pressure distribution for  $\eta = 0.877$ . Additionally, vortex separation is apparent for  $\eta = 0.492$  and  $0.638$ , with the approximate vortex locations at these spanwise stations indicated by the pressure peaks at  $x/c \approx 0.35$  and  $0.40$ . The coalescence of surface pressure values for the upper and lower surfaces aft of the vortex location is indicative of completely separated flow for wing stations  $\eta = 0.492$  and  $0.638$ .

The deflection of leading- and trailing-edge flaps to experimentally determined optimal positions for the original DAC 2.2 planform produced the results shown in figure 23. From this figure, a significant increase in local wing lift is apparent on the outboard section of the wing as indicated by the enhanced surface pressure distribution at  $\eta = 0.877$ . Also, the large region of separated flow observed in figure 22 at station  $\eta = 0.492$  is no longer

evident for deflected leading- and trailing-edge flaps. However, some vortex separated flow may still exist for  $\eta = 0.638$  and  $0.877$ . The spreading of the wing lift over the entire wing span favorably alters the wing wake, which reduces drag and greatly improves the level of  $S_s$ . Interpolating values of  $S_s$  to the design lift coefficient of 0.5 produced levels of  $S_s = 0.402$  and  $0.813$  for the undeflected and deflected leading- and trailing-edge flaps, respectively. Although a dramatic improvement in  $S_s$  was achieved for deflected leading- and trailing-edge flaps, some overdeflection was apparent for the inboard leading-edge flap sections. The overdeflection is indicated by the relatively high negative surface pressures existing for  $\eta = 0.263, 0.492,$  and  $0.638$  at the extreme forward locations on the lower surface of the leading-edge flaps.

Additional improvements in  $S_s$  were realized by deflecting the ailerons symmetrically. Figure 24 presents the wing-surface pressure distribution for the same leading- and trailing-edge flap deflections used in figure 23 but with  $\delta_{a,s} = 10^\circ$ . Symmetric aileron deflection reduced the angle of attack required to generate the design  $C_L$ , and also alleviated the overdeflection problem of the inboard leading-edge flap segments. Both these effects were significant; however, the alleviation of the apparent overdeflection of the inboard leading-edge flap segments was particularly interesting given the fact that the angle of attack necessary to achieve the design  $C_L$  was reduced approximately  $0.6^\circ$  from that for  $\delta_{a,s} = 0^\circ$ . Generally, lower angles of attack would exacerbate the overdeflection of the inboard leading-edge flaps, but apparently symmetric aileron deflection increased the upwash angle at the leading edge more than it reduced the angle of attack. Similar results were observed in reference 16; however, in those tests the effects of inboard trailing-edge flap deflection influenced the upwash mainly at the outboard sections of the wing. Increasing symmetric aileron deflections to  $\delta_{a,s} = 20^\circ$  yielded no significant increase in  $S_s$  but did decrease the angle of attack required to generate the design  $C_L$  by approximately  $0.4^\circ$ . Figure 25 presents wing surface pressure data for  $\delta_{a,s} = 20^\circ$ . Examination of this figure reveals no significant differences in pressure distribution between  $\delta_{a,s} = 20^\circ$  and  $\delta_{a,s} = 10^\circ$ .

A similar analysis of results, as performed for the original DAC 2.2 planform, was conducted for the modified planform. Figure 26 presents results for the undeflected leading- and trailing-edge flap condition. Comparing figure 22 with figure 26 shows very similar results for the two planforms, that is, vortex-dominated flow acting on the inboard section of the wing and completely unorganized separated flow acting on the outboard section.

Deflection of leading- and trailing-edge flaps to experimentally optimized positions produced the data shown in figure 27. From this figure, it can be seen that the leading-edge flaps were very nearly aligned with the local upwash angle for  $\eta = 0.125, 0.263,$  and  $0.492$  as indicated by the coalescence of upper and lower surface pressures near the leading edge and also by the smooth increase of negative surface pressure on the upper surface of the wing. Improved flow quality was also apparent at the leading edge of the trailing-edge flaps and is indicated by the increased negative surface pressure values acting in this area. This effect was much more pronounced for the modified planform than for the original DAC 2.2 planform. Interpolating values of  $S_s$  to the design lift coefficient of 0.5 produced levels of  $S_s = 0.461$  and  $0.831$  for the undeflected and deflected leading- and trailing-edge flaps, respectively.

An undesired feature of the modified planform was a large gap which formed between leading-edge flap segments 4 and 5 when these flap segments were deflected. A filler piece was fabricated and installed, which produced a relatively smooth surface between these leading-edge flap segments. Surface pressure data for this configuration are presented in figure 28. Comparison of this figure with figure 27 shows that the effect of filling the flap gap on the surface pressure distribution was small and that the resulting increase in  $S_s$  was probably due to a reduction of drag components which are not identifiable from analysis of surface pressure distributions. The effect of gap fairing increased  $S_s$  from  $0.831$  to  $0.866$  at the design lift coefficient of 0.5.

Similar symmetric aileron deflections, as evaluated for the original DAC 2.2 planform, only slightly increased  $S_s$  for the modified planform. Figures 29 and 30 contain results for  $\delta_{a,s} = 10^\circ$  and  $20^\circ$ , respectively. A significant increase in lift acting on the outboard section of the wing is indicated by the improved surface pressure distribution for  $\eta = 0.877$ . In addition, the slight overdeflection of leading-edge flap segment 5, for the gap-filled configuration with  $\delta_{a,s} = 0^\circ$  (fig. 28), is no longer evident for  $\delta_{a,s} = 10^\circ$  or  $20^\circ$ . Symmetric aileron deflections also reduced the angle of attack required to achieve the design  $C_L$ , as was demonstrated for the original planform. However, symmetric aileron deflections for the modified planform only had a significant effect on the surface pressure distribution at  $\eta = 0.877$ , whereas a much larger area was affected for the original planform. As a result of the reduced area affected by symmetric aileron deflections, the increase in  $S_s$  was much smaller than that for the original planform. Overall the increase in  $S_s$  due to symmetric aileron deflection was less than 1 percent and, with the possible sacrifice of lateral

control caused by symmetric aileron deflection, would indicate the cost could outweigh the benefits.

### **Lateral-Directional Characteristics of Original DAC 2.2 Planform**

**Lateral-directional stability.** Although the primary objective of the test program was to evaluate the effectiveness of the two high-lift systems on longitudinal characteristics, an examination of the lateral-directional characteristics of this configuration was also made. The effect of the various configuration components on lateral-directional stability is shown in figure 31. All sideslip derivatives in this paper were computed by using data obtained at sideslip angles of  $+5^\circ$  and  $-5^\circ$ . As expected, the wing dominated the lateral stability characteristics ( $C_{l_\beta}$ ). Variations in lateral stability due to the horizontal and vertical tail (including the ventral) were slight and occurred primarily below  $\alpha = 15^\circ$ . The vortical flows associated with highly swept wings, such as employed with this configuration, result in relatively high levels of lateral stability, particularly at takeoff and approach-to-landing conditions. The impact of these high levels of lateral stability as they relate to crosswind operations is discussed later. Although the vertical tail had little effect on lateral stability, it did provide a substantial stabilizing increment directionally. With the addition of the vertical tail, the configuration exhibited stable directional characteristics up to  $\alpha = 18^\circ$ , which is greater than takeoff and landing angles of attack but could possibly be encountered during abnormal operating conditions. The ventral fin increased directional stability slightly at the lower angles of attack but did not extend the angle-of-attack range over which the configuration was stable.

The effect of deflecting the leading- and trailing-edge flaps is shown in figure 32(a) for the WBNLEF1 test configuration. In general, deflection of the flaps resulted in a slight decrease in lateral stability for the WBN test configuration. Flap deflections did not significantly affect the level of directional stability although they did increase the level of side force due to sideslip angle. This effect is possibly due to the increase in projected vertical surface area caused by the deflection of the leading-edge flaps. Since the centroid of the increased projected area is near the moment reference center, little effect on directional stability would be expected. Flap deflection reduced the level of directional stability, as shown in figure 32(b), over most of the test angle-of-attack range for the complete test configuration. This reduction is most likely a result of reduced dynamic pressure at the vertical tail due to the larger wake generated by the high-lift system. Even so, directional stability is maintained to at least  $\alpha = 15^\circ$ .

**Lateral-directional control.** The lateral-directional control characteristics for the original planform are shown in figures 33 through 36. Because of the relatively high levels of lateral stability associated with HSC-T-type configurations, adequate roll control during crosswind landing approaches is an issue. This concern stems from an operations requirement which imposes a 30-knot crosswind component capability for transport-type aircraft (ref. 17). As can be seen from the data in figure 33(a), aileron effectiveness is maintained over the entire angle-of-attack range. Deflection of the leading- and trailing-edge flaps increased aileron effectiveness at all angles of attack (fig. 33(b)). As can be seen more clearly in figure 34, flap deflection significantly increased the effectiveness of the ailerons over much of the angle-of-attack range. A brief analysis of lateral trim capability was performed for configurations with flaps undeflected and flaps deflected. Required roll control authority was assumed to be equal to the required approach sideslip angle multiplied by the lateral stability for each angle of attack as was done in reference 18. The approach sideslip angle was based on an assumed approach wing loading of  $50 \text{ lb/ft}^2$  and employed the 30-knot crosswind component specified previously. Maximum aileron deflection was limited to  $\pm 20^\circ$ , which reserves approximately one third of maximum travel for maneuvering control and stability augmentation. Results from the roll trim capability evaluation, shown in figure 35, indicate that, for the zero leading- and trailing-edge flap deflections, a minimum approach speed of 238 knots would be required. Deflection of leading- and trailing-edge flaps to the optimum schedule required an approach speed of 196 knots, which is a reduction of 41 knots. Note that the yawing moments due to roll control were negligible, particularly for the high-lift configuration.

Rudder effectiveness for this configuration is not only linear but virtually independent of angle of attack (fig. 36(a)). The level of yaw control is quite good and would only require approximately 50 percent of maximum deflection to trim during crosswind landing approaches. Leading- and trailing-edge flap deflection had relatively little impact on rudder effectiveness (figs. 35(b) and 37). The only effect, as might be expected given the effect of flap deflection on directional stability, was a slight reduction in rudder power for the high-lift configuration.

### **Lateral-Directional Characteristics of Modified DAC 2.2 Planform**

**Lateral-directional stability.** The effect of component buildup on the lateral-directional characteristics of the modified planform is shown in figure 38. As can be

seen, the addition of the horizontal and vertical tails had a much greater effect on lateral stability than was true for the original planform. At low angles of attack, both these surfaces provided nearly equal stabilizing increments to lateral stability. Directional stability starts to decrease, however, at a lower angle of attack as compared with the original planform. Although the modified configuration becomes directionally unstable by  $\alpha = 17^\circ$  as did the original planform, the original configuration maintains a more constant level of stability until  $\alpha = 15^\circ$  followed by a sharp decrease in directional stability. In contrast, directional stability for the modified planform gradually decreases after  $\alpha = 5^\circ$ . The model buildup data for the modified planform were generated with the B' forebody, which was designed to allow the testing of canards on this configuration. Although the B' forebody was manufactured from a casting of the B forebody, significant differences were observed in the aerodynamic data, depending on which forebody was selected. The effect of different forebodies is discussed in detail later.

The effect of deflecting the leading- and trailing-edge flaps is shown in figure 39. A significant decrease in lateral stability can be seen over most of the angle-of-attack range when the leading- and trailing-edge flaps are deflected to the experimentally optimized positions. Also, a marked decrease occurs in directional stability, which results in the configuration becoming directionally unstable by  $\alpha = 13^\circ$  as opposed to  $\alpha = 17^\circ$  for the cruise configuration. These effects are, as were the component buildup effects, much larger for the modified planform than they were for the original leading-edge configuration. As shown in figure 40, however, the lateral-directional stability characteristics of the two planforms when configured for optimized performance are essentially the same. Note that figures 38 and 39 show data obtained with the second forebody, whereas figure 40 shows data obtained with the original forebody. Although the geometry of the two forebodies was intended to be identical, slight differences due to manufacturing tolerances resulted in variations in lateral-directional characteristics between the two sets of data. These differences were consistently repeatable and greater than could be accounted for by balance accuracy. A comparison of the two forebodies for the optimized performance configuration on LEF2 is shown in figure 41. From this figure, it can be seen that installation of the second forebody resulted in a slight destabilization of both lateral and directional stability. This sensitivity to forebody geometry is quite common for fuselages with high fineness ratios.

**Lateral-directional control.** The aileron effectiveness for the modified planform is shown in figure 42. Roll control decreases slightly with increasing angle of

attack, and the yawing moments due to aileron deflection are essentially zero. With the flaps deflected, the aileron effectiveness, unlike the original planform (shown in fig. 34), is reduced over much of the test angle-of-attack range (fig. 43). The directional control characteristics of the modified planform (fig. 44) are nearly the same as those presented earlier for the original planform (fig. 35(b)); this is not unexpected given the location of the vertical tail relative to the wing.

Because of the relatively high levels of lateral stability that these configurations exhibit, either improving the effectiveness of existing roll control devices, developing new and more powerful control effectors, or permitting a higher approach speed is necessary. To evaluate the effect of increased approach speed, an analysis of minimum approach speed was also conducted for the modified planform. Required roll control authority was again assumed to be equal to the approach sideslip angle multiplied by the lateral stability for each angle of attack. Maximum roll control available was again limited to  $\pm 20^\circ$  of aileron deflection. The approach sideslip angle was based on an assumed approach wing loading of  $50 \text{ lb/ft}^2$  and employed the 30-knot crosswind component previously specified. This calculation was carried out for each angle of attack. Figure 45(a) shows that with flaps undeflected a minimum approach speed for the modified planform would be 258 knots. Results for the modified planform with leading- and trailing-edge flaps deflected to the experimentally optimized positions (fig. 45(b)) indicate that a minimum approach speed of 195 knots, which corresponds to approximately an angle of attack of  $7^\circ$ , would be needed to satisfy the 30-knot crosswind requirement. An interesting observation is that the original planform required an approach speed of 196 knots, which also occurred at approximately an angle of attack of  $7^\circ$ . As can be seen from figures 34, 40, and 43, both planforms have almost the same levels of roll control and lateral stability for this angle of attack so this result is not surprising.

## Summary of Results

Results from a low-speed wind tunnel investigation of two leading-edge flap systems for a High-Speed Civil Transport type configuration can be summarized as follows:

1. Although predictions from the AERO2S analysis code provide a good indication of the potential untrimmed leading-edge suction improvements obtainable for attached-flow flaps, experimental optimization can improve the results.
2. The combination of inboard and outboard leading-edge flaps and trailing-edge flaps provide significant

improvements in wing performance over the configuration with flaps undeflected.

3. Combined inboard and outboard leading-edge flaps provide significantly larger improvements in wing performance over either inboard or outboard leading-edge flaps alone.

4. A complete wing and high-lift system design utilizing state-of-the-art design and analysis codes can result in significant improvements in aerodynamic performance over the methods available 25 years ago. This improvement results from optimizing both flap geometry and flap deflections.

5. Addition of a horizontal tail has minimal impact on the longitudinal stability characteristics of this configuration.

6. Deflection of leading- and trailing-edge flaps can improve crosswind landing performance.

7. More effective roll control is needed to overcome the high levels of lateral stability characteristic of this type of configuration in order to achieve required crosswind landing performance.

NASA Langley Research Center  
Hampton, VA 23681-0001  
August 13, 1996

## References

1. Douglas Aircraft Co., New Commercial Programs: *Study of High-Speed Civil Transports—Summary*. NASA CR-4236, 1990.
2. Boeing Commercial Airplanes: *High-Speed Civil Transport Study—Special Factors*. NASA CR-181881, 1990.
3. Noise Standards: *Aircraft Type and Airworthiness Certification*. FAR Part 36, FAA, Jan. 1996.
4. Olson, E. D.: Advanced Takeoff Procedures for High-Speed Civil Transport Community Noise Reduction. SAE Paper 921939, Oct. 1992.
5. Glaab, Louis J.; Riley, Donald R.; Brandon, Jay M.; Person, Lee H., Jr.; and Glaab, Patricia C.: *Piloted Simulation Study of the Effect of High-Lift Aerodynamics on the Takeoff Noise of a Representative High-Speed Civil Transport*. NASA/TP-1999-209696, 1999.
6. Yip, Long P.; and Parlett, Lysle P.: *Low-Speed Wind-Tunnel Tests of a 1/10-Scale Model of an Advanced Arrow-Wing Supersonic Cruise Configuration Designed for Cruise at Mach 2.2*. NASA TM-80152, 1979.
7. Radkey, R. L.; Welge, H. R.; and Roensch, R. L.: Aerodynamic Design of a Mach 2.2 Supersonic Cruise Aircraft. *J. Aircr.*, vol. 15, no. 6, June 1978, pp. 351–357.
8. Theodorsen, Theodore; and Silverstein, Abe: *Experimental Verification of the Theory of Wind-Tunnel Boundary Interference*. NACA Rep. 478, 1934.
9. Coe, Paul L., Jr.; and Graham, A. B.: Results of Recent NASA Research on Low-Speed Aerodynamic Characteristics of Supersonic Cruise Aircraft. *Proceedings of the SCAR Conference—Part 1*, NASA CP-001, [1977], pp. 123–136.
10. Shivers, James P.; McLemore, H. Clyde; and Coe, Paul L., Jr.: *Low-Speed Wind-Tunnel Investigation of a Large-Scale Advanced Arrow-Wing Supersonic Transport Configuration With Engines Mounted Above Wing for Upper-Surface Blowing*. NASA TN D-8350, 1976.
11. Coe, Paul L., Jr.; Huffman, Jarrett K.; and Fenbert, James W.: *Leading-Edge Deflection Optimization for a Highly Swept Arrow-Wing Configuration*. NASA TP-1777, 1980.
12. Coe, Paul L., Jr.; and Weston, Robert P.: *Effects of Wing Leading-Edge Deflection on Low-Speed Aerodynamic Characteristics of a Low-Aspect-Ratio Highly Swept Arrow-Wing Configuration*. NASA TP-1434, 1979.
13. Frink, Neal T.: *Concept for Designing Vortex Flap Geometries*. NASA TP-2233, 1983.
14. Frink, Neal T.: Refinements of a Vortex Flap Design Method With Systematic Applications. *Vortex Flow Aerodynamics*, Volume III, James F. Campbell, Russell F. Osborn, and Jerome T. Foughner, Jr., eds., NASA CP-2418, 1986, pp. 1–25.
15. Carlson, Harry W.; and Darden, Christine M.: *Validation of a Pair of Computer Codes for Estimation and Optimization of Subsonic Aerodynamic Performance of Simple Hinged-Flap Systems for Thin Swept Wings*. NASA TP-2828, 1988.
16. Coe, Paul L., Jr.; Kjelgaard, Scott O.; and Gentry, Garl L., Jr.: *Low-Speed Aerodynamic Characteristics of a Highly Swept, Untwisted, Uncambered Arrow Wing*. NASA TP-2176, 1983.
17. Military Specifications—Flying Qualities of Piloted Airplanes. MIL-F-8785C, Sept. 24, 1991.
18. Coe, Paul L., Jr.; Smith, Paul M.; and Parlett, Lysle P.: *Low-Speed Wind Tunnel Investigation of an Advanced Supersonic Cruise Arrow-Wing Configuration*. NASA TM-74043, 1977.

Table I. Geometric Characteristics of Model

Overall length, ft .....		31.00
	Original planform	Modified planform
Wing:		
Reference area, ft <sup>2</sup> .....	98.94	102.78
Span, ft .....	13.55	13.55
Mean aerodynamic chord, ft .....	9.84	9.35
Aspect ratio .....	1.86	1.79
Inboard leading-edge sweep, deg .....	71.00	68.00
Outboard leading-edge sweep, deg .....	57.00	58.00
Inboard flap area (each), ft <sup>2</sup> .....	0.97	0.97
Outboard flap area (each), ft <sup>2</sup> .....	2.08	2.08
Aileron area (each), ft <sup>2</sup> .....	1.08	1.08
Moment reference center, percent $\bar{c}$ .....	0.52	0.48
Leading-edge flap:		
Root chord (fuselage side), ft .....	1.57	0.78
Break chord, ft .....	0.68	1.63
Tip chord, ft .....	0.38	0.63
Horizontal tail:		
Area, ft <sup>2</sup> .....	7.82	7.82
Span, ft .....	3.96	3.96
Aspect ratio .....	2.00	2.00
Leading-edge sweep, deg .....	50.00	50.00
Root chord, ft .....	3.42	3.42
Tip chord, ft .....	0.53	0.53
Vertical tail:		
Area, ft <sup>2</sup> .....	7.00	7.00
Span, ft .....	2.51	2.51
Aspect ratio .....	0.90	0.90
Leading-edge sweep, deg .....	50.00	50.00
Root chord, ft .....	4.46	4.46
Tip chord, ft .....	1.12	1.12
Rudder area, ft <sup>2</sup> .....	2.03	2.03
Ventral:		
Area, ft <sup>2</sup> .....	0.74	0.74

Table II. Locations of Pressure Port

(a) Baseline wing

Station 1: $2y/b = 0.125$		Station 2: $2y/b = 0.263$		Station 3: $2y/b = 0.492$		Station 4: $2y/b = 0.638$		Station 5: $2y/b = 0.877$	
$x/c$	Surface								
LE flap		LE flap		LE flap		LE flap		LE flap	
0.116	Lower	0.143	Lower	0.230	Lower	0.171	Lower	0.215	Lower
0.094	Lower	0.114	Lower	0.185	Lower	0.131	Lower	0.166	Lower
0.071	Lower	0.085	Lower	0.138	Lower	0.099	Lower	0.123	Lower
0.048	Lower	0.056	Lower	0.092	Lower	0.066	Lower	0.082	Lower
0.025	Lower	0.027	Lower	0.046	Lower	0.034	Lower	0.040	Lower
0.008	Lower	0.006	Lower	0.012	Lower	0.008	Lower	0.000	
0.005	Lower	0.003	Lower	0.005	Lower	0.003	Lower	0.018	Upper
0.004	Lower	0.002	Lower	0.002	Lower	0.002	Lower	0.038	Upper
0.000		0.000		0.000		0.000		0.060	Upper
0.001	Upper	0.0001	Upper	0.001	Upper	0.002	Upper	0.080	Upper
0.003	Upper	0.001	Upper	0.003	Upper	0.003	Upper	0.122	Upper
0.006	Upper	0.004	Upper	0.011	Upper	0.008	Upper	0.164	Upper
0.012	Upper	0.012	Upper	0.023	Upper	0.016	Upper	0.182	Upper
0.023	Upper	0.027	Upper	0.046	Upper	0.032	Upper	Wing	
0.035	Upper	0.041	Upper	0.069	Upper	0.050	Upper	1.000	Lower
0.036	Upper	0.056	Upper	0.092	Upper	0.066	Upper	0.900	Lower
0.069	Upper	0.084	Upper	0.138	Upper	0.098	Upper	0.800	Lower
0.092	Upper	0.113	Upper	0.184	Upper	0.130	Upper	0.750	Lower
0.104	Upper	0.127	Upper	0.207	Upper	0.147	Upper	0.700	Lower
Wing		Wing		Wing		Wing		0.650	Lower
1.000		0.800	Lower	0.700	Lower	0.600	Lower	0.600	Lower
0.900	Lower	0.700	Lower	0.600	Lower	0.500	Lower	0.500	Lower
0.850	Lower	0.600	Lower	0.500	Lower	0.400	Lower	0.400	Lower
0.800	Lower	0.500	Lower	0.400	Lower	0.300	Lower	0.300	Lower
0.700	Lower	0.400	Lower	0.300	Lower	0.250	Lower	0.250	Lower
0.600	Lower	0.300	Lower	0.250	Lower	0.200	Lower	0.220	Upper
0.500	Lower	0.200	Lower	0.270	Upper	0.175	Lower	0.250	Upper
0.400	Lower	0.150	Lower	0.300	Lower	0.150	Upper	0.300	Upper
0.300	Lower	0.200	Upper	0.350	Upper	0.175	Upper	0.350	Upper
0.200	Lower	0.250	Upper	0.400	Upper	0.200	Upper	0.400	Upper
0.150	Lower	0.350	Upper	0.450	Upper	0.220	Upper	0.450	Upper
0.125	Lower	0.400	Upper	0.500	Upper	0.250	Upper	0.500	Upper
0.125	Upper	0.450	Upper	0.550	Upper	0.270	Upper	0.600	Upper
0.150	Upper	0.500	Upper	0.600	Upper	0.300	Upper	0.650	Upper
0.200	Upper	0.550	Upper	0.650	Upper	0.350	Upper	0.690	Upper
0.250	Upper	0.600	Upper	0.700	Upper	0.400	Upper	0.750	Upper
0.300	Upper	0.650	Upper	0.750	Upper	0.450	Upper	0.800	Upper
0.350	Upper	0.700	Upper	0.800	Upper	0.500	Upper	0.850	Upper
0.400	Upper	0.750	Upper	0.850	Upper	0.550	Upper	0.900	Upper
0.450	Upper	0.800	Upper	TE flap		0.600	Upper	0.950	Upper
0.500	Upper	0.850	Upper	1.000	Lower	0.650	Upper		
0.550	Upper	TE flap		0.982	Lower	TE flap			
0.600	Upper	1.000	Lower	0.936	Lower	1.000	Lower		
0.650	Upper	0.987	Lower	0.900	Lower	0.976	Lower		
0.700	Upper	0.958	Lower	0.873	Lower	0.917	Lower		
0.750	Upper	0.933	Lower	0.836	Lower	0.871	Lower		
0.800	Upper	0.914	Lower	0.827	Lower	0.836	Lower		
0.850	Upper	0.890	Lower	0.820	Upper	0.790	Lower		
0.900	Upper	0.884	Lower	0.823	Upper	0.779	Lower		
0.950	Upper	0.878	Upper	0.838	Upper	0.767	Upper		
		0.881	Upper	0.837	Upper	0.773	Upper		
		0.885	Upper	0.856	Upper	0.779	Upper		
		0.891	Upper	0.873	Upper	0.790	Upper		
		0.903	Upper	0.901	Upper	0.813	Upper		
		0.915	Upper	0.937	Upper	0.836	Upper		
		0.933	Upper	0.955	Upper	0.871	Upper		
		0.950	Upper	0.982	Upper	0.918	Upper		
		0.970	Upper			0.941	Upper		
		0.988	Upper			0.976	Upper		

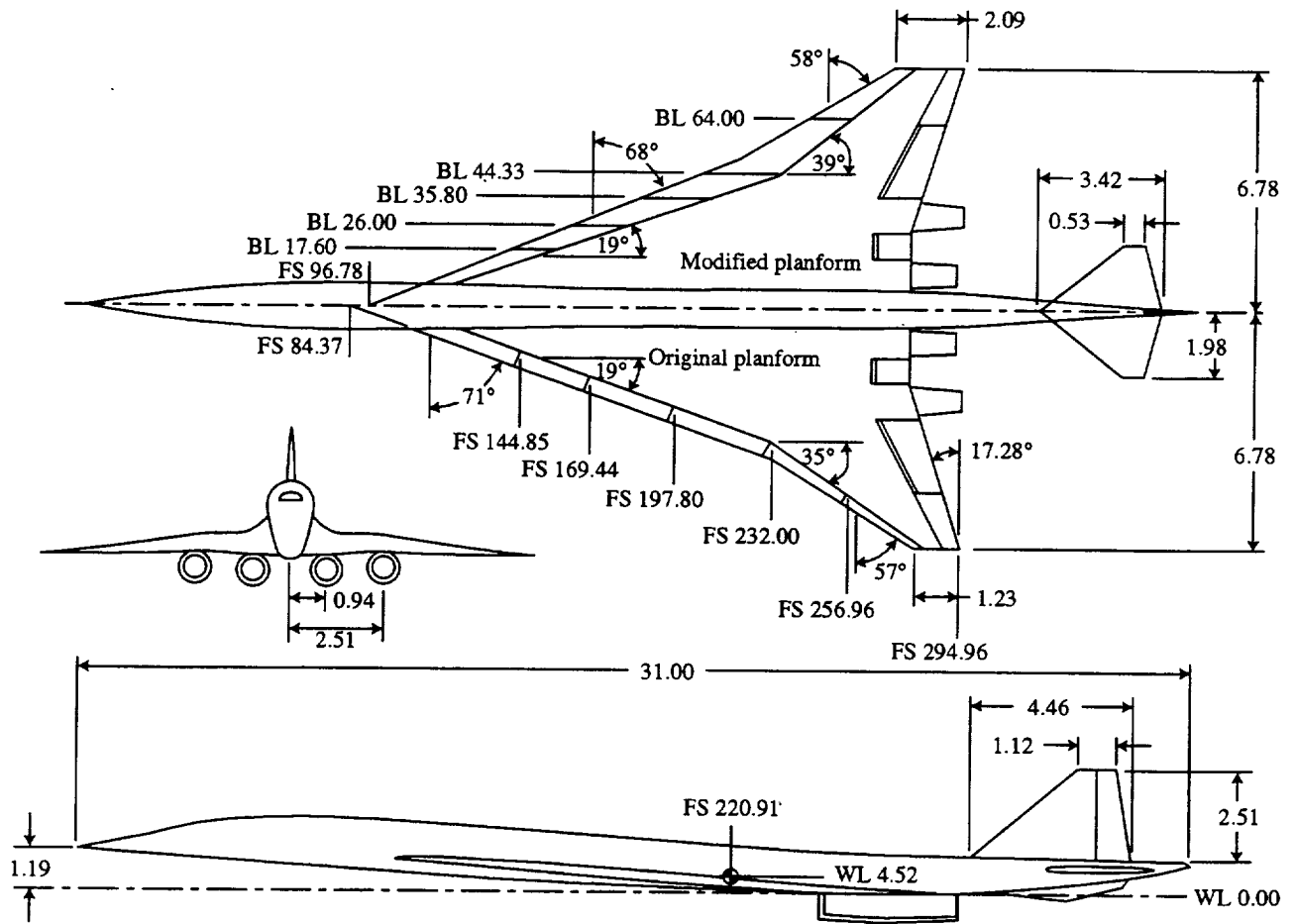
Table II. Concluded

(b) Modified wing

Station 1: $2y/b = 0.125$		Station 2: $2y/b = 0.263$		Station 3: $2y/b = 0.492$		Station 4: $2y/b = 0.638$		Station 5: $2y/b = 0.877$	
$x/c$	Surface								
LE flap		LE flap		LE flap		LE flap		LE flap	
0.069	Lower	0.122	Lower	0.230	Lower	0.314	Lower	0.443	Lower
0.050	Lower	0.114	Lower	0.185	Lower	0.171	Lower	0.215	Lower
0.035	Lower	0.085	Lower	0.138	Lower	0.131	Lower	0.166	Lower
0.023	Lower	0.056	Lower	0.092	Lower	0.099	Lower	0.123	Lower
0.012	Lower	0.027	Lower	0.046	Lower	0.066	Lower	0.082	Lower
0.003	Lower	0.006	Lower	0.012	Lower	0.034	Lower	0.040	Lower
0.000		0.002	Lower	0.005	Lower	0.008	Lower	0.000	
0.008	Upper	0.000		0.002	Lower	0.003	Lower	0.018	Upper
0.025	Upper	0.004	Upper	0.000		0.000		0.038	Upper
0.048	Upper	0.012	Upper	0.001	Upper	0.003	Upper	0.060	Upper
0.065	Upper	0.027	Upper	0.003	Upper	0.008	Upper	0.080	Upper
Wing		0.041	Upper	0.011	Upper	0.016	Upper	0.122	Upper
1.000		0.056	Upper	0.023	Upper	0.032	Upper	0.164	Upper
0.895	Lower	0.084	Upper	0.046	Upper	0.050	Upper	Wing	
0.842	Lower	0.113	Upper	0.069	Upper	0.066	Upper	1.000	Lower
0.789	Lower	Wing		0.092	Upper	0.098	Upper	0.929	Lower
0.684	Lower	0.795	Lower	0.138	Upper	0.130	Upper	0.858	Lower
0.579	Lower	0.693	Lower	0.184	Upper	0.147	Upper	0.822	Lower
0.473	Lower	0.590	Lower	0.207	Upper	Wing		0.787	Lower
0.368	Lower	0.488	Lower	Wing		0.669	Lower	0.751	Lower
0.263	Lower	0.385	Lower	0.716	Lower	0.586	Lower	0.716	Lower
0.158	Lower	0.283	Lower	0.622	Lower	0.504	Lower	0.645	Lower
0.105	Lower	0.181	Lower	0.527	Lower	0.421	Lower	0.574	Lower
0.079	Lower	0.129	Lower	0.433	Lower	0.380	Lower	0.503	Lower
0.079	Upper	0.181	Upper	0.338	Lower	0.338	Lower	0.467	Lower
0.105	Upper	0.232	Upper	0.291	Lower	0.318	Lower	0.446	Upper
0.158	Upper	0.334	Upper	0.310	Upper	0.297	Upper	0.467	Upper
0.210	Upper	0.385	Upper	0.338	Lower	0.318	Upper	0.503	Upper
0.263	Upper	0.437	Upper	0.385	Upper	0.338	Upper	0.538	Upper
0.316	Upper	0.488	Upper	0.433	Upper	0.355	Upper	0.574	Upper
0.368	Upper	0.539	Upper	0.480	Upper	0.380	Upper	0.609	Upper
0.421	Upper	0.590	Upper	0.527	Upper	0.396	Upper	0.645	Upper
0.473	Upper	0.642	Upper	0.574	Upper	0.421	Upper	0.716	Upper
0.526	Upper	0.693	Upper	0.622	Upper	0.462	Upper	0.751	Upper
0.579	Upper	0.744	Upper	0.669	Upper	0.504	Upper	0.780	Upper
0.631	Upper	0.795	Upper	0.716	Upper	0.545	Upper	0.822	Upper
0.684	Upper	0.846	Upper	0.764	Upper	0.586	Upper	0.858	Upper
0.737	Upper	TE flap		0.811	Upper	0.628	Upper	0.893	Upper
0.789	Upper	1.000	Lower	0.858	Upper	0.669	Upper	0.929	Upper
0.842	Upper	0.987	Lower	TE flap		0.711	Upper	0.964	Upper
0.895	Upper	0.957	Lower	1.000	Lower	TE flap			
0.947	Upper	0.931	Lower	0.983	Lower	1.000	Lower		
		0.912	Lower	0.940	Lower	0.980	Lower		
		0.887	Lower	0.905	Lower	0.931	Lower		
		0.881	Lower	0.880	Lower	0.893	Lower		
		0.875	Upper	0.845	Lower	0.864	Lower		
		0.878	Upper	0.836	Lower	0.826	Lower		
		0.882	Upper	0.830	Upper	0.817	Lower		
		0.888	Upper	0.833	Upper	0.807	Upper		
		0.901	Upper	0.847	Upper	0.812	Upper		
		0.913	Upper	0.846	Upper	0.817	Upper		
		0.931	Upper	0.864	Upper	0.826	Upper		
		0.949	Upper	0.880	Upper	0.845	Upper		
		0.969	Upper	0.906	Upper	0.864	Upper		
		0.988	Upper	0.940	Upper	0.893	Upper		
				0.958	Upper	0.932	Upper		
				0.983	Upper	0.951	Upper		
						0.980	Upper		

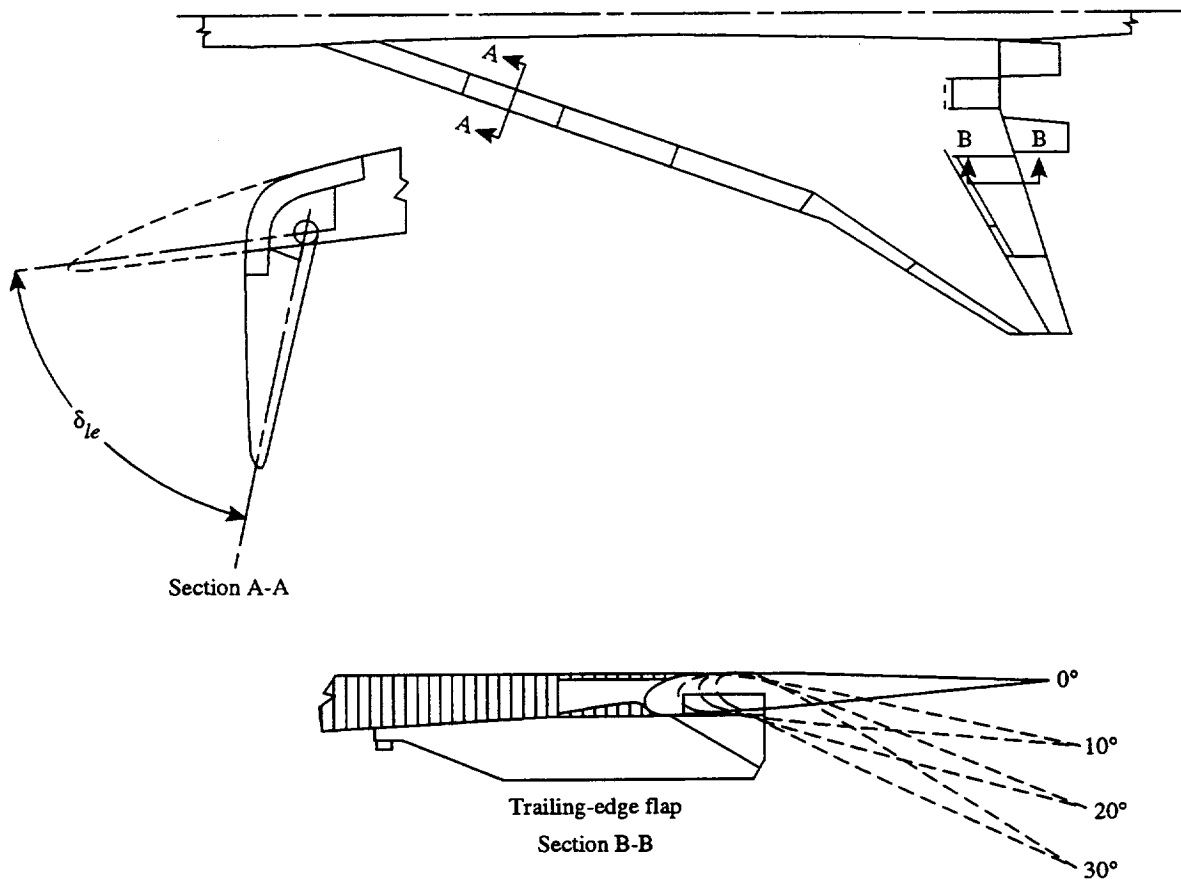
Table III. Leading-Edge Flap Deflections Tested

Deflection name	$\delta_{le}$ , deg, for segment—					
	1	2	3	4	5	6
LEF1						
Schedule R (ref. 6)	13	34	35	35	19	29
AERO2S optimized	18	29	38	44	40	43
1.10 AERO2S optimized	20	32	42	48	44	47
0.90 AERO2S optimized	16	26	34	40	36	39
0.90 to 1.10 AERO2S optimized (mod 1)	16	28	39	44	42	47
1.10 to 0.90 AERO2S optimized (mod 2)	20	31	38	44	38	39
No relation to AERO2S optimized (mod 3)	29	34	39	44	42	39
LEF2						
AERO2S optimized	25	32	37	41	28	33
0.95 AERO2S optimized	24	30	35	39	27	31
1.10 to 0.95 AERO2S optimized (mod 2)	28	34	37	41	27	31
1.45 to 0.95 AERO2S optimized (mod 3)	36	46	45	43	31	31
1.45 to 0.95 AERO2S optimized (mod 4, gap filled between seg 4 and 5)	36	46	45	43	31	31
Mod 5	31	31	31	31	31	31
Mod 6	31	31	31	31	23	23



(a) Three-view sketch of model.

Figure 1. Sketches of model geometry. Linear dimensions are in feet.



(b) Details of flap geometry.

Figure 1. Concluded.

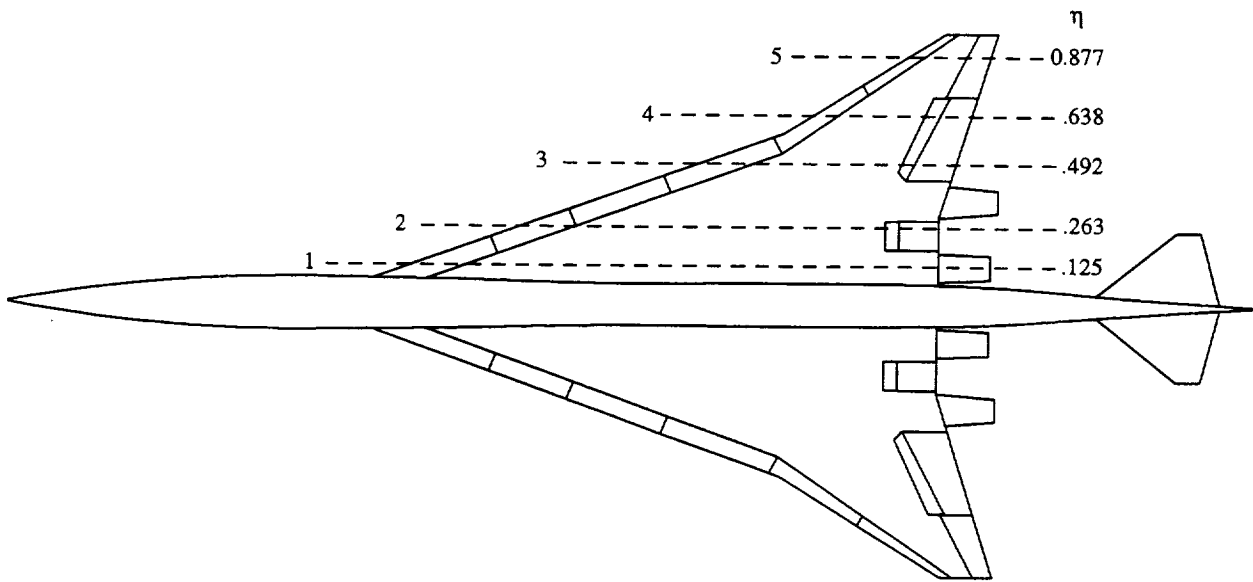


Figure 2. Location of pressure port rows.

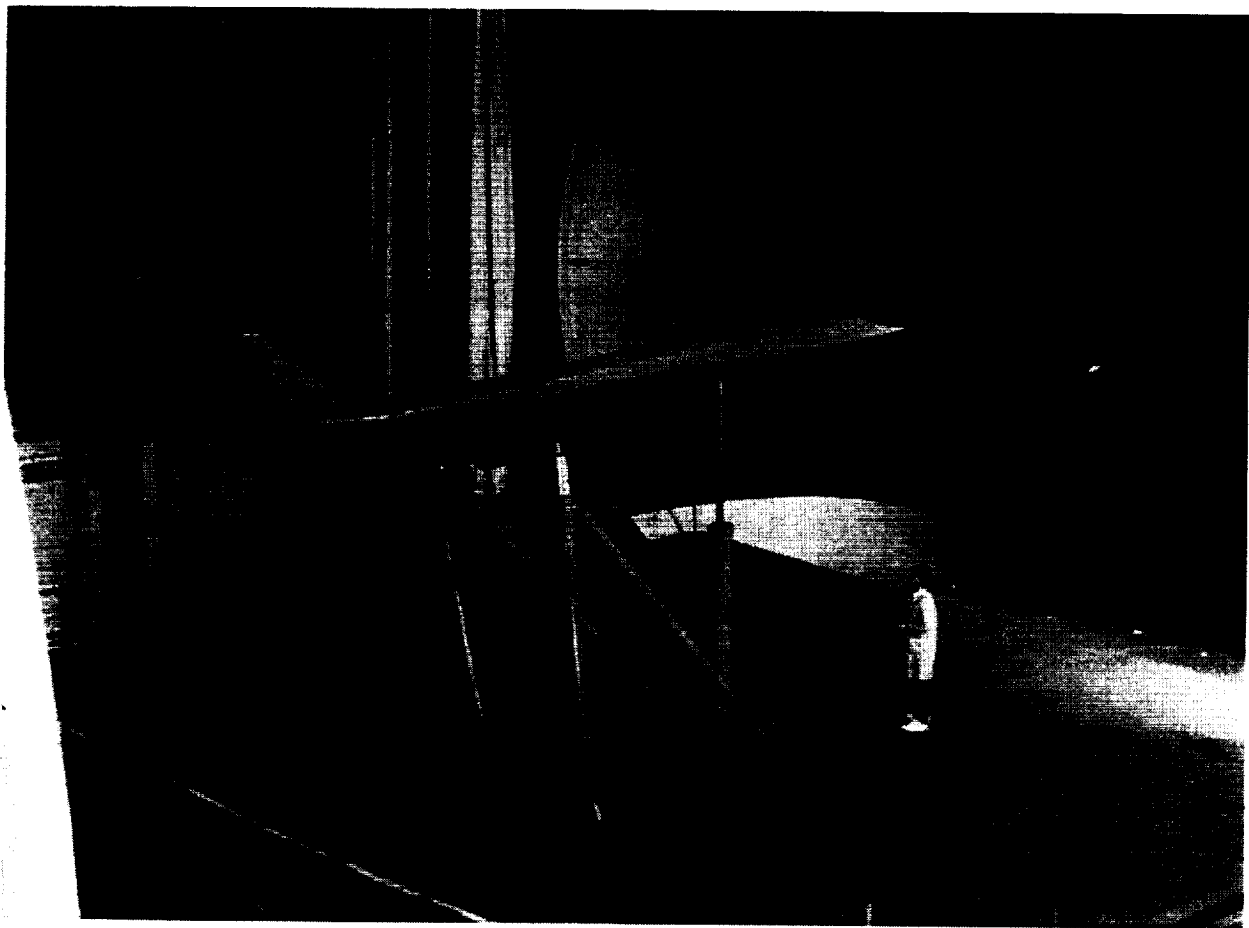


Figure 3. Model in Langley 30- by 60-Foot Tunnel.

L-92-11467

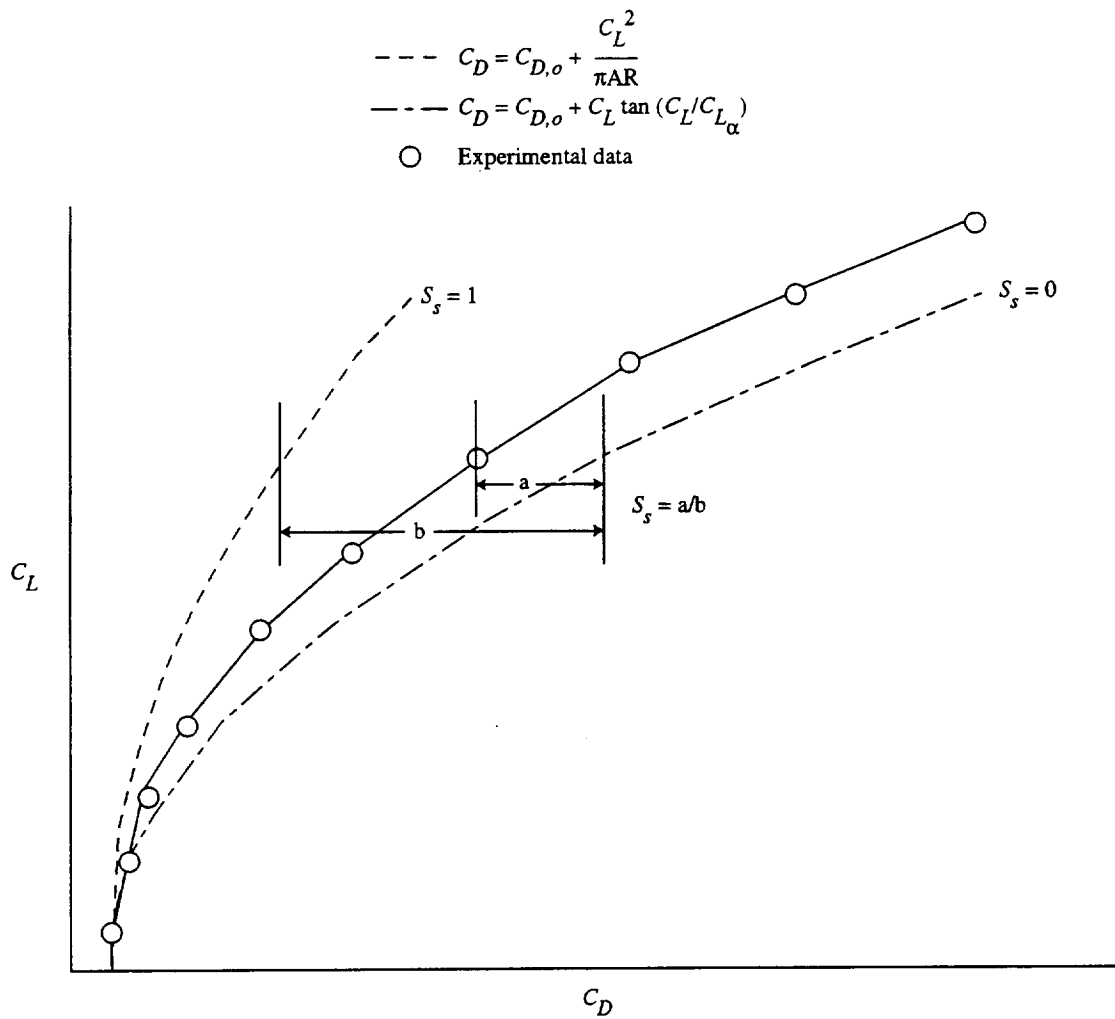
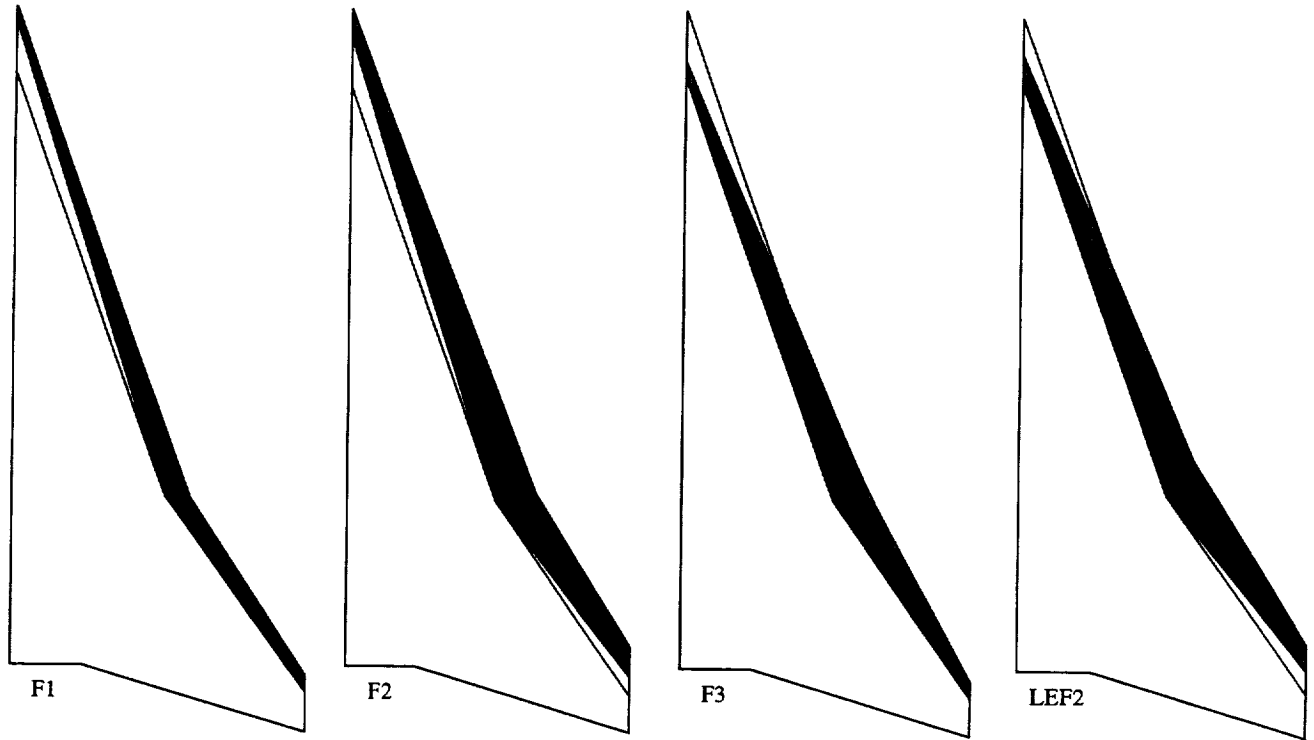
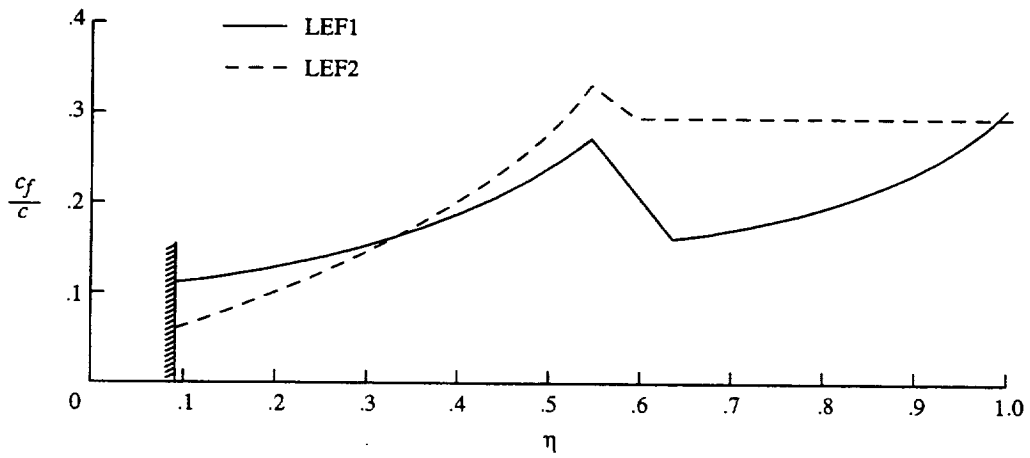


Figure 4. Graphical depiction of leading-edge suction parameter.

	LE sweeps, deg	
	IB	OB
Original	71	57
F1	71	57
F2	69	57
F3	67.4	61.5
LEF2	68	58



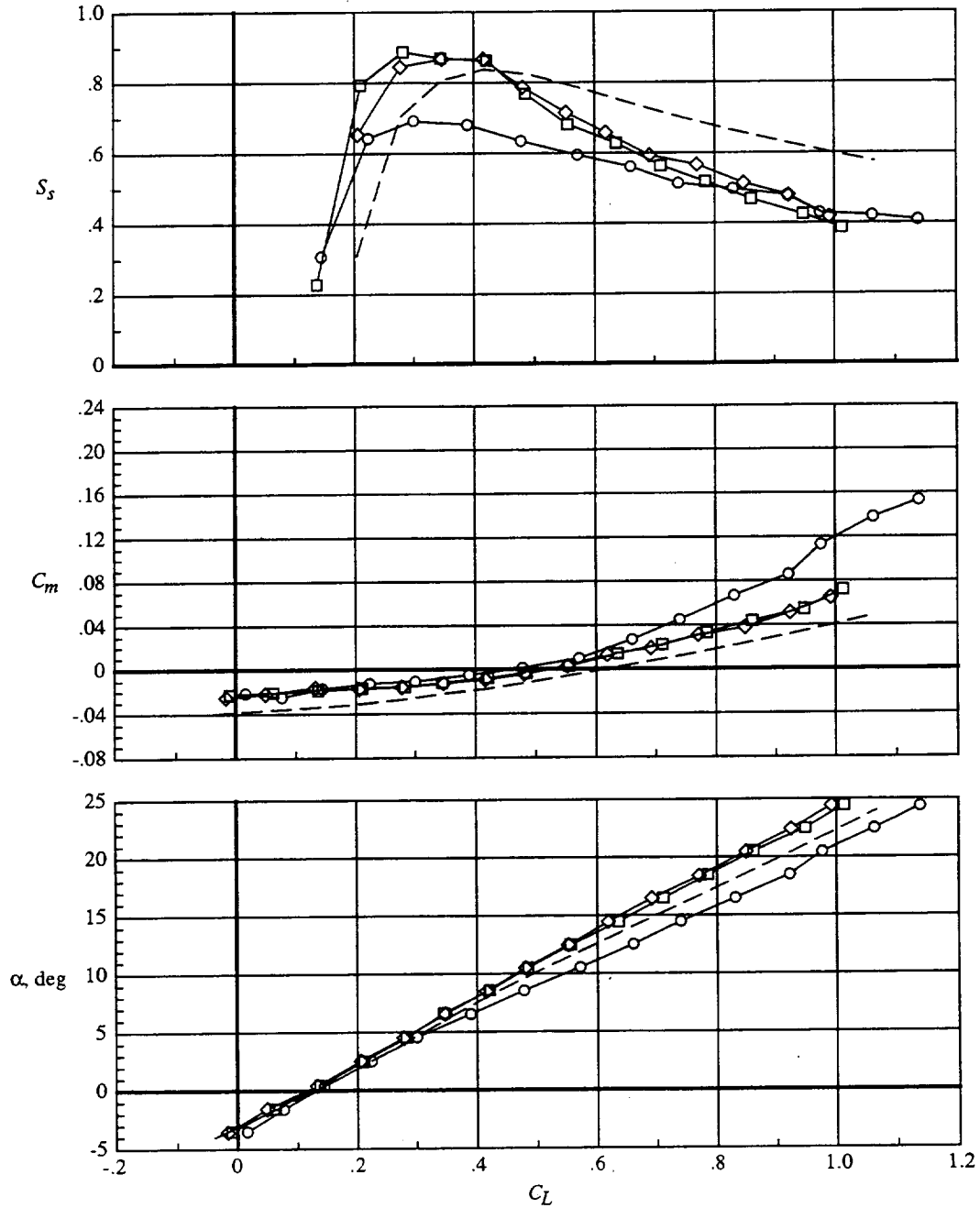
(a) Modified flaps and original geometry.



(b) Original flap chord distribution and final modified flap chord distribution.

Figure 5. Details of wing modifications.

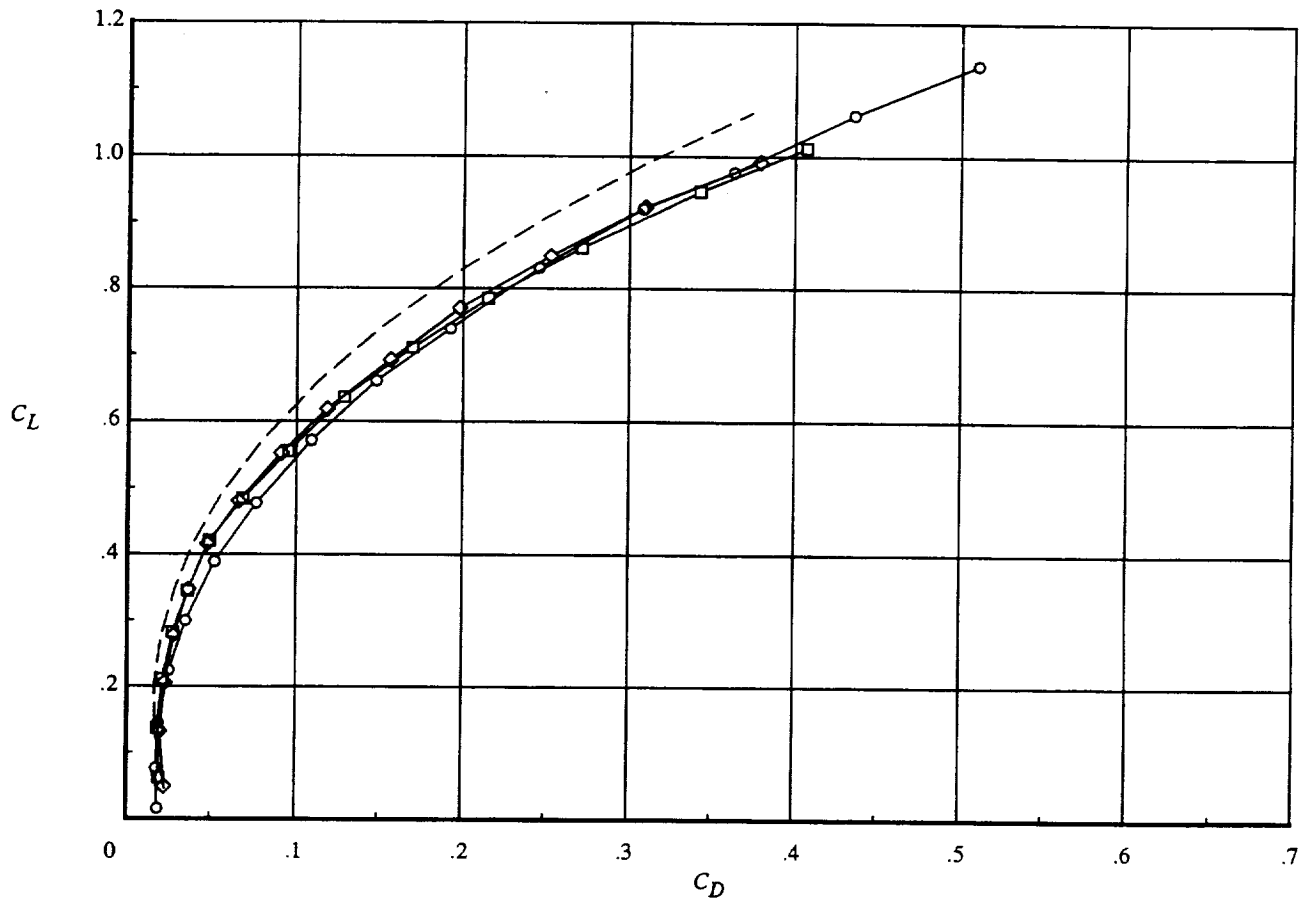
		$\delta_{le}$ , deg, for —						
		Seg 1	Seg 2	Seg 3	Seg 4	Seg 5	Seg 6	
○		0	0	0	0	0	0	Zero
□		13	34	35	35	19	29	Schedule R (ref. 6)
◇		18	29	38	44	40	43	AERO2S (experimental)
---		18	29	38	44	40	43	AERO2S (predicted)



(a) Lift, pitching moment, and suction parameter.

Figure 6. Effect of leading-edge flap deflection on longitudinal characteristics for WBNLEF1.  $\delta_{le} = 13^\circ$ .

	$\delta_{le}$ , deg, for —						
	Seg 1	Seg 2	Seg 3	Seg 4	Seg 5	Seg 6	
○	0	0	0	0	0	0	Zero
□	13	34	35	35	19	29	Schedule R (ref. 6)
◇	18	29	38	44	40	43	AERO2S (experimental)
---	18	29	38	44	40	43	AERO2S (predicted)



(b) Drag polar.

Figure 6. Concluded.

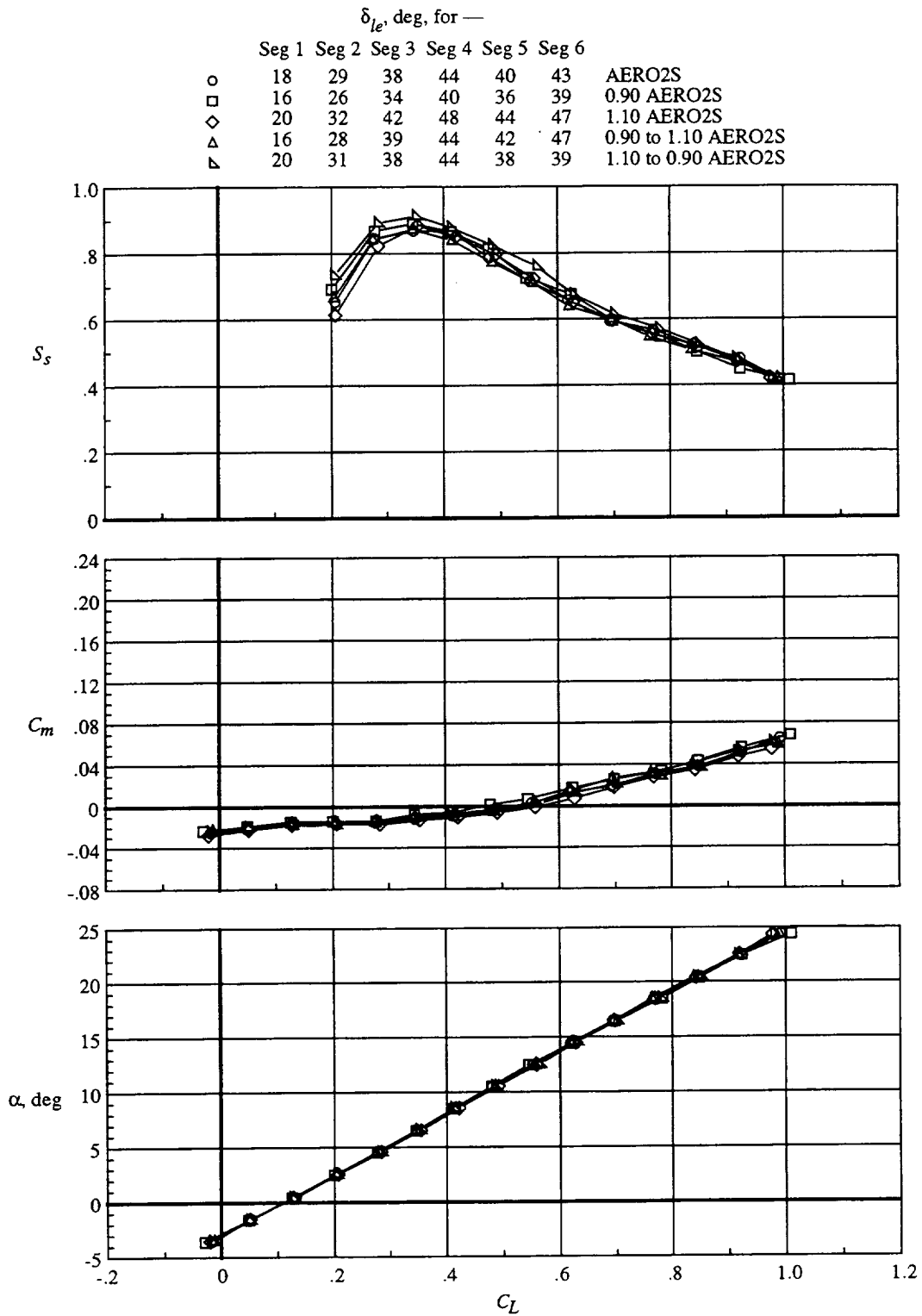
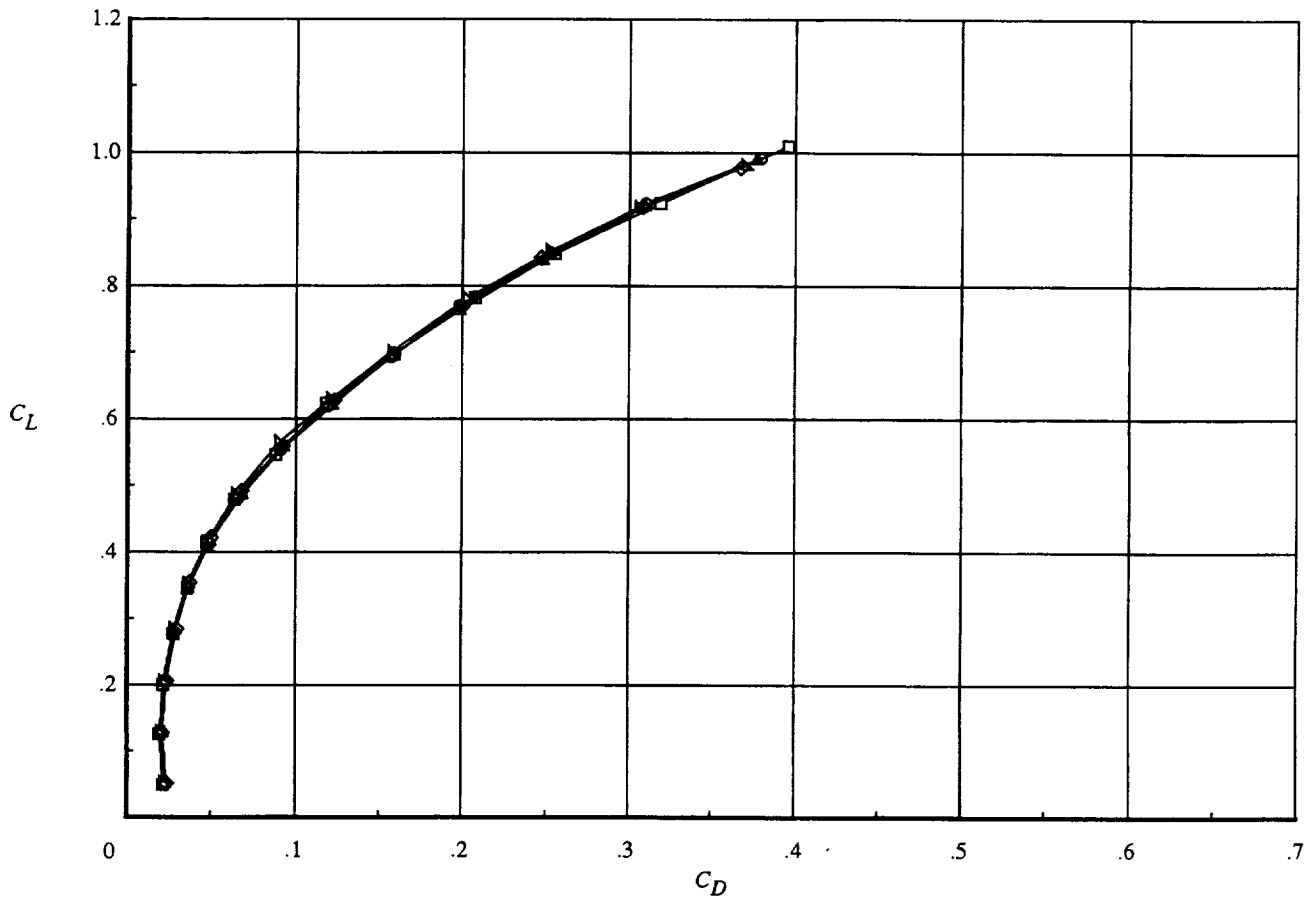


Figure 7. Effect of perturbations about AERO2S leading-edge flap design deflections for WBNLEF1.  $\delta_{le} = 13^\circ$ .

$\delta_{te}$ , deg. for —							
	Seg 1	Seg 2	Seg 3	Seg 4	Seg 5	Seg 6	
○	18	29	38	44	40	43	AERO2S
□	16	26	34	40	36	39	0.90 AERO2S
◇	20	32	42	48	44	47	1.10 AERO2S
△	16	28	39	44	42	47	0.90 to 1.10 AERO2S
▽	20	31	38	44	38	39	1.10 to 0.90 AERO2S



(b) Drag polar.

Figure 7. Concluded.

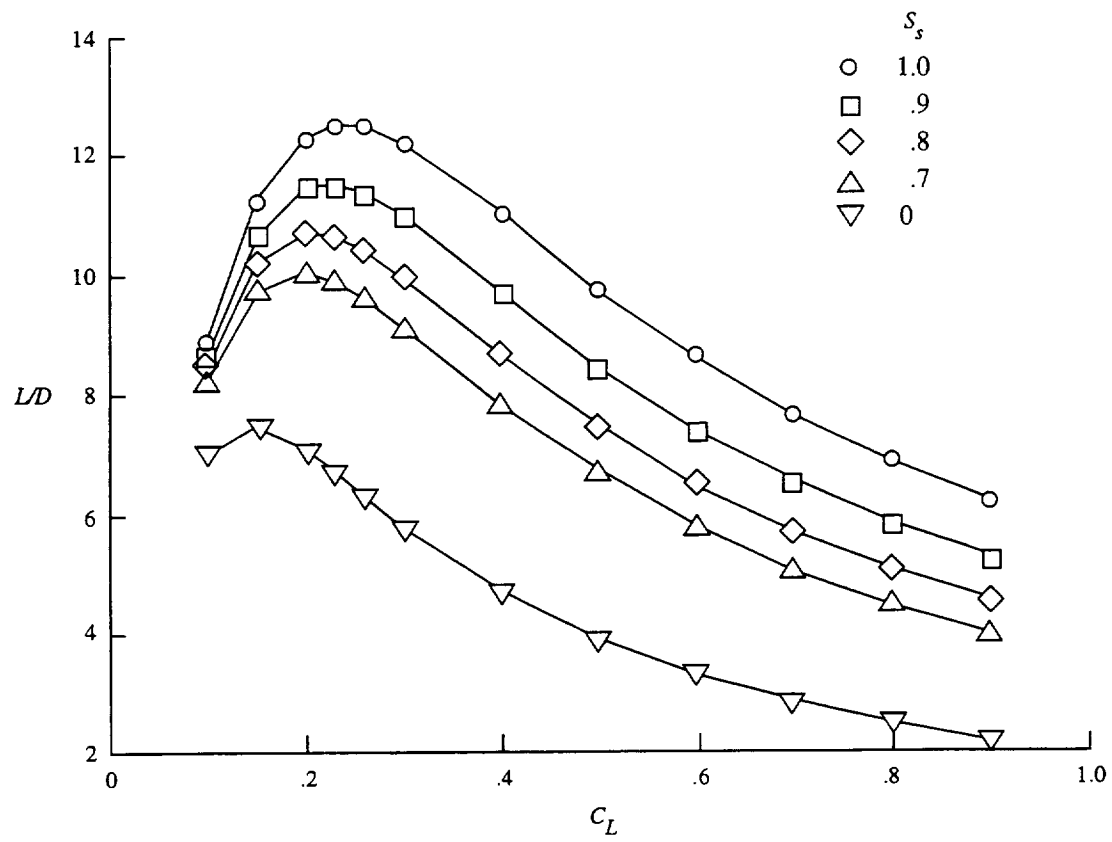
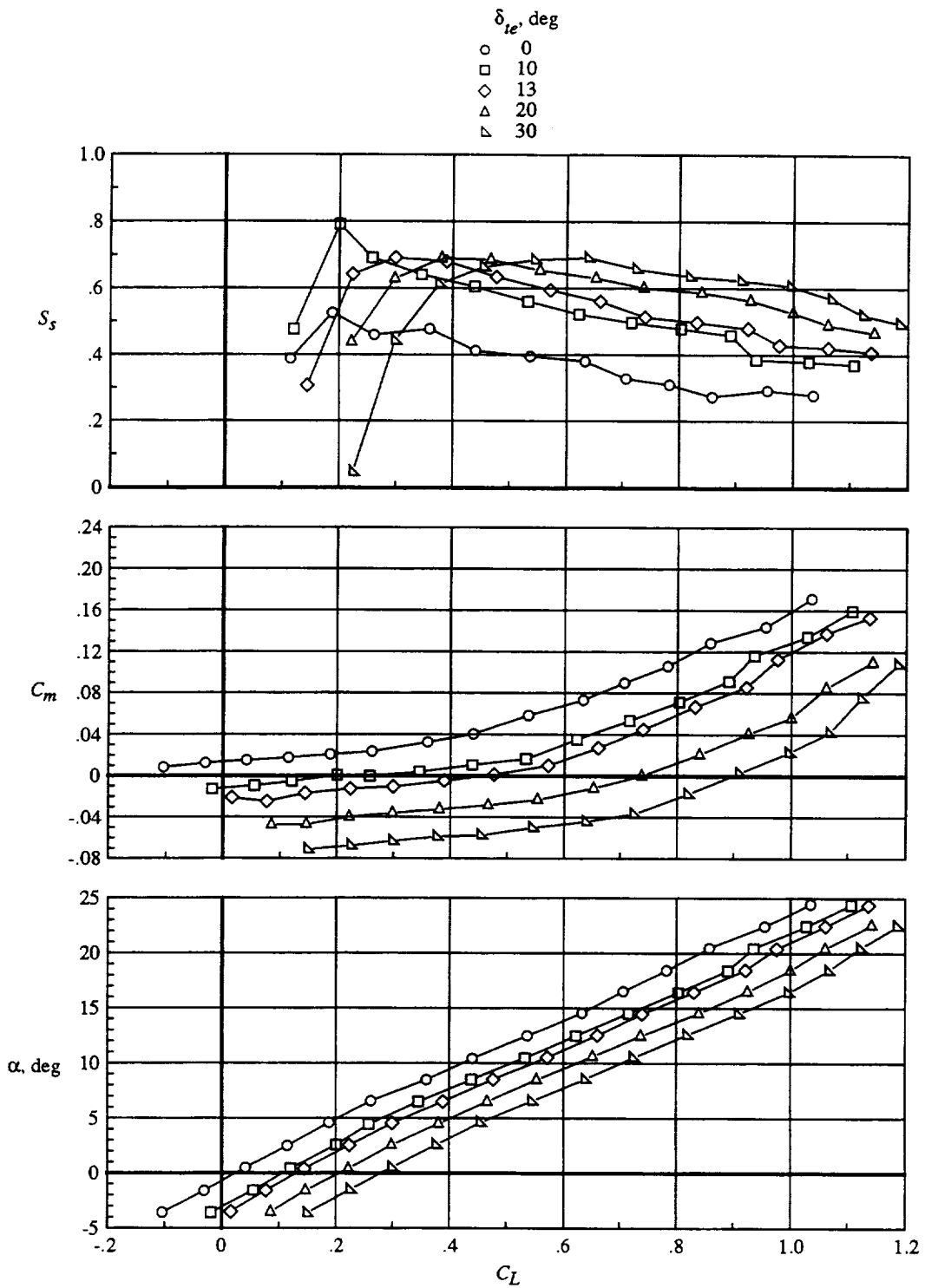
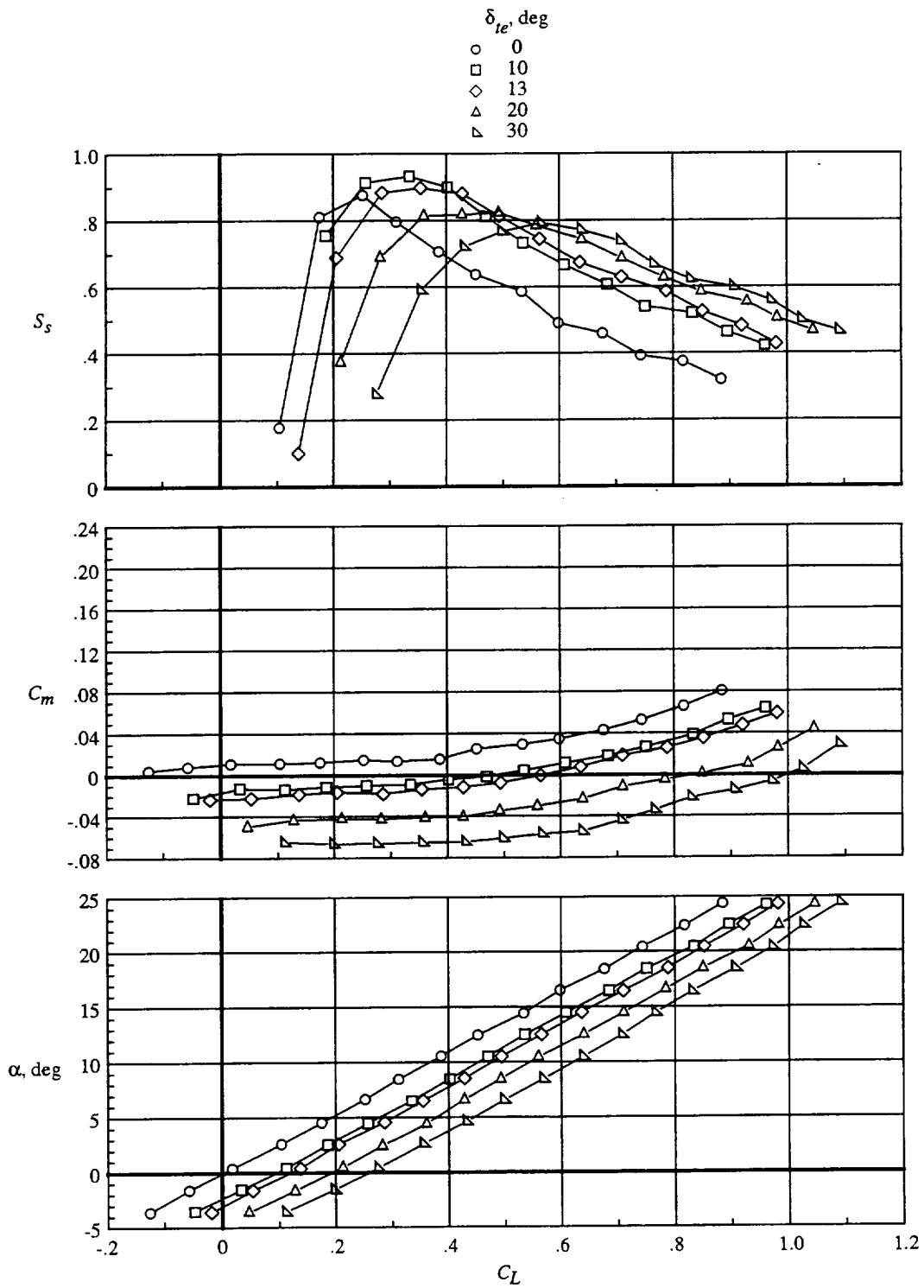


Figure 8. Variation of  $L/D$  with leading-edge suction parameter. Data from reference 11.



(a) Leading-edge flaps undeflected.

Figure 9. Effect of trailing-edge flap deflection on longitudinal characteristics for WBNLEF1.



(b) Leading-edge flaps deflected 20°, 31°, 38°, 44°, 38°, and 39° (1.10 to 0.90 AERO2S).

Figure 9. Concluded.

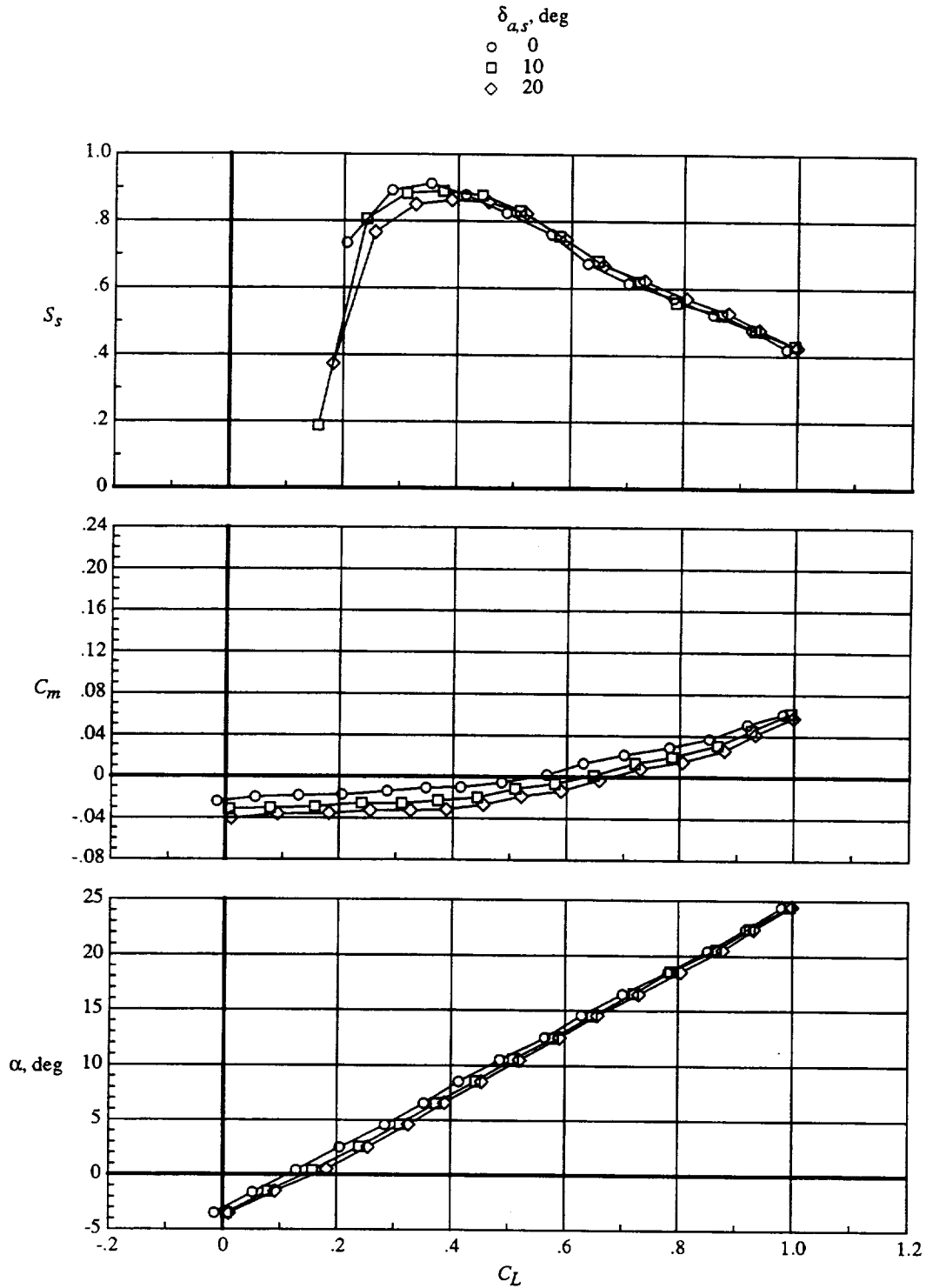
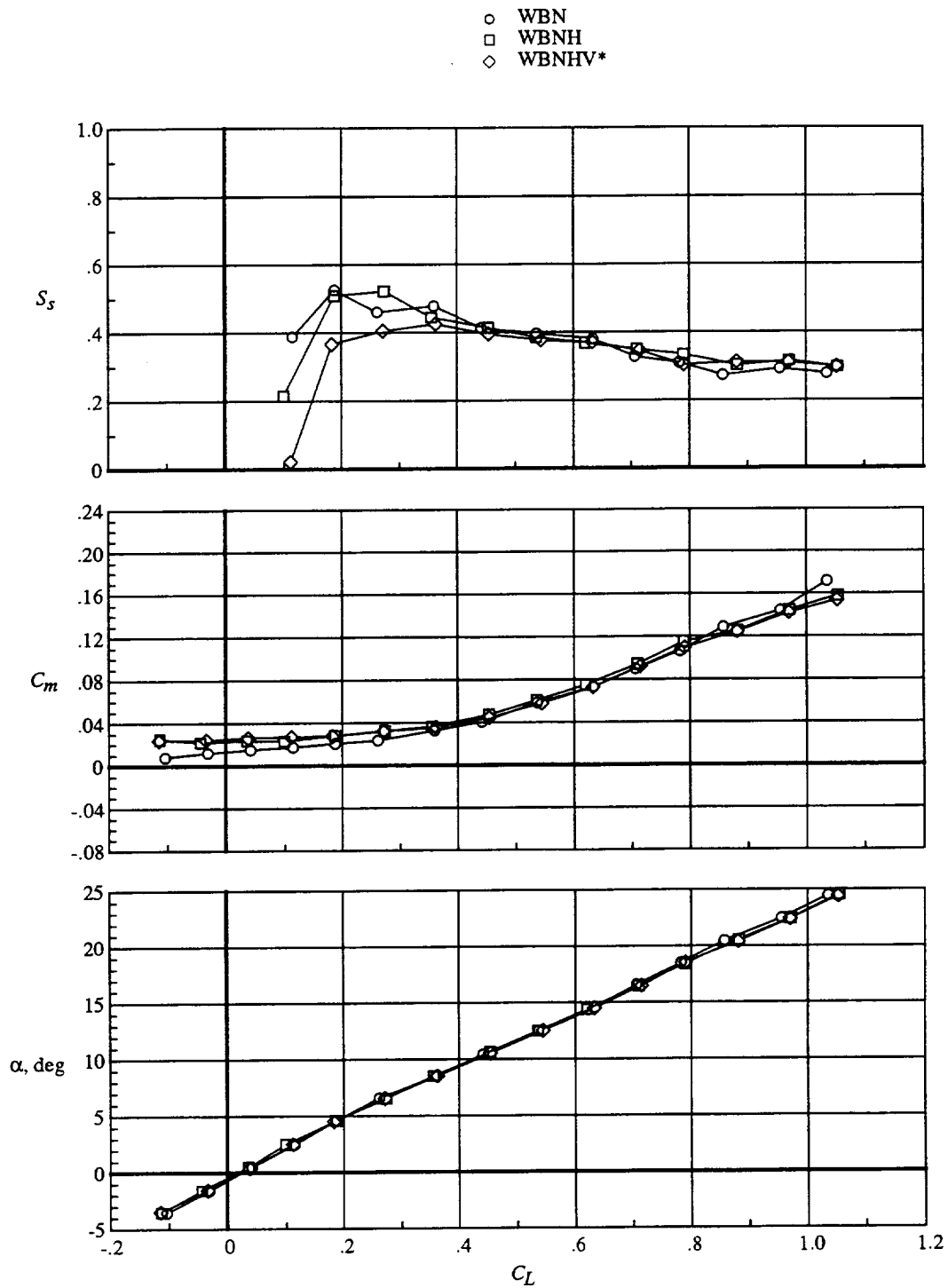
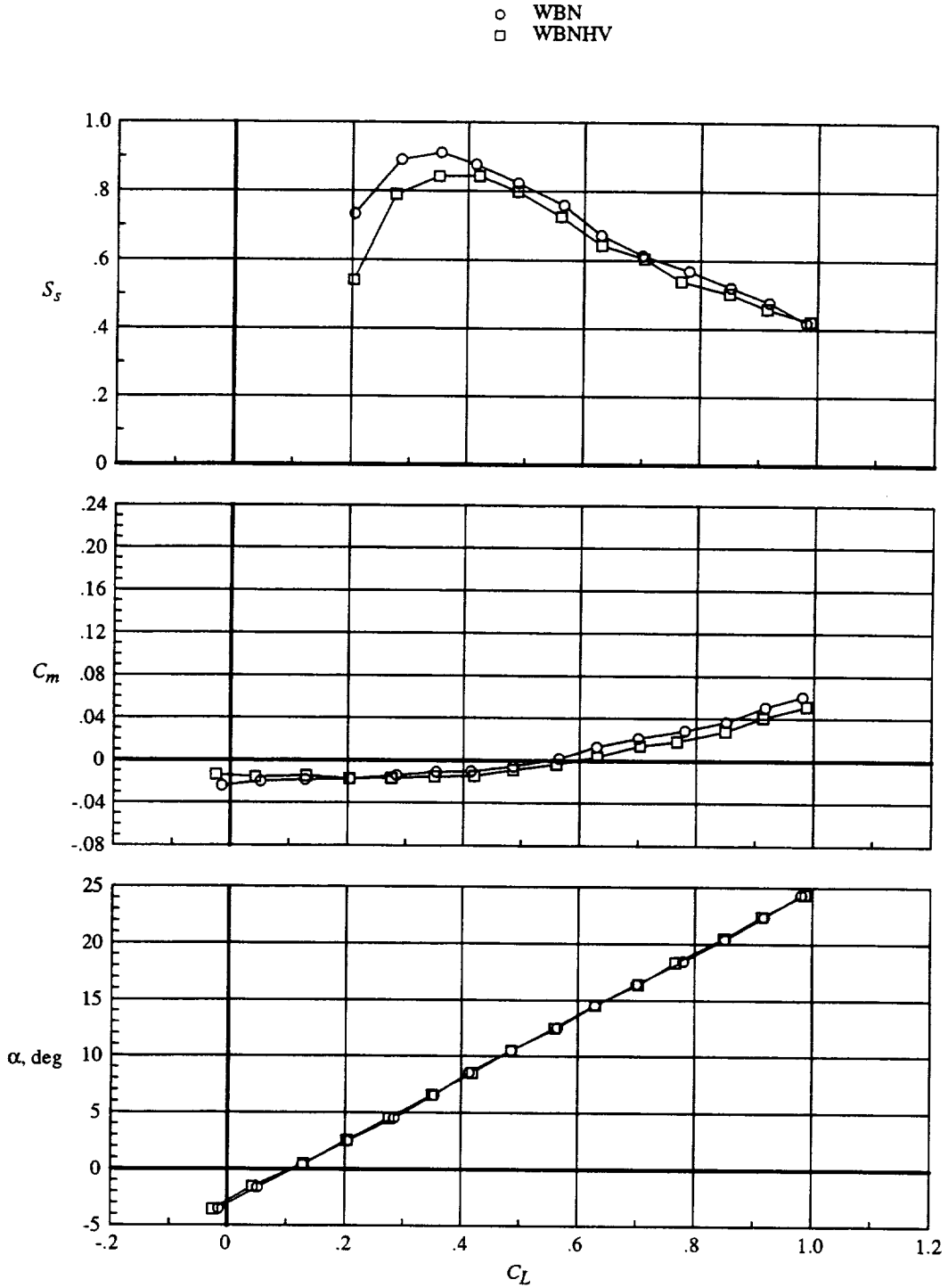


Figure 10. Effect of symmetric aileron deflection on longitudinal characteristics for WBNLEF1.  $\delta_{te} = 13^\circ$ ; leading-edge flaps deflected  $20^\circ, 31^\circ, 38^\circ, 44^\circ, 38^\circ,$  and  $39^\circ$  (1.10 to 0.90 AERO2S).



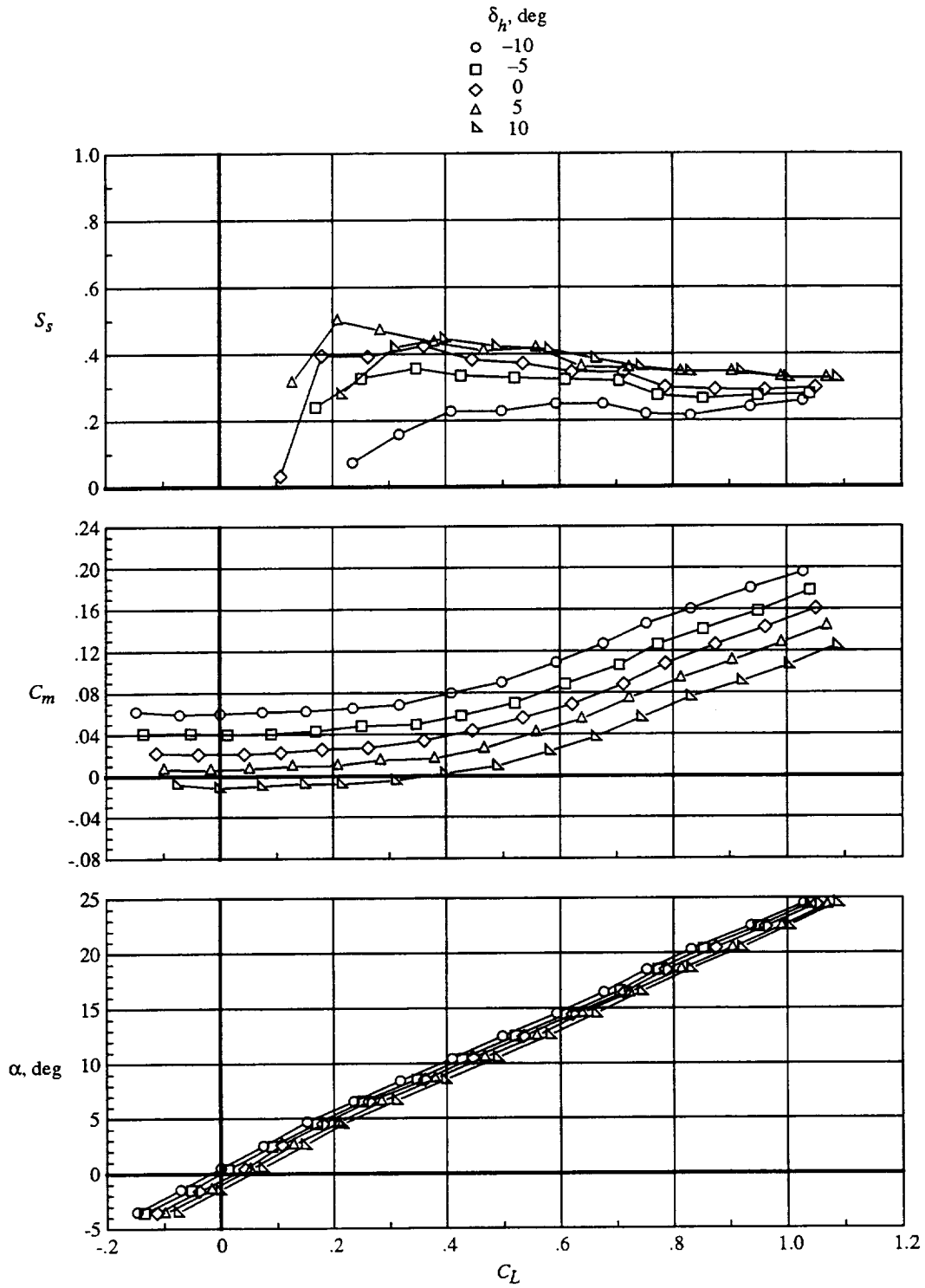
(a) Leading- and trailing-edge flaps undeflected.

Figure 11. Effect of component buildup on longitudinal characteristics for LEF1.



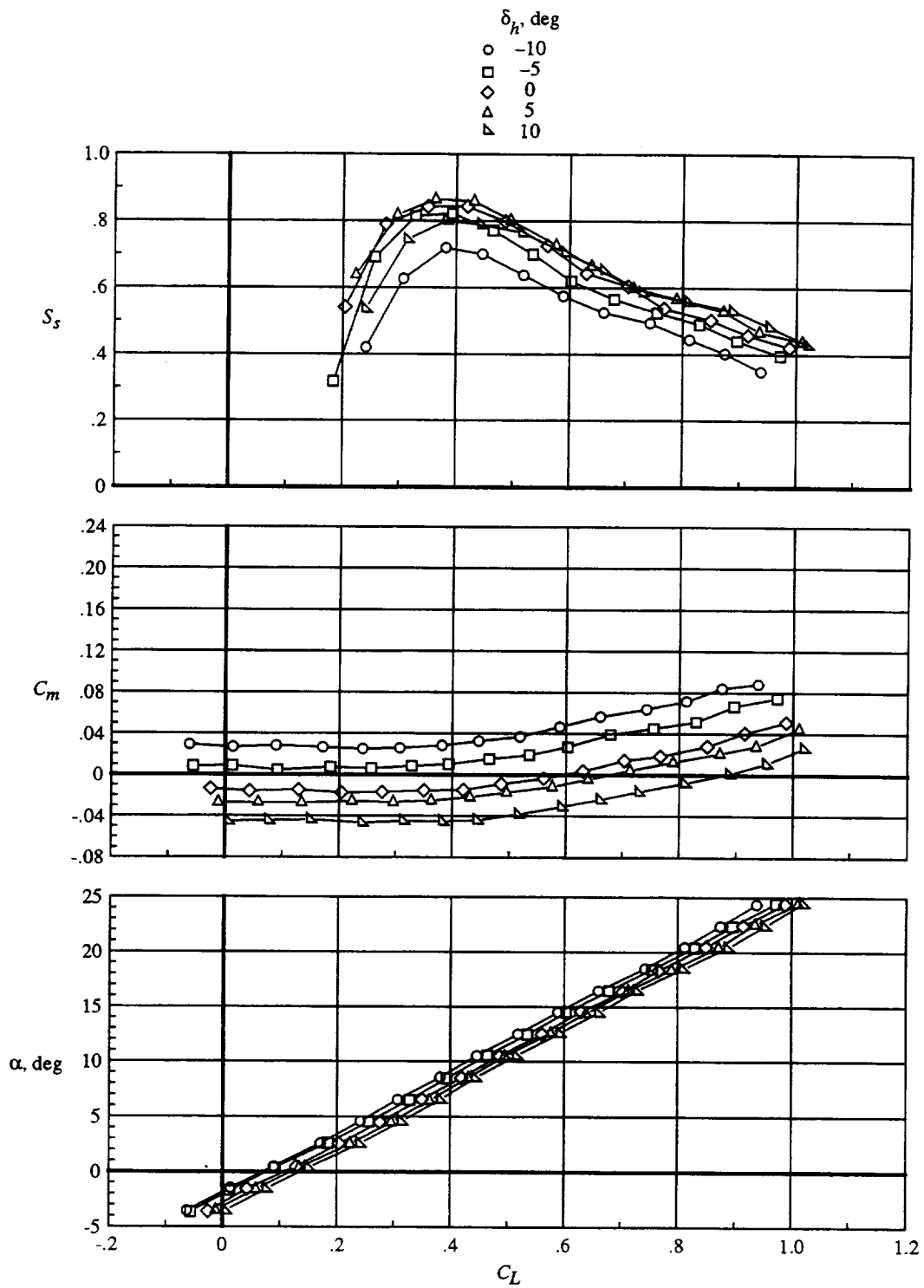
(b) Leading-edge flaps deflected 20°, 31°, 38°, 44°, 38°, and 39° (1.10 to 0.90 AERO2S);  $\delta_{te} = 13^\circ$ .

Figure 11. Concluded.



(a) Leading- and trailing-edge flaps undeflected.

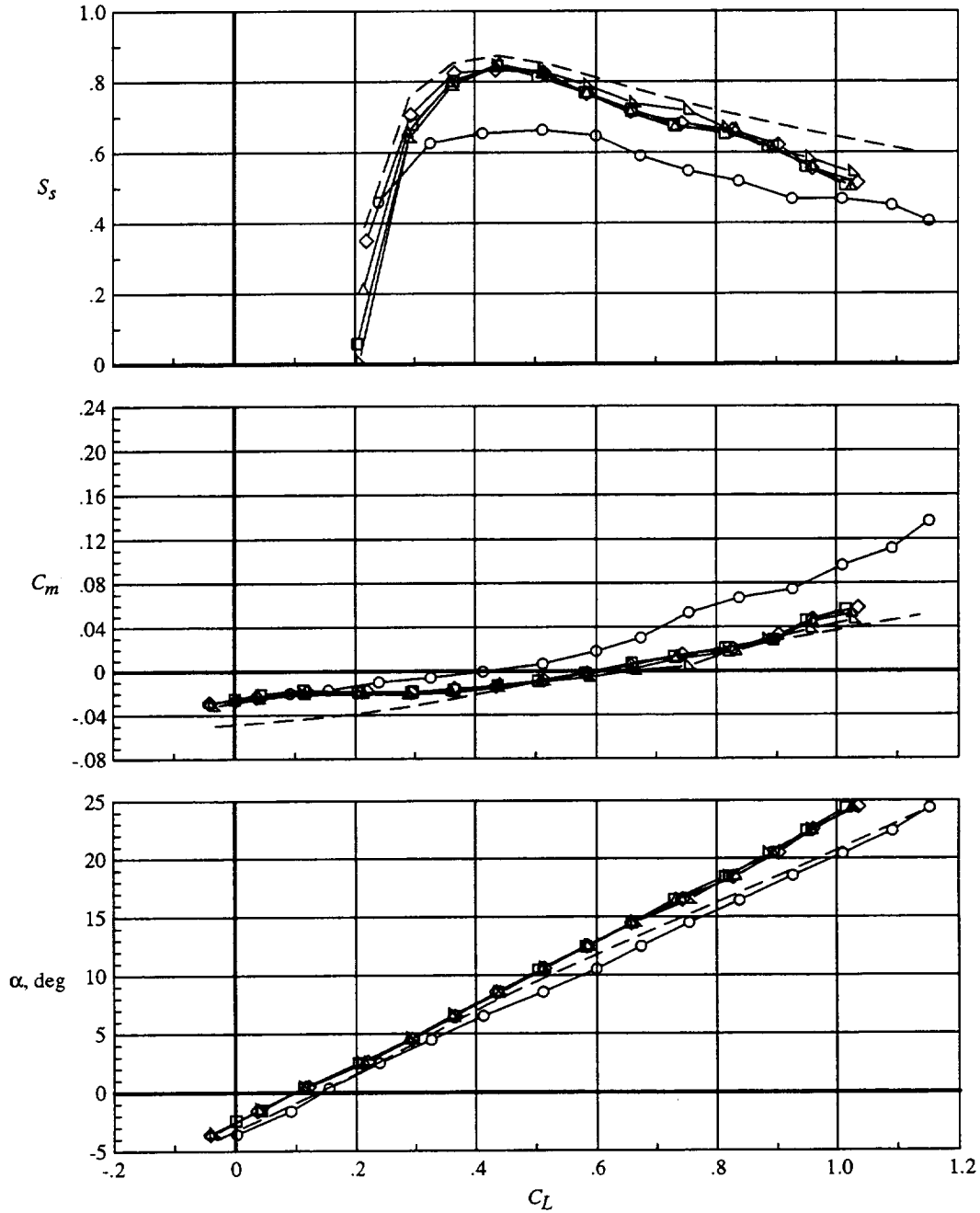
Figure 12. Effect of horizontal tail deflection on longitudinal characteristics for WBNHVLEF1.



(b) Leading-edge flaps deflected 20°, 31°, 38°, 44°, 38°, and 39° (1.10 to 0.90 AERO2S);  $\delta_{te} = 13^\circ$ .

Figure 12. Concluded.

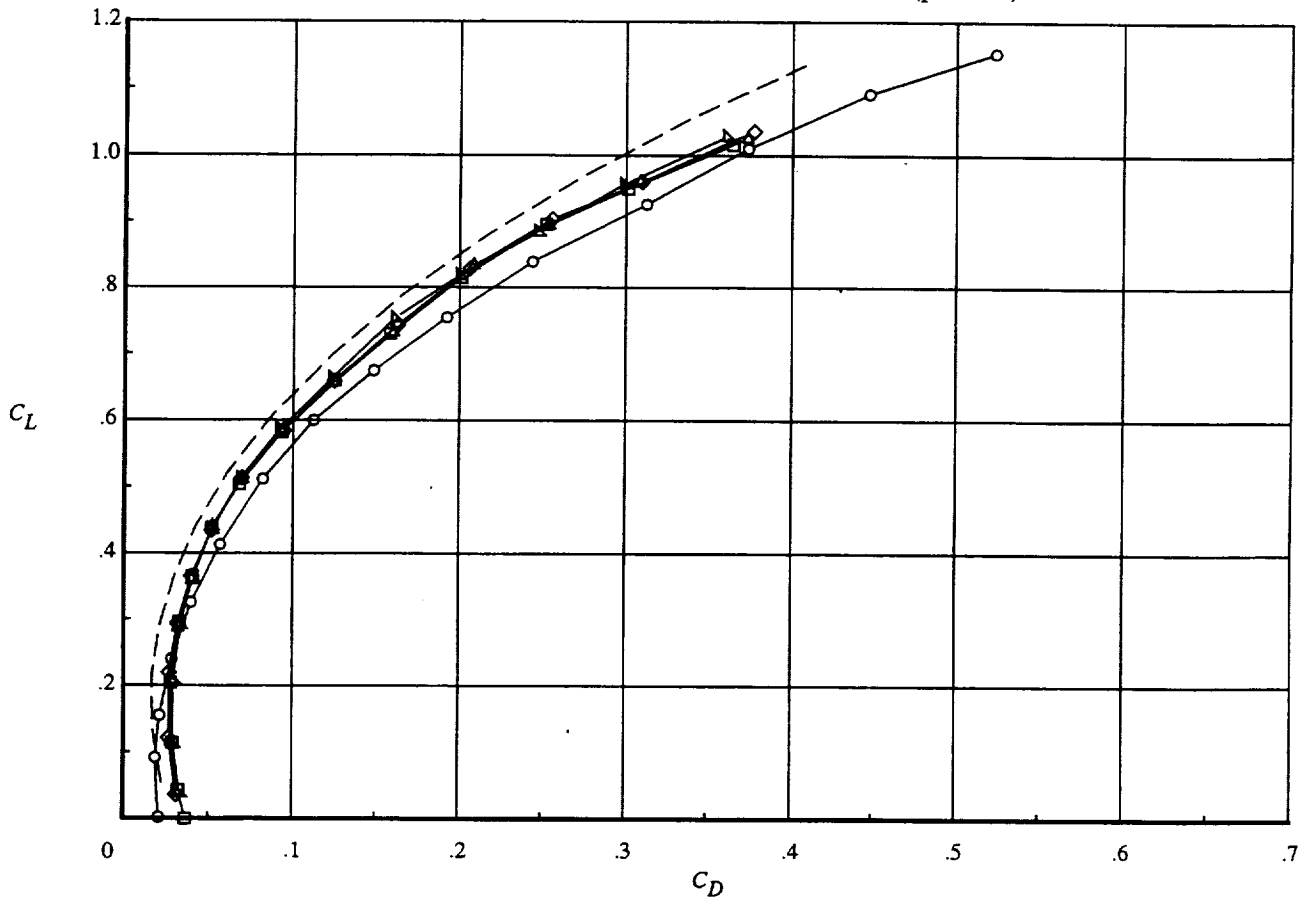
		$\delta_{le}$ , deg, for —						
		Seg 1	Seg 2	Seg 3	Seg 4	Seg 5	Seg 6	
○		0	0	0	0	0	0	Zero
□		25	32	37	41	28	33	AERO2S (experimental)
◇		24	30	35	39	27	31	0.95 AERO2S
△		28	34	37	41	27	31	1.10 to 0.95 AERO2S
▽		36	46	45	43	31	31	1.45 to 0.95 AERO2S
— —		25	32	37	41	28	33	AERO2S (predicted)



(a) Lift, pitching moment, and suction parameter.

Figure 13. Effect of perturbations about AERO2S leading-edge flap design deflections for WBNLEF2.  $\delta_{le} = 15^\circ$ .

	$\delta_{le}$ , deg, for —						
	Seg 1	Seg 2	Seg 3	Seg 4	Seg 5	Seg 6	
○	0	0	0	0	0	0	Zero
□	25	32	37	41	28	33	AERO2S (experimental)
◇	24	30	35	39	27	31	0.95 AERO2S
△	28	34	37	41	27	31	1.10 to 0.95 AERO2S
▽	36	46	45	43	31	31	1.45 to 0.95 AERO2S
— —	25	32	37	41	28	33	AERO2S (predicted)



(b) Drag polar.

Figure 13. Concluded.

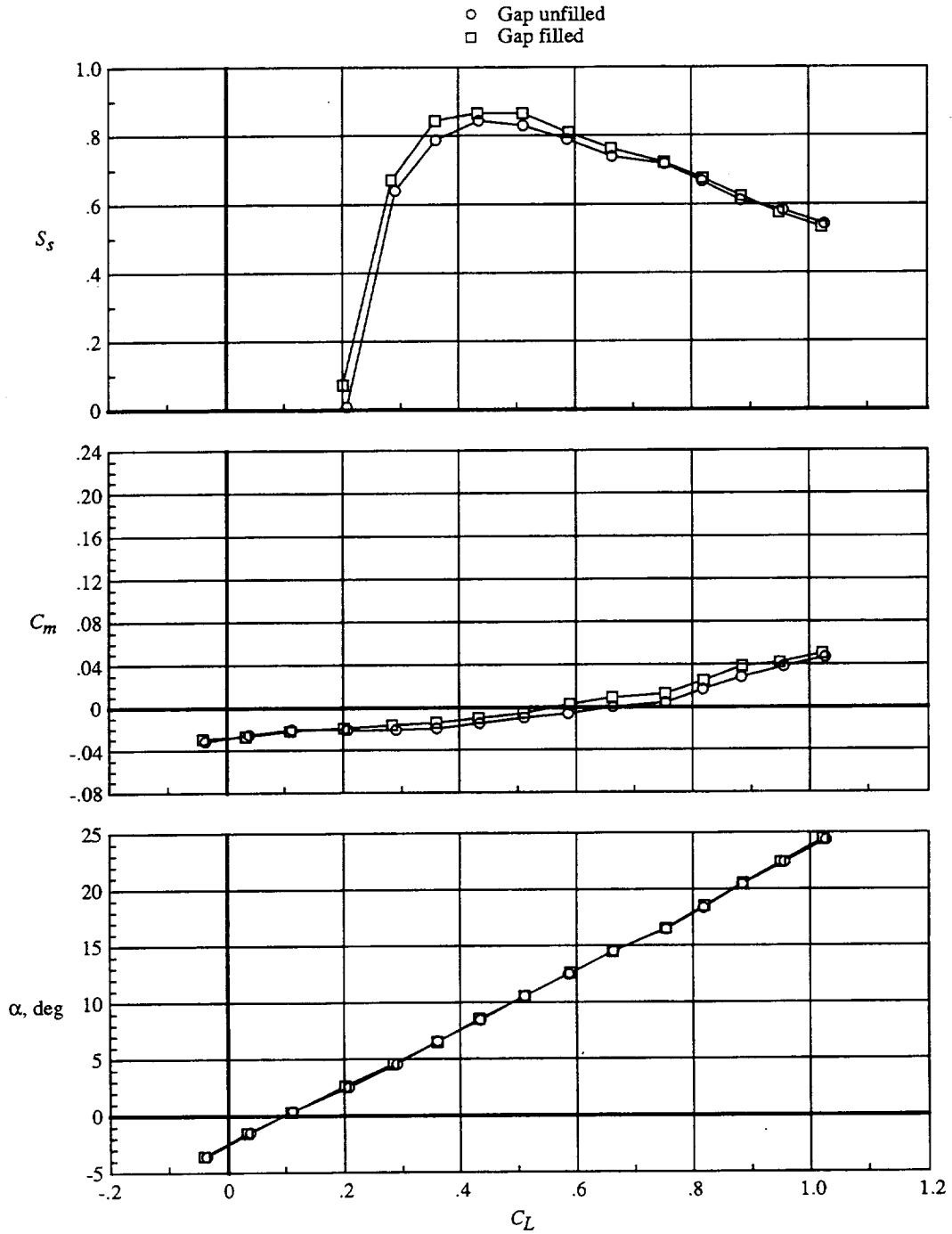
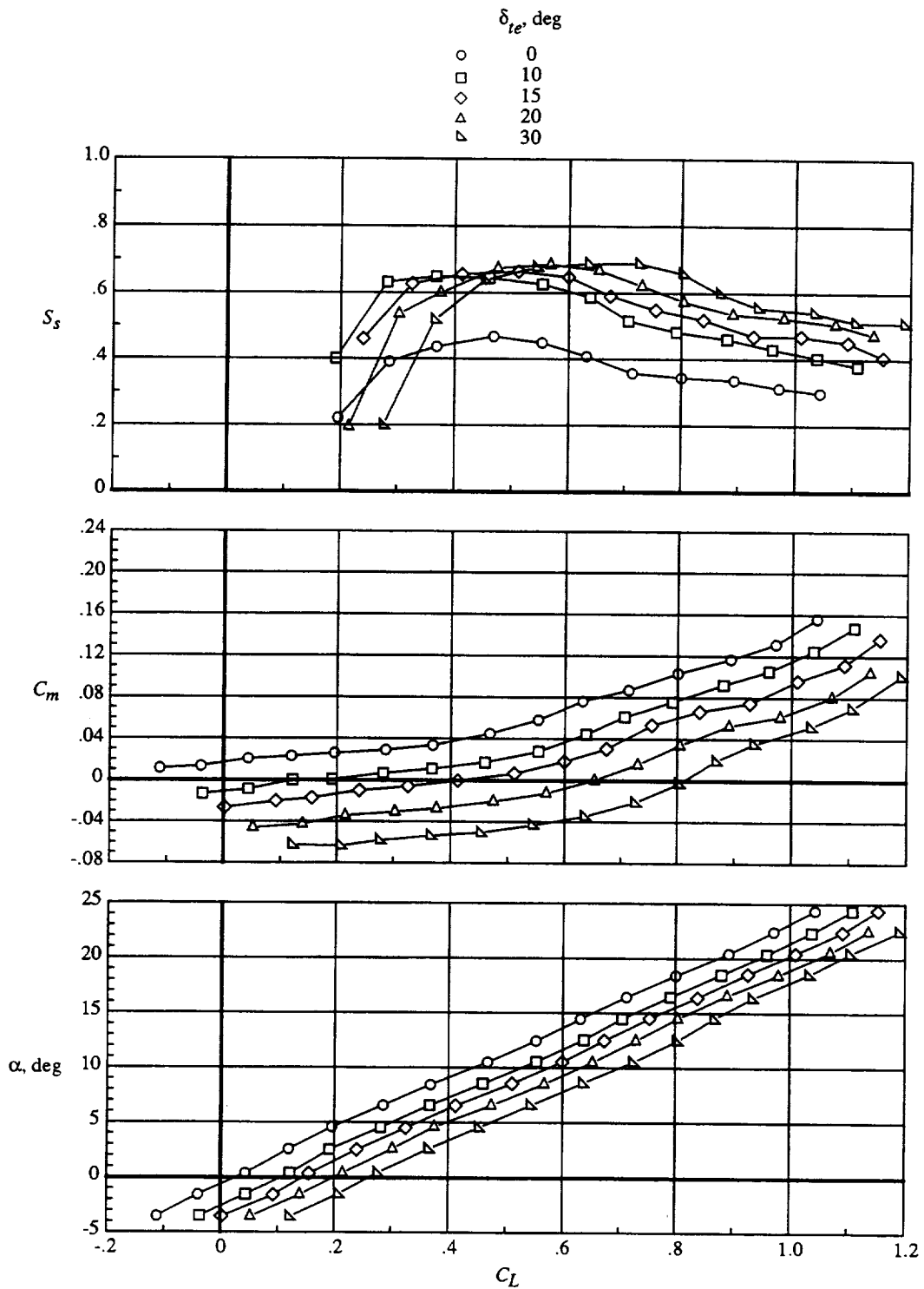
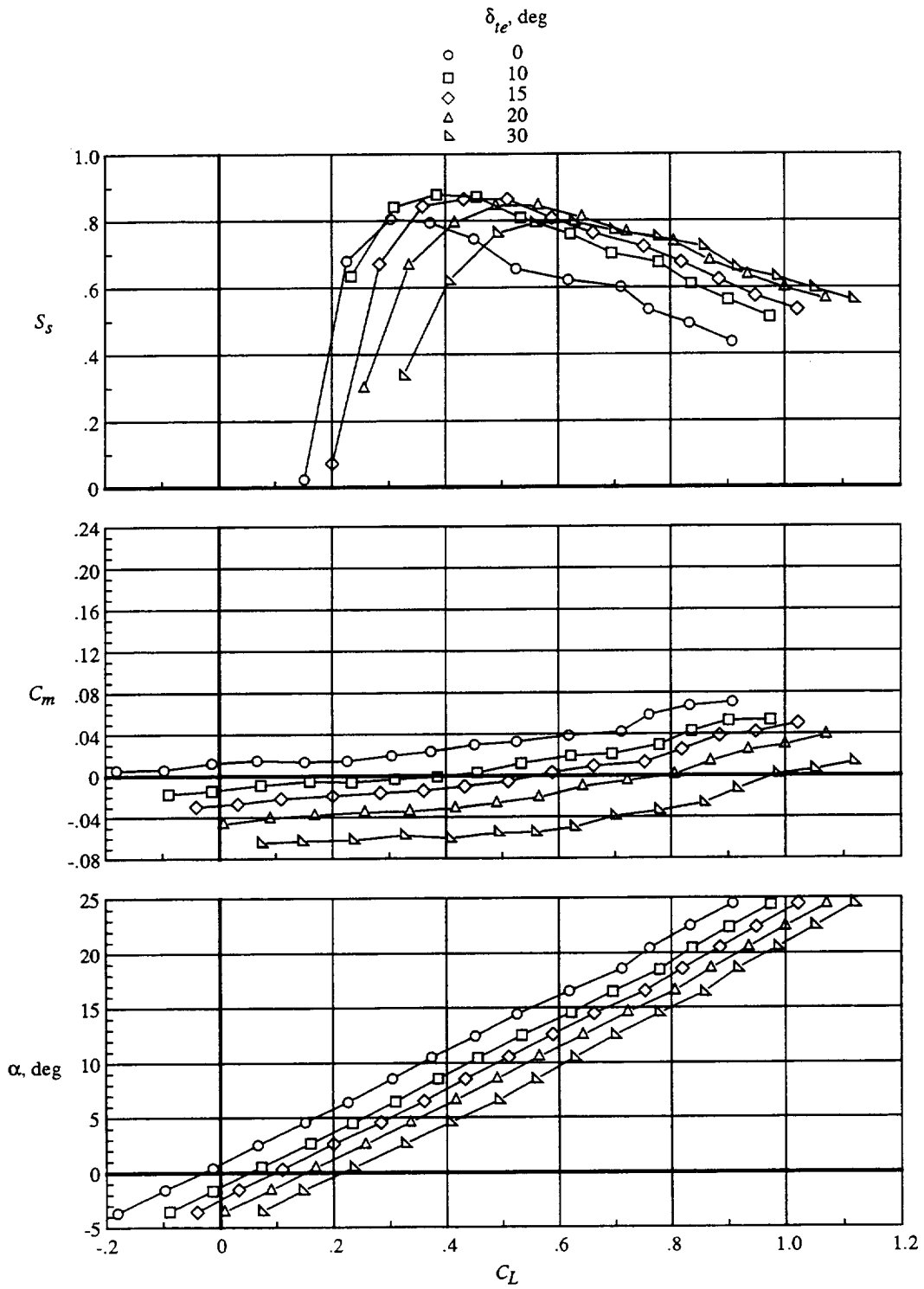


Figure 14. Effect of gap filler between leading-edge flap segments 4 and 5 on longitudinal characteristics. WBNLEF2;  $\delta_{te} = 15^\circ$ ; leading-edge flaps deflected  $36^\circ, 46^\circ, 45^\circ, 43^\circ, 31^\circ$ , and  $31^\circ$  (1.45 to 0.95 AERO2S).



(a) Leading-edge flaps undeflected.

Figure 15. Effect of trailing-edge flap deflection on longitudinal characteristics for WBNLEF2.



(b) Leading-edge flaps deflected 36°, 46°, 45°, 43°, 31°, and 31° (1.45 to 0.95 AERO2S); gap between leading-edge flap segments 4 and 5 filled.

Figure 15. Concluded.

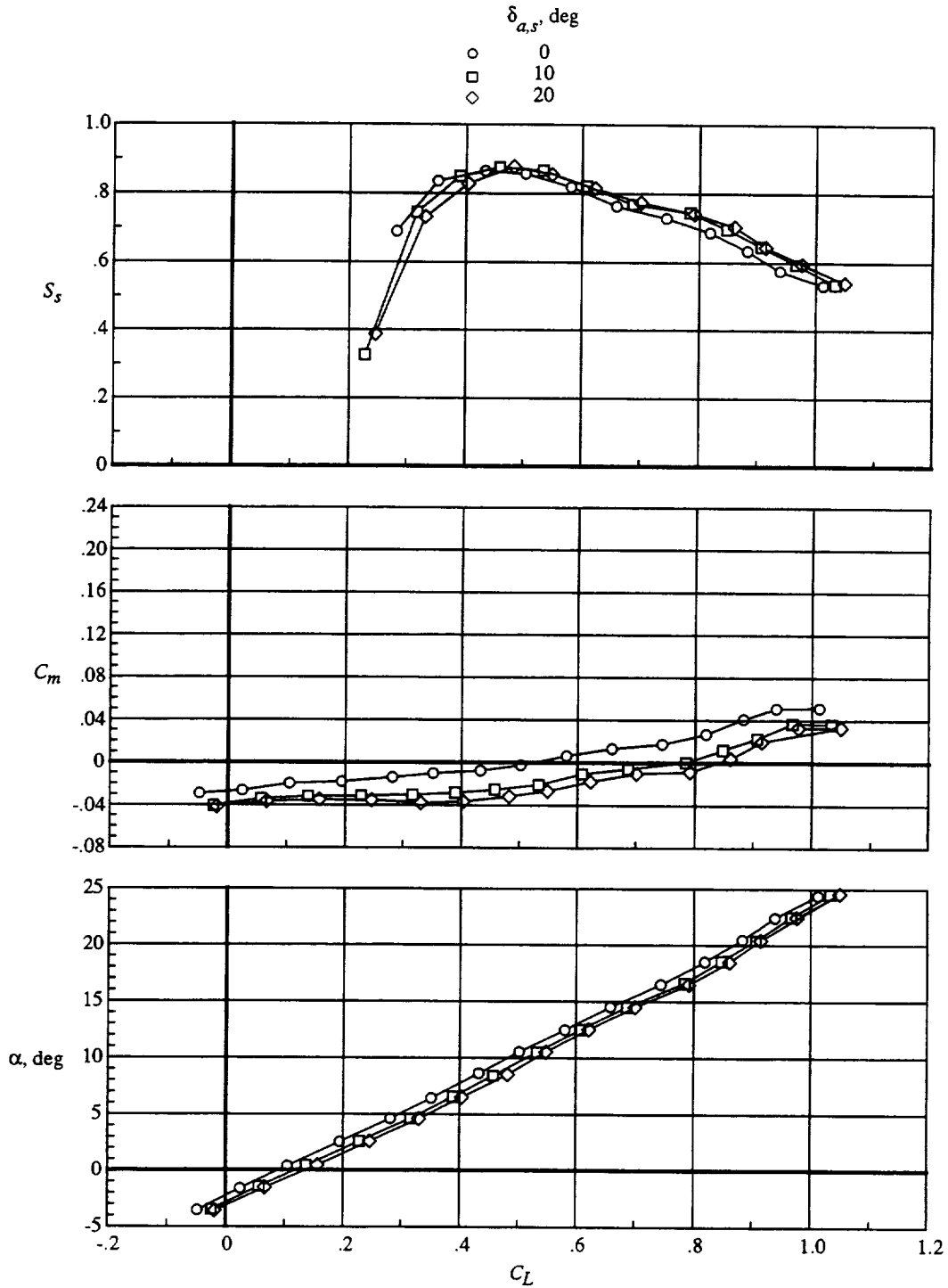


Figure 16. Effect of symmetric aileron deflection on longitudinal characteristics for WBNLEF2.  $\delta_{te} = 15^\circ$ ; leading-edge flaps deflected  $36^\circ$ ,  $46^\circ$ ,  $45^\circ$ ,  $43^\circ$ ,  $31^\circ$ , and  $31^\circ$  (1.45 to 0.95 AERO2S); gap between leading-edge flap segments 4 and 5 filled.

	$\delta_{le}$ , deg, for —						
	Seg 1	Seg 2	Seg 3	Seg 4	Seg 5	Seg 6	
○	0	0	0	0	0	0	Zero
□	36	46	45	43	31	31	1.45 to 0.95 AERO2S
◇	36	46	45	43	0	0	Outboard zero
△	0	0	0	0	31	31	Inboard zero

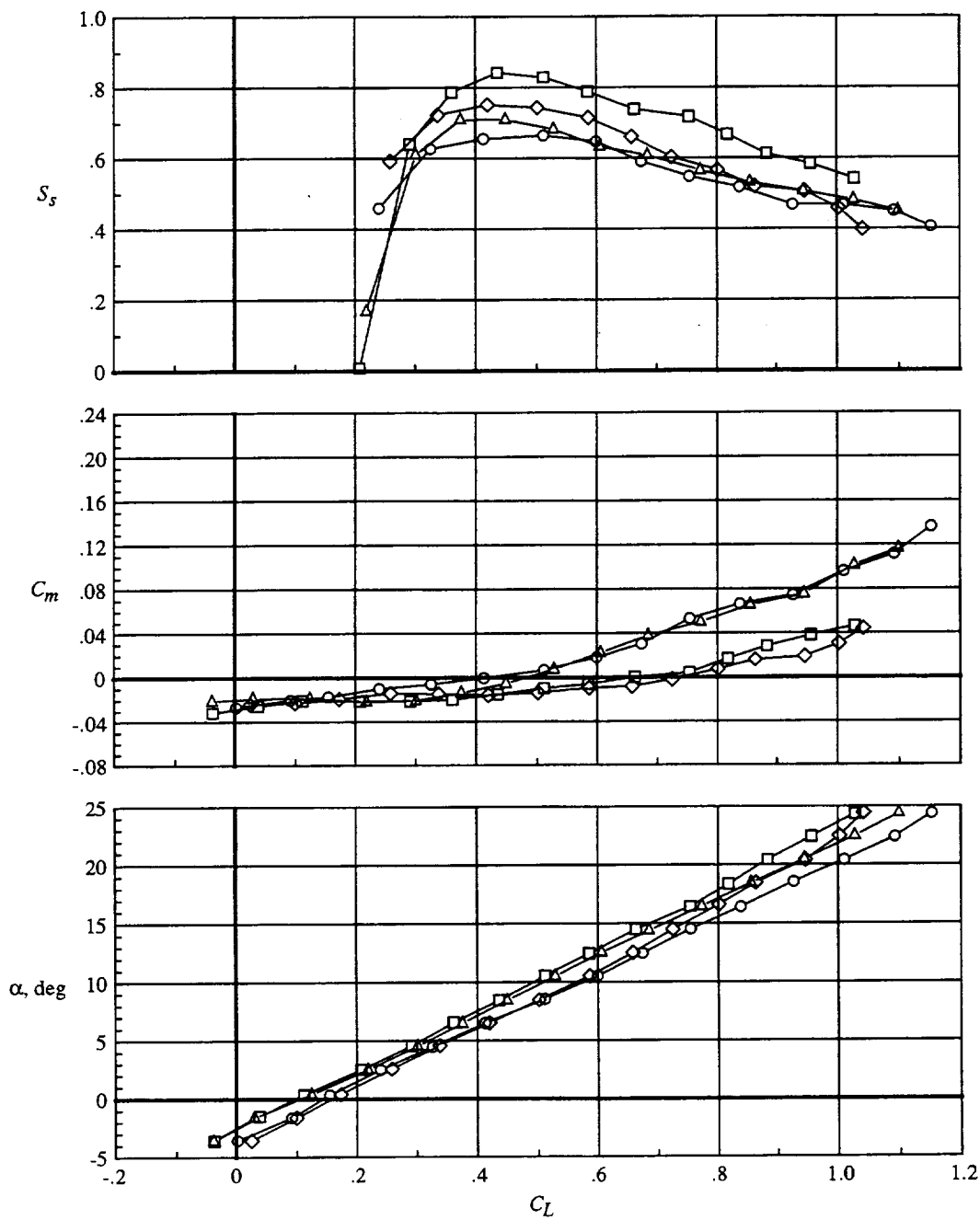
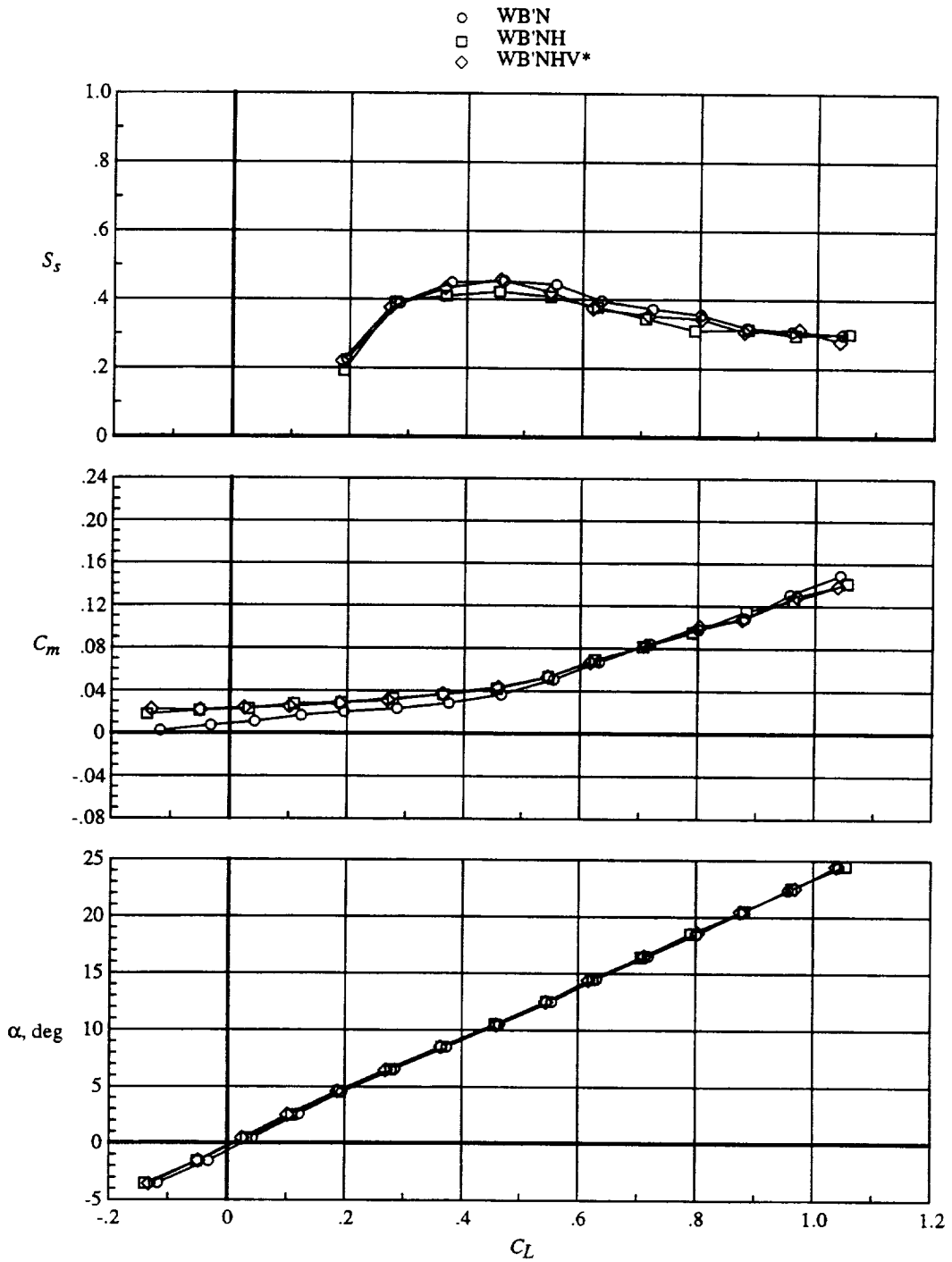
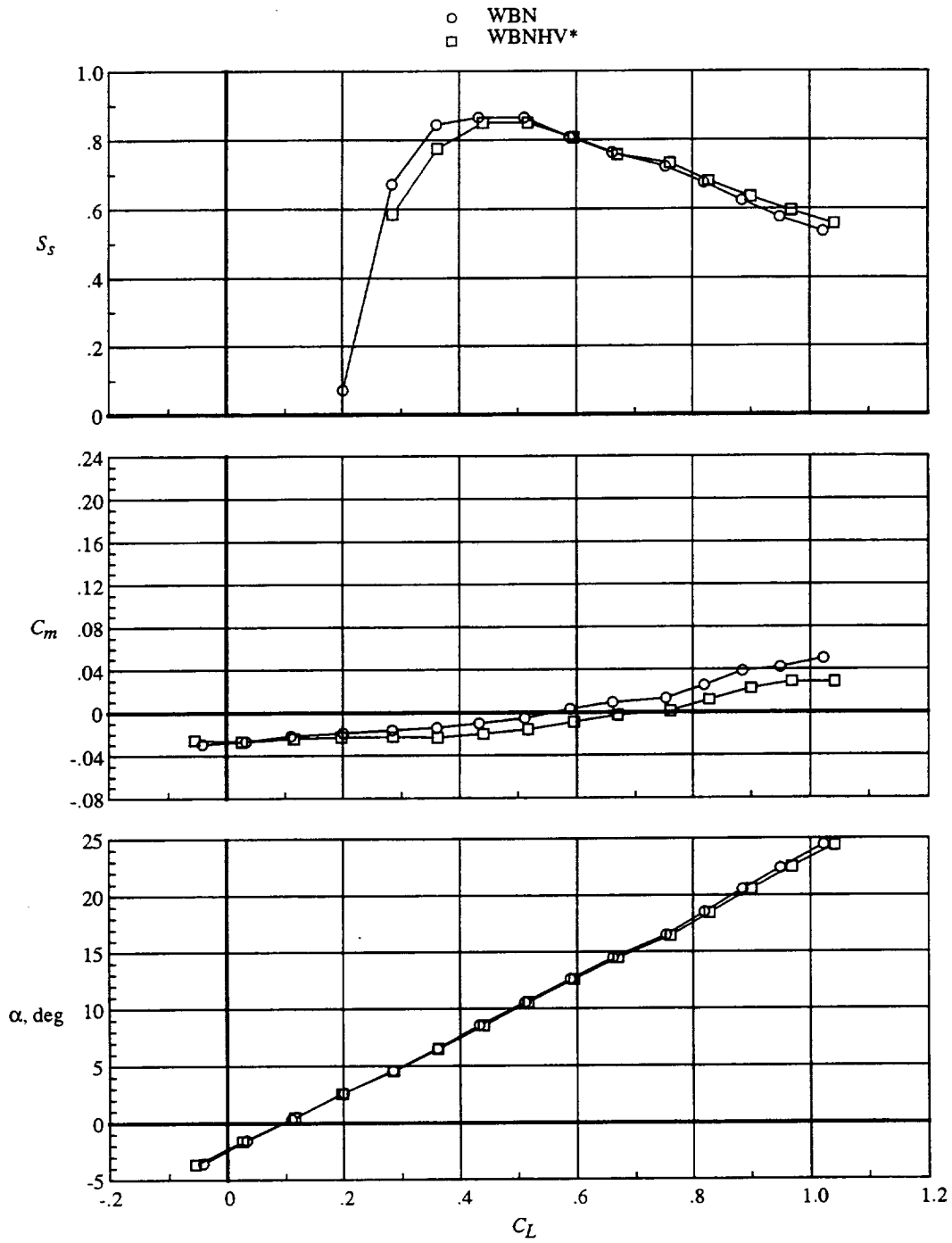


Figure 17. Effect of inboard and outboard leading-edge flap deflections on longitudinal characteristics. WBNLEF2;  $\delta_{le} = 15^\circ$ .



(a) Leading- and trailing-edge flaps undeflected.

Figure 18. Effect of component buildup on longitudinal characteristics for LEF2.



(b) Leading-edge flaps deflected 36°, 46°, 45°, 43°, 31°, and 31° (1.45 to 0.95 AERO2S); gap between leading-edge flap segments 4 and 5 filled;  $\delta_{te} = 15^\circ$ .

Figure 18. Concluded.

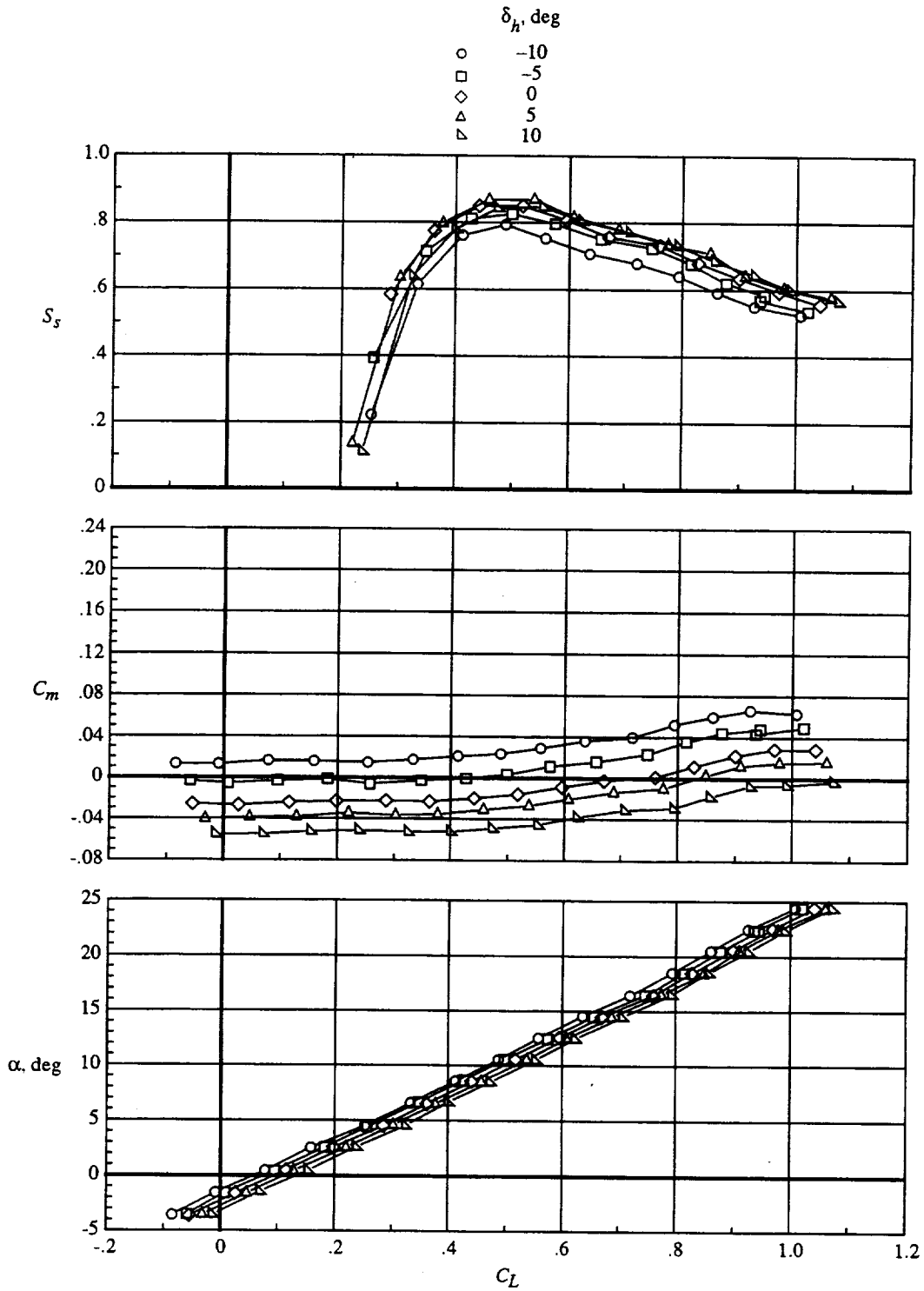


Figure 19. Effect of horizontal tail deflection on longitudinal characteristics for WBNHVLEF2. Leading-edge flaps deflected 36°, 46°, 45°, 43°, 31°, and 31° (1.45 to 0.95 AERO2S); gap between leading-edge flap segments 4 and 5 filled;  $\delta_{le} = 15^\circ$ .

	$\delta_{le}$ , deg						$\delta_{te}$ , deg		LEF1	LEF2	AERO2S
	Seg 1	Seg 2	Seg 3	Seg 4	Seg 5	Seg 6					
○	0	0	0	0	0	0	0	0	Zero		
□	20	31	38	44	38	39	13	13	LEF1	1.10 to 0.90 AERO2S	
◇	0	0	0	0	0	0	0	0	LEF2	Zero	
△	36	46	45	43	31	31	15	15	LEF2	1.45 to 0.95 AERO2S (gap filled)	

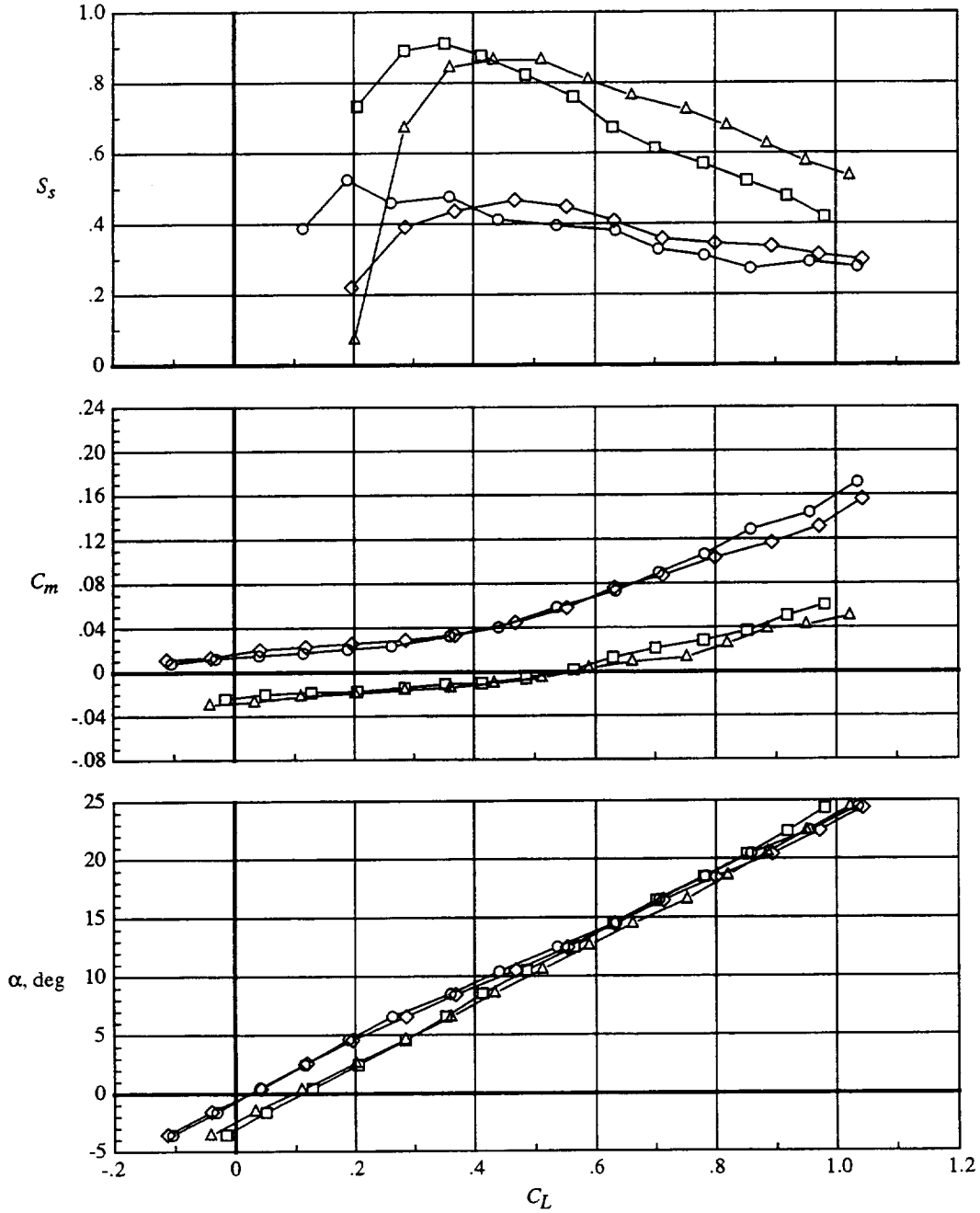


Figure 20. Original and modified leading-edge flap systems. WBN.

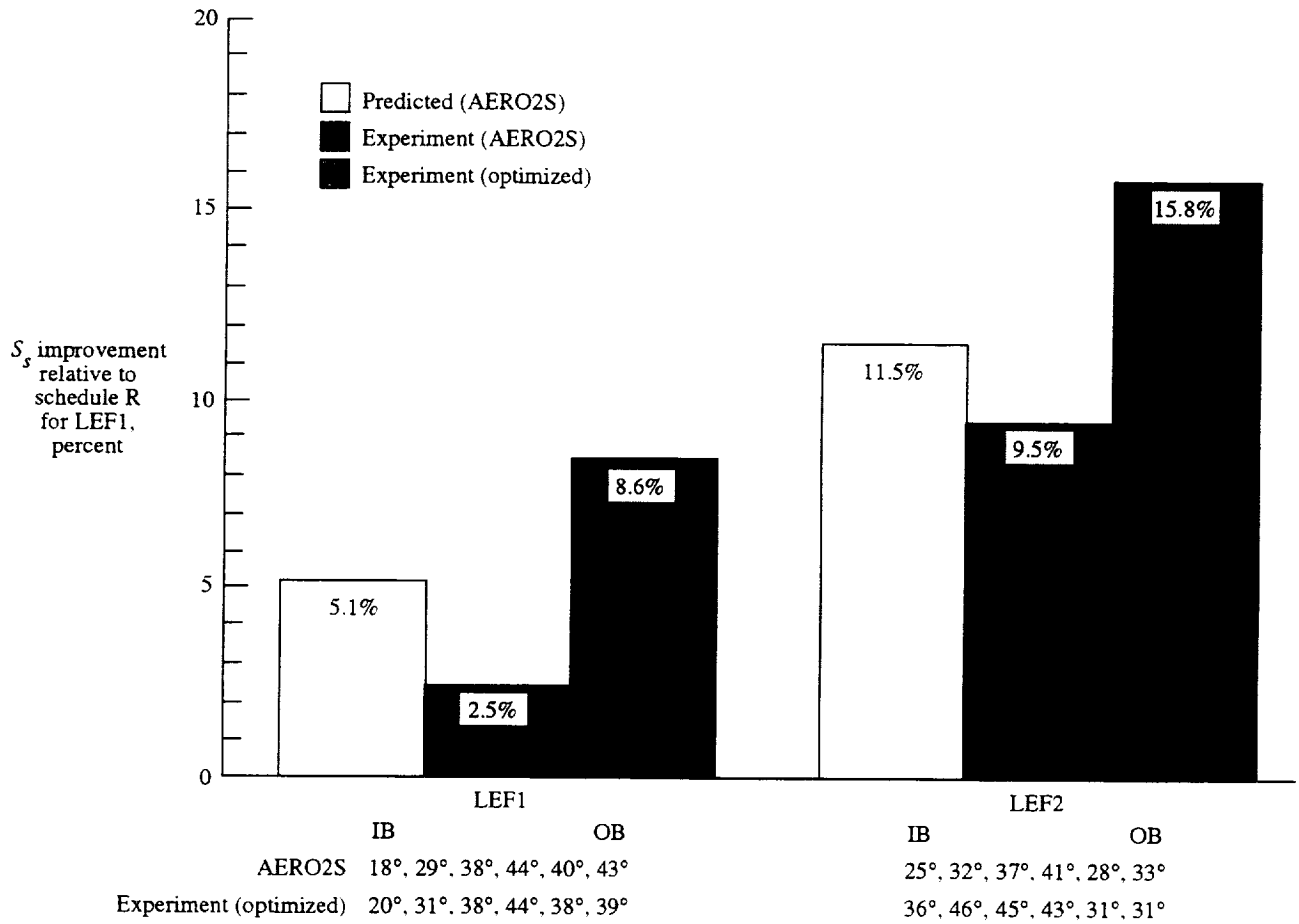
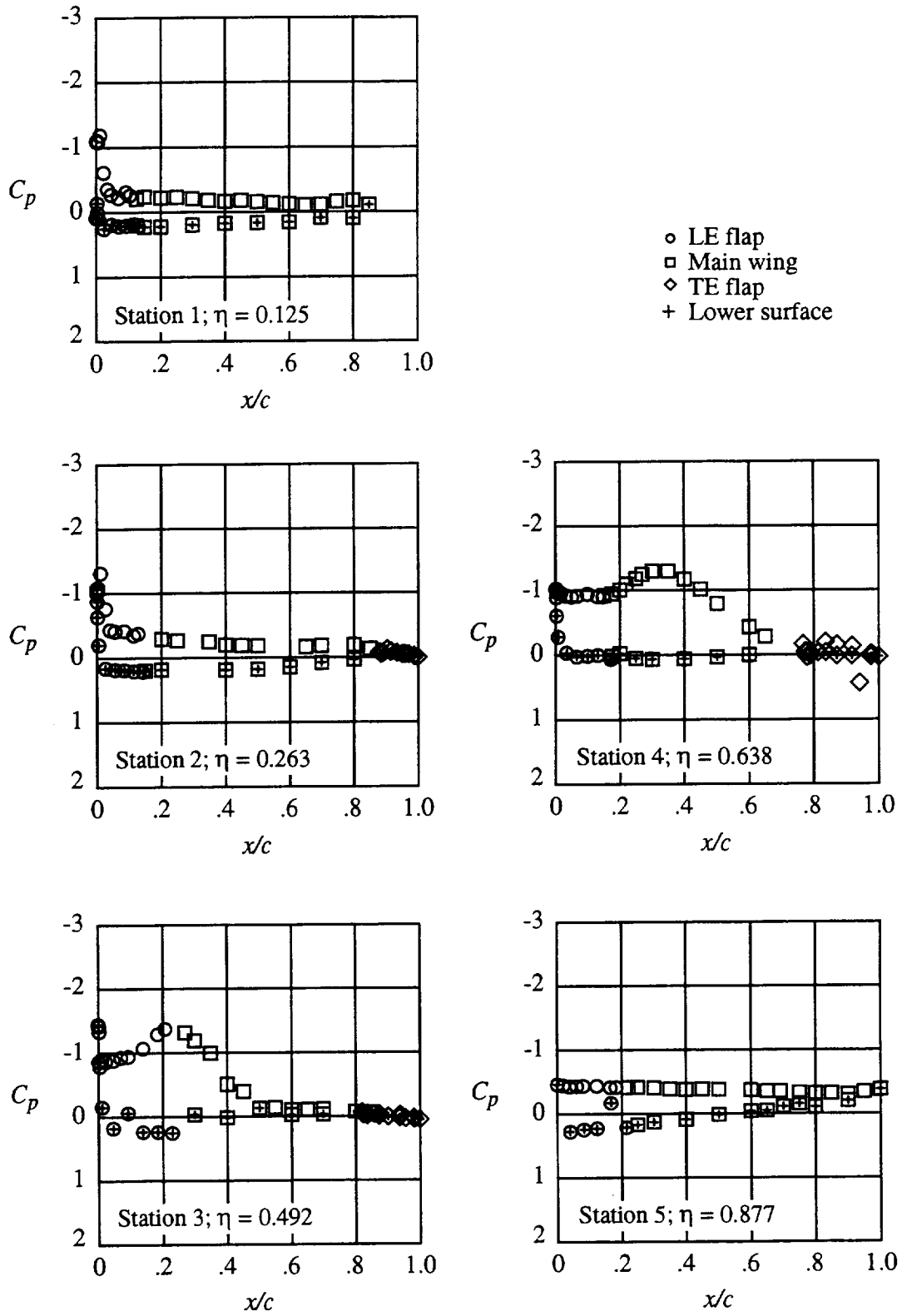
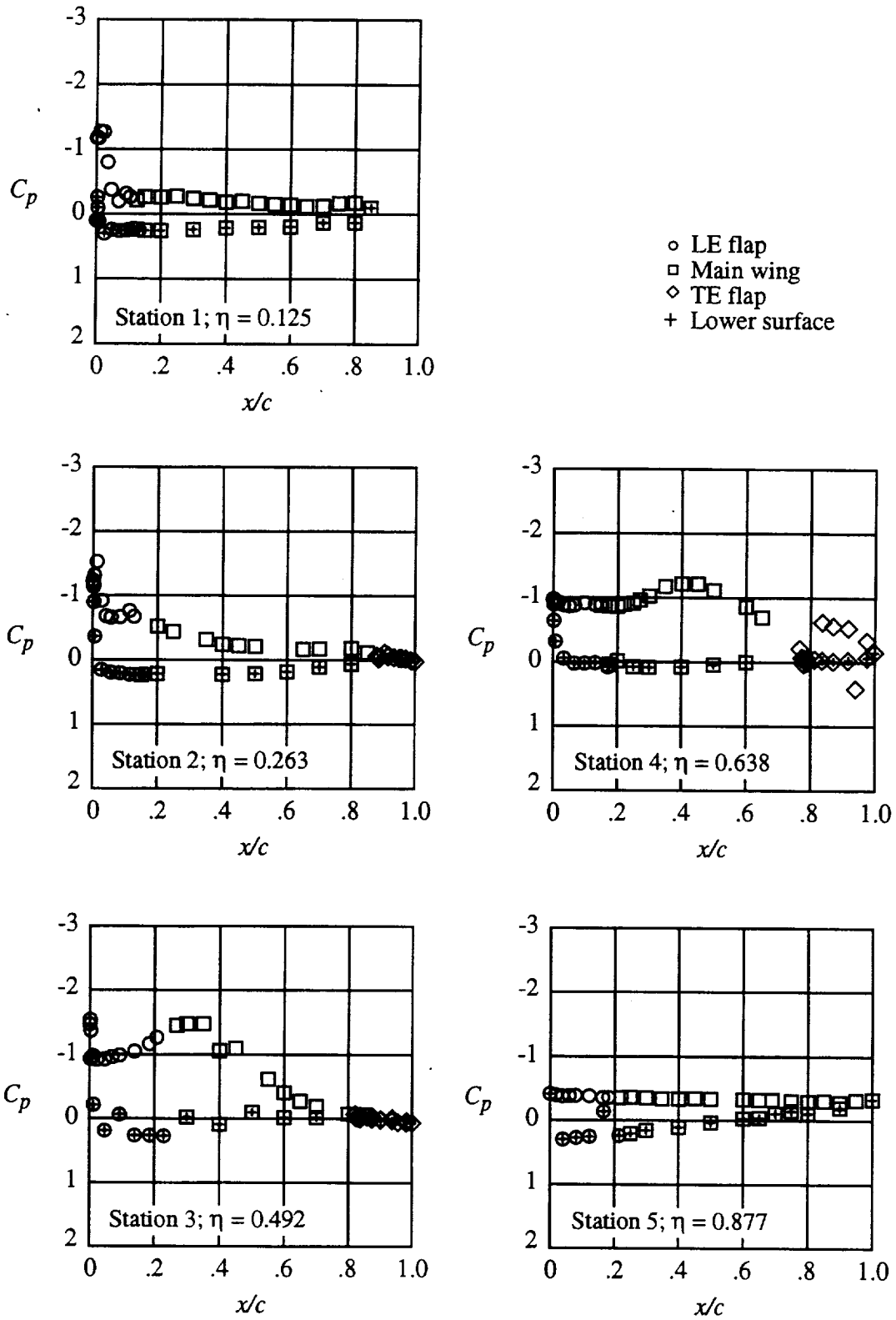


Figure 21. Untrimmed predicted and experimental leading-edge suction parameter results.  $C_L = 0.5$ .



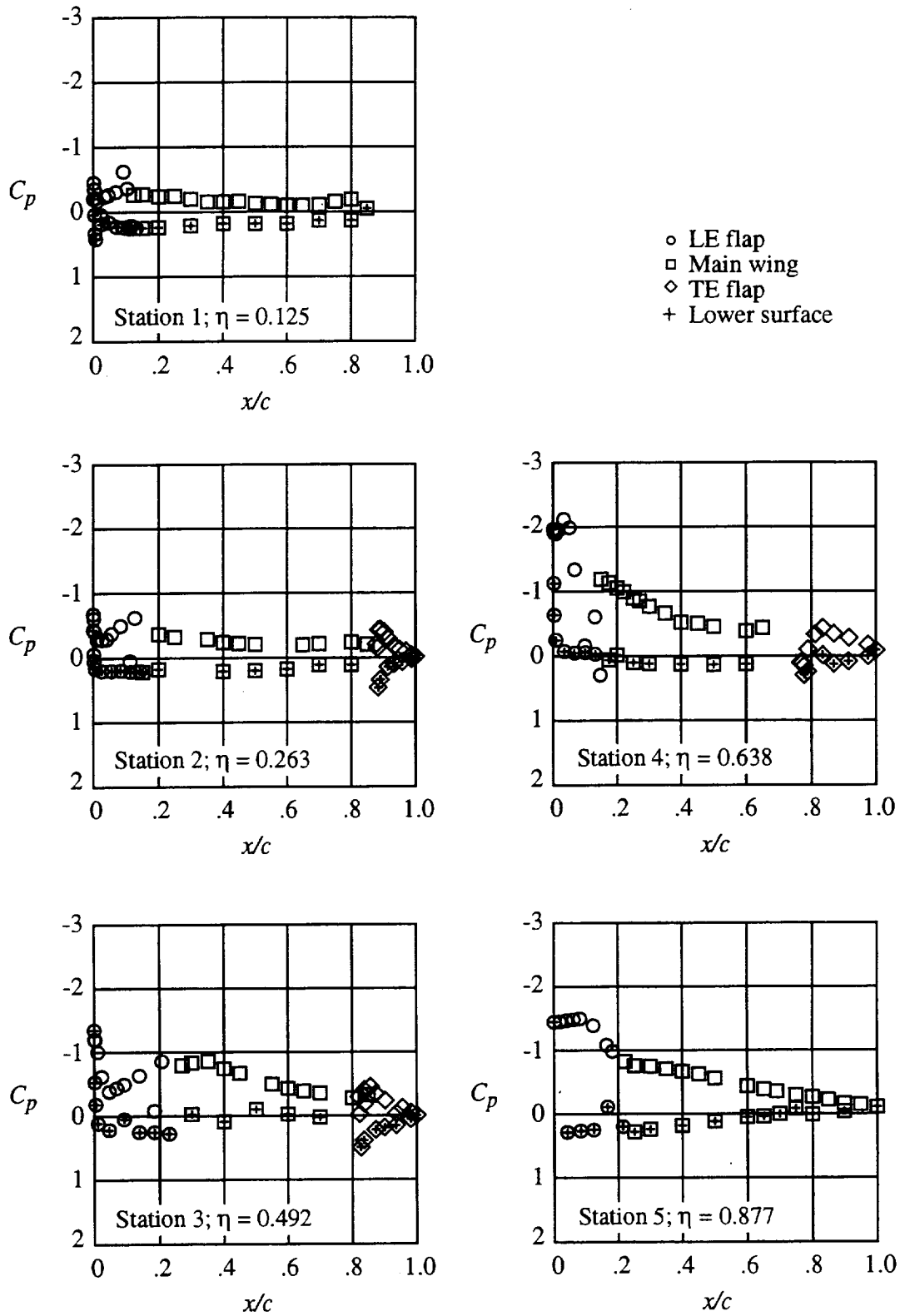
(a)  $C_L = 0.441$ ;  $\alpha = 10.4^\circ$ ;  $S_s = 0.413$ .

Figure 22. Pressure distribution for WBNLEF1 with  $\delta_{le} = \delta_{te} = 0^\circ$ .



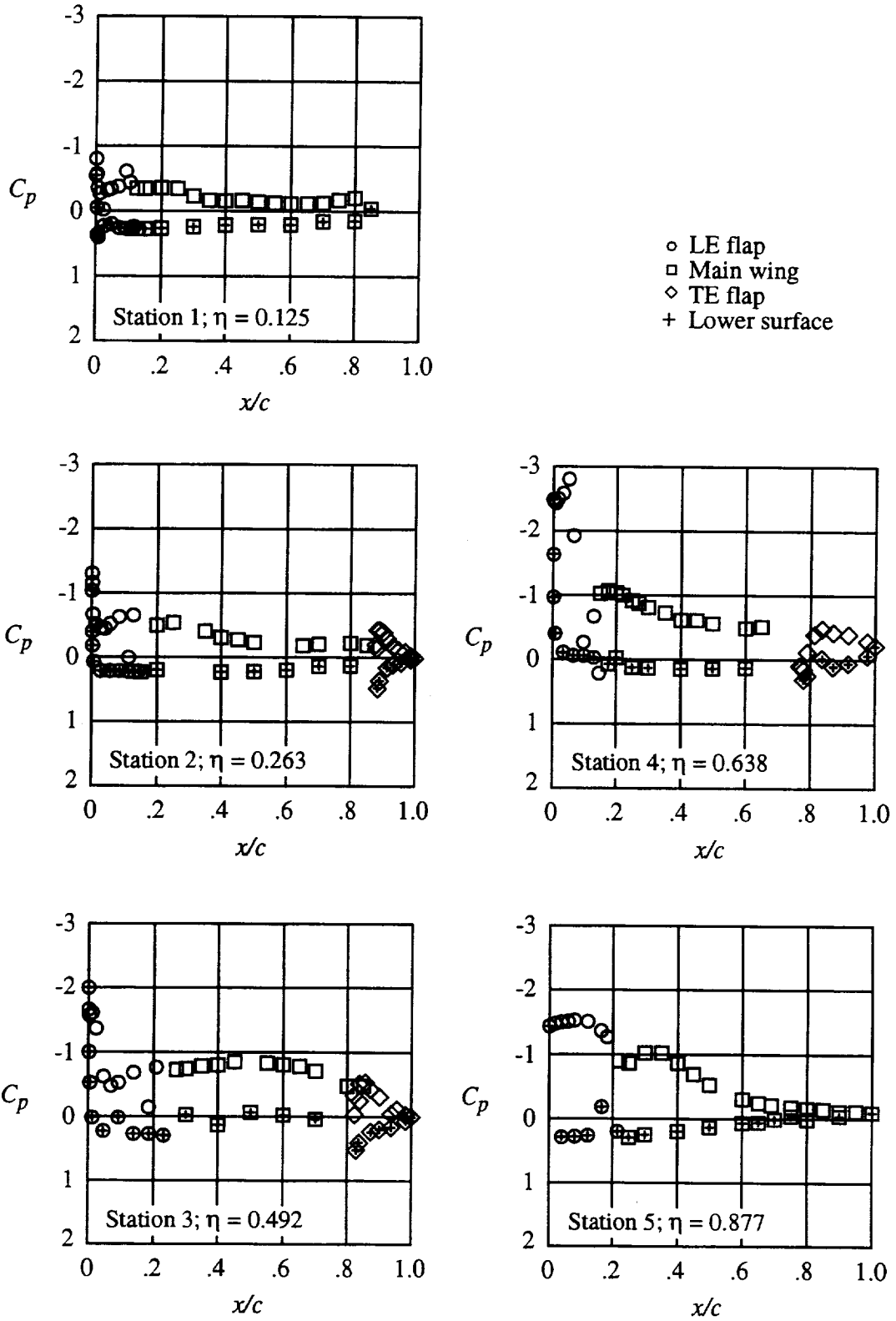
(b)  $C_L = 0.536$ ;  $\alpha = 12.5^\circ$ ;  $S_f = 0.396$ .

Figure 22. Concluded.



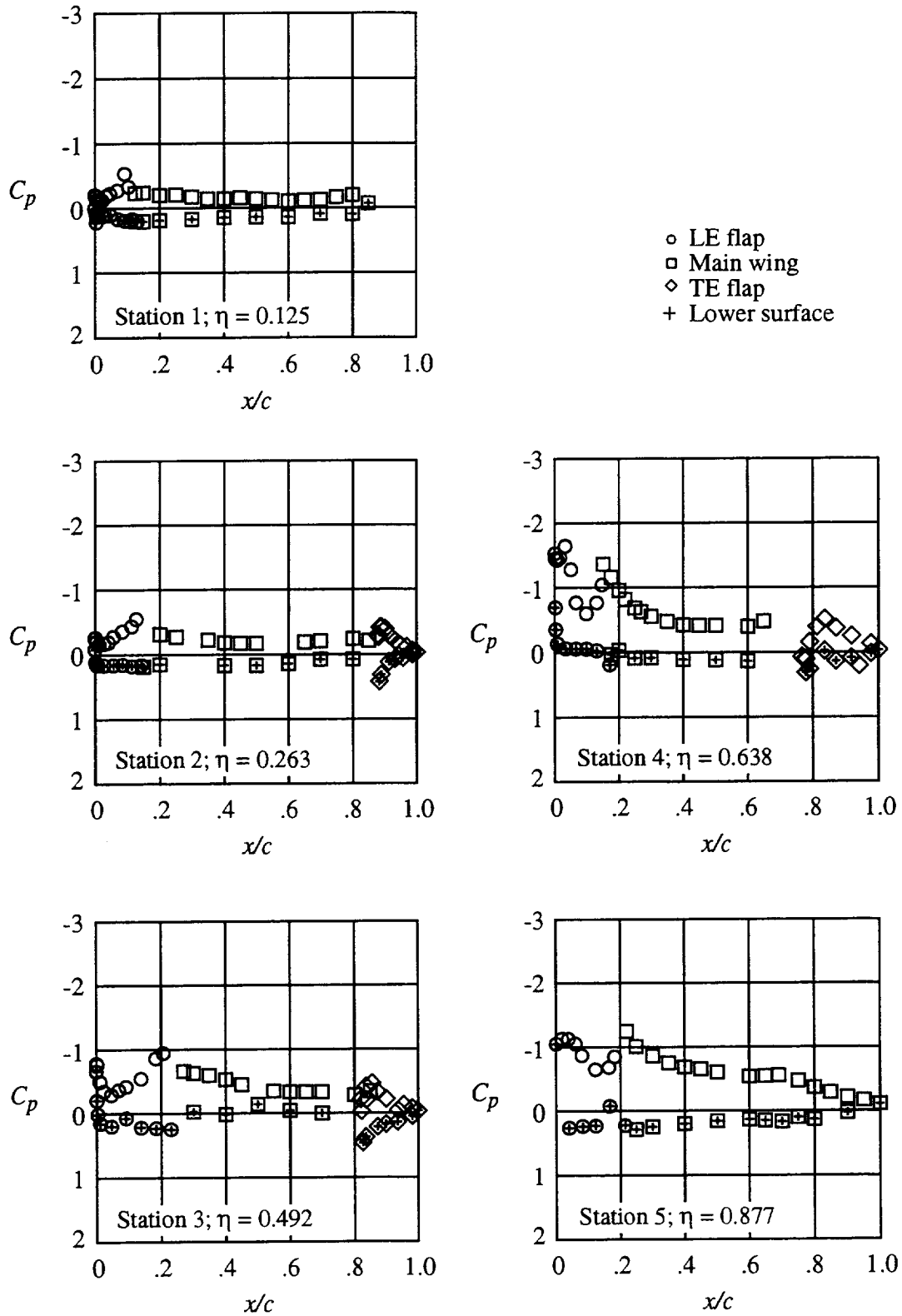
(a)  $C_L = 0.486$ ;  $\alpha = 10.5^\circ$ ;  $S_s = 0.824$ .

Figure 23. Pressure distribution for WBNLEF1 with  $\delta_{te} = 13^\circ$ . Leading-edge flaps deflected  $20^\circ$ ,  $31^\circ$ ,  $38^\circ$ ,  $44^\circ$ ,  $38^\circ$ , and  $39^\circ$  (1.10 to 0.90 AERO2S).



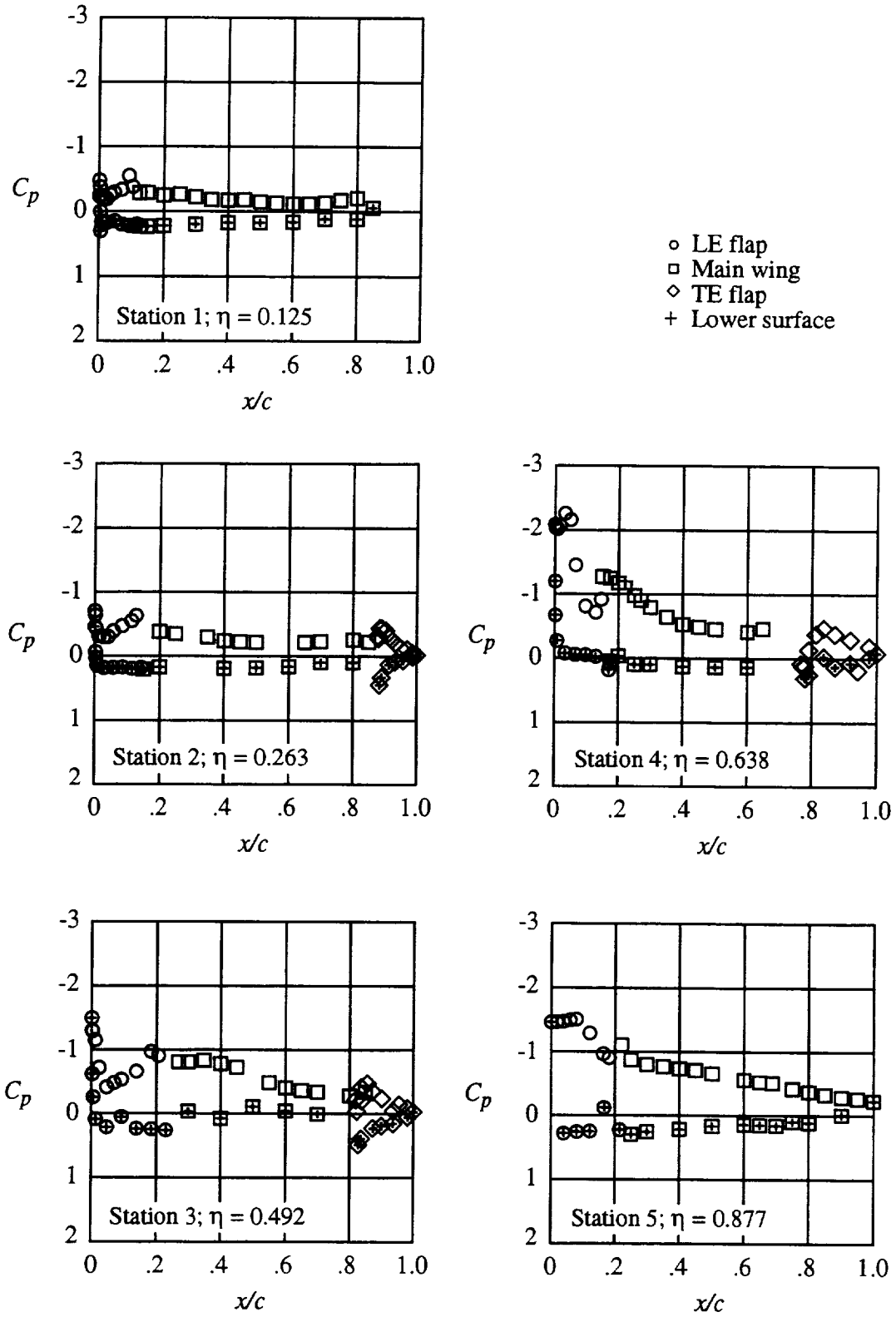
(b)  $C_L = 0.564$ ;  $\alpha = 12.5^\circ$ ;  $S_s = 0.760$ .

Figure 23. Concluded.



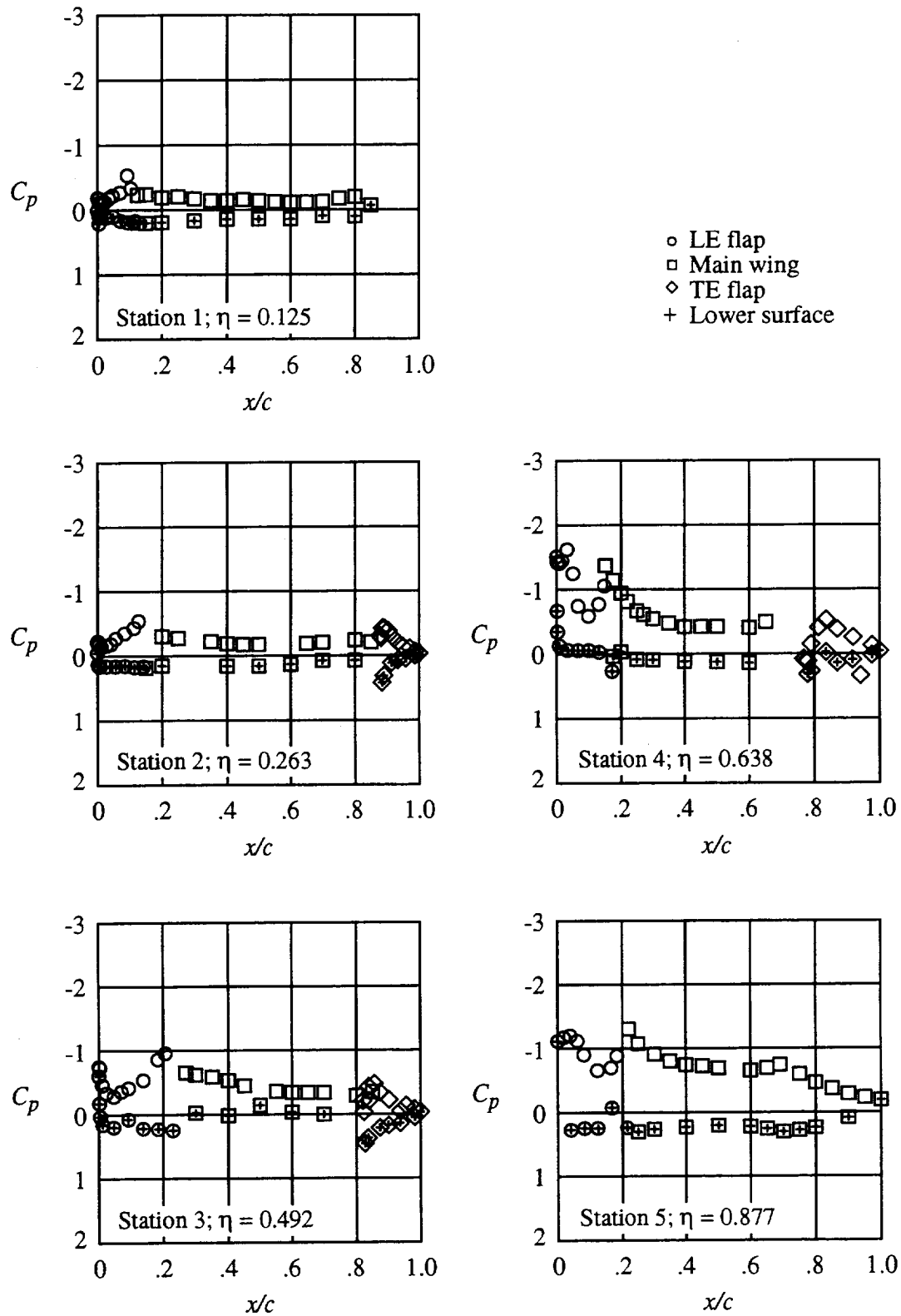
(a)  $C_L = 0.443$ ;  $\alpha = 8.6^\circ$ ;  $S_s = 0.877$ .

Figure 24. Pressure distribution for WBNLEF1 with  $\delta_{le} = 13^\circ$  and  $\delta_{a,s} = 10^\circ$ . Leading-edge flaps deflected  $20^\circ$ ,  $31^\circ$ ,  $38^\circ$ ,  $44^\circ$ ,  $38^\circ$ , and  $39^\circ$  (1.10 to 0.90 AERO2S).



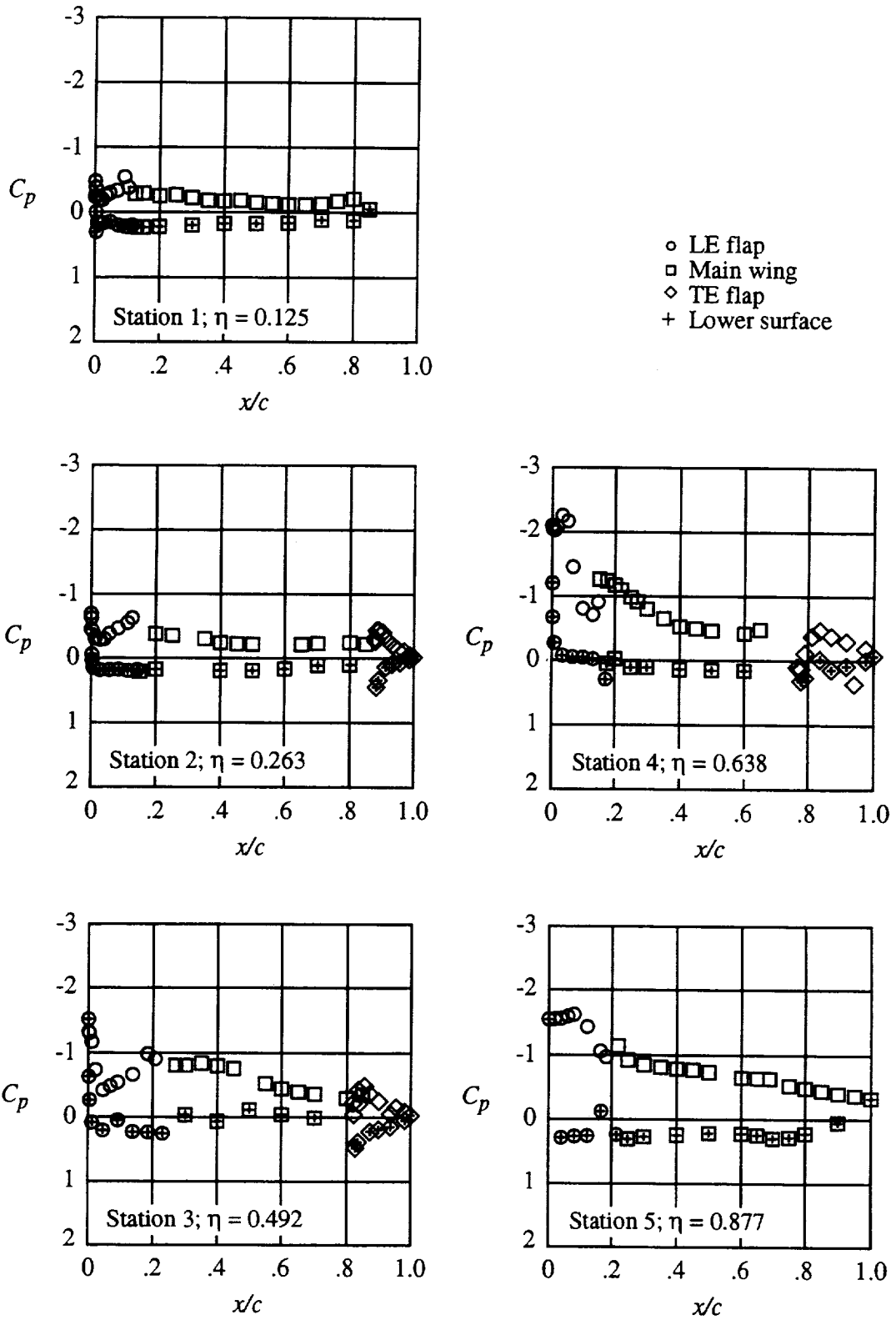
(b)  $C_L = 0.510$ ;  $\alpha = 10.6^\circ$ ;  $S_s = 0.832$ .

Figure 24. Concluded.



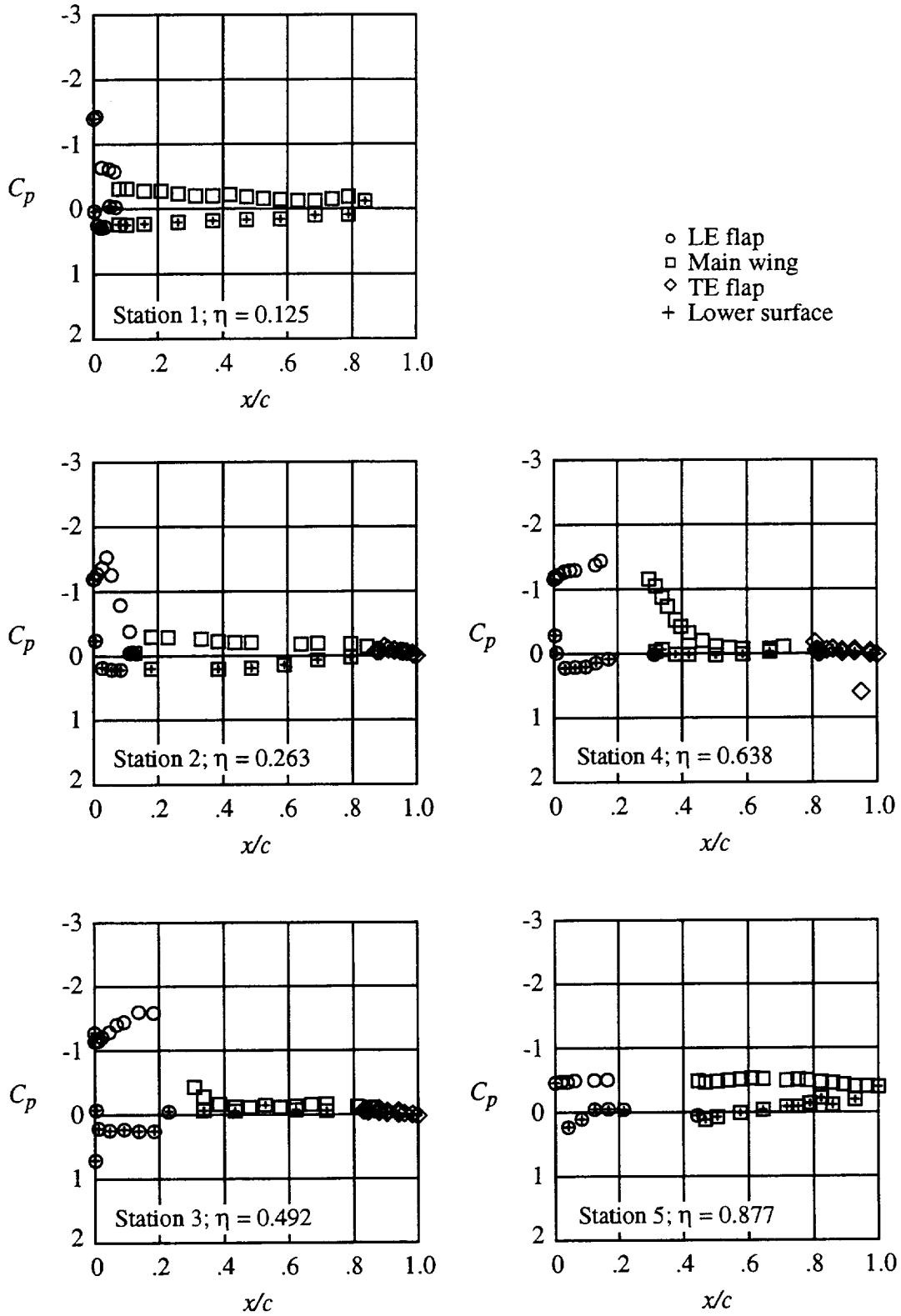
(a)  $C_L = 0.454$ ;  $\alpha = 8.5^\circ$ ;  $S_s = 0.857$ .

Figure 25. Pressure distribution for WBNLEF1 with  $\delta_{te} = 13^\circ$  and  $\delta_{a,s} = 20^\circ$ . Leading-edge flaps deflected  $20^\circ$ ,  $31^\circ$ ,  $38^\circ$ ,  $44^\circ$ ,  $38^\circ$ , and  $39^\circ$  (1.10 to 0.90 AERO2S).



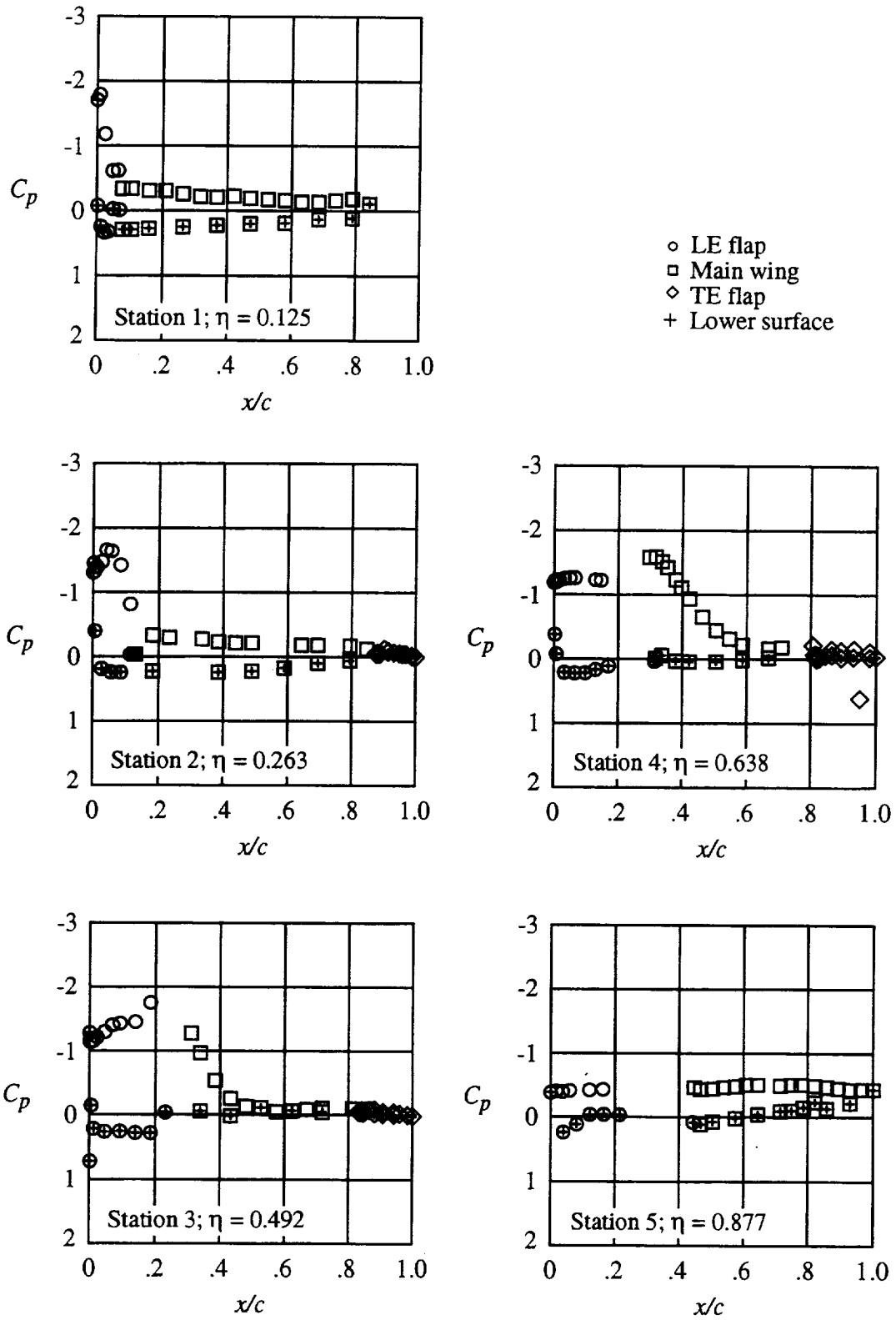
(b)  $C_L = 0.520$ ;  $\alpha = 10.5^\circ$ ;  $S_s = 0.823$ .

Figure 25. Concluded.



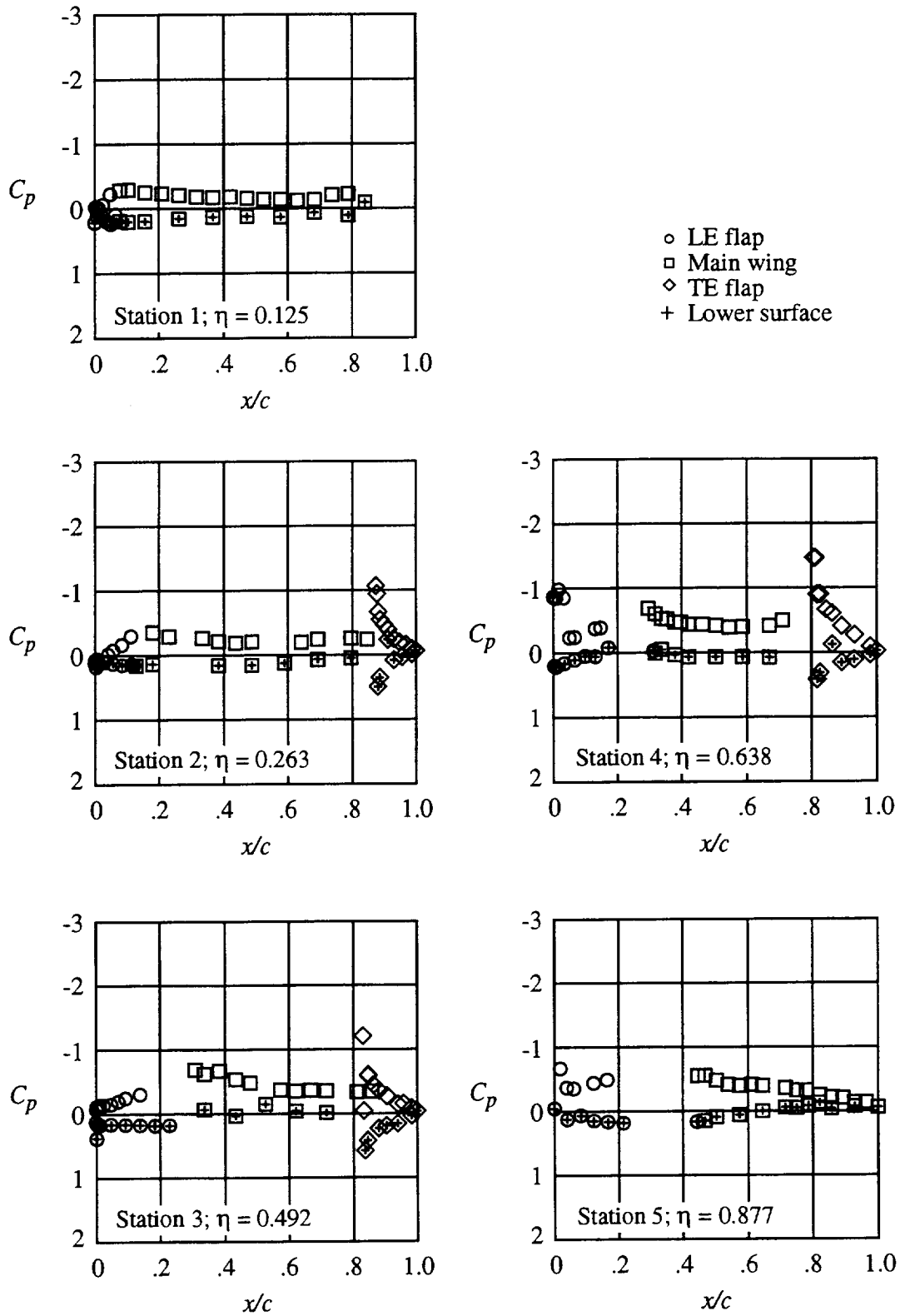
(a)  $C_L = 0.468$ ;  $\alpha = 10.5^\circ$ ;  $S_f = 0.468$ .

Figure 26. Pressure distribution for WBNLEF2 with  $\delta_{le} = \delta_{te} = 0^\circ$ .



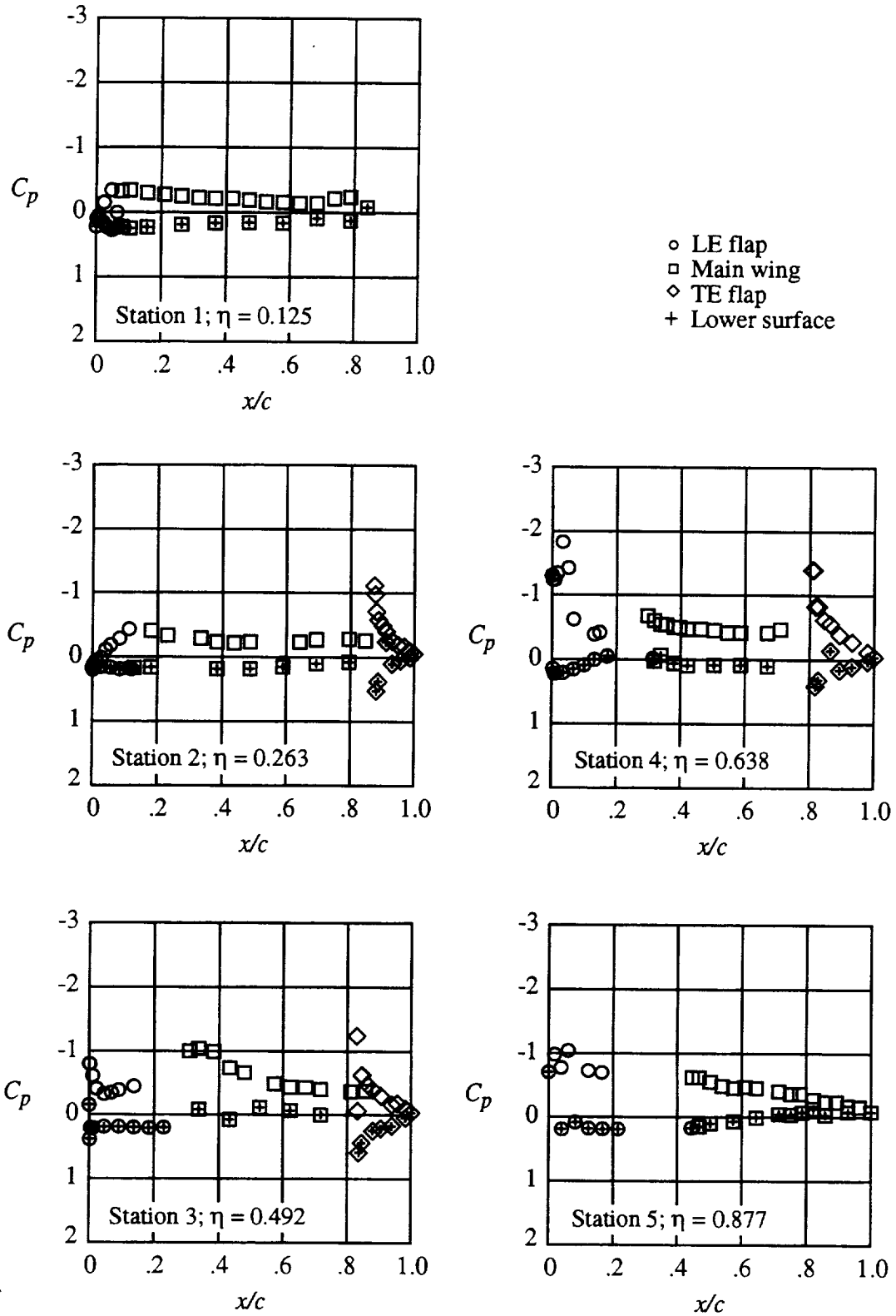
(b)  $C_L = 0.553$ ;  $\alpha = 12.5^\circ$ ;  $S_f = 0.449$ .

Figure 26. Concluded.



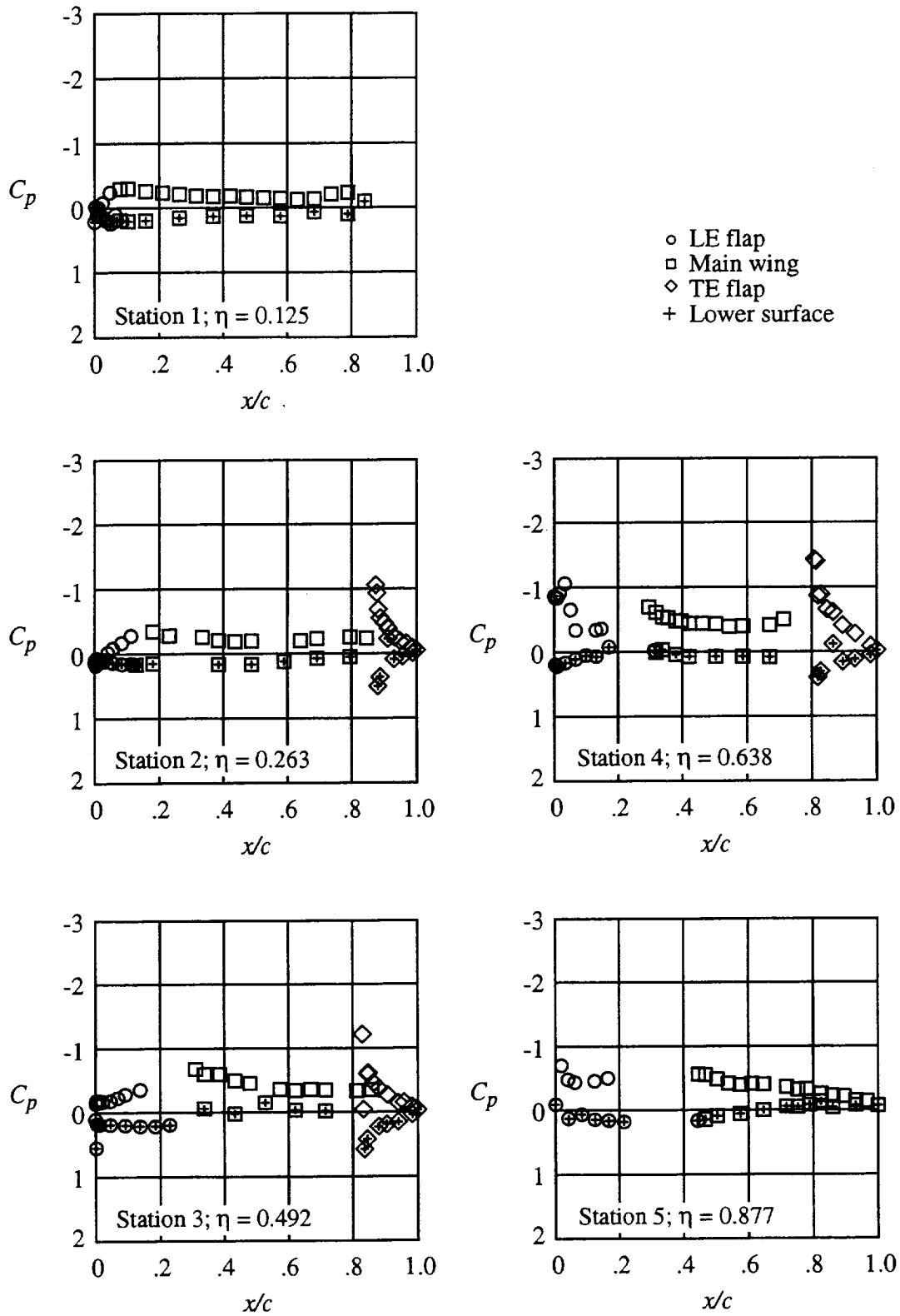
(a)  $C_L = 0.435$ ;  $\alpha = 8.5^\circ$ ;  $S_f = 0.843$ .

Figure 27. Pressure distribution for WB NLEF2 with leading-edge flaps deflected  $36^\circ$ ,  $46^\circ$ ,  $45^\circ$ ,  $43^\circ$ ,  $31^\circ$ , and  $31^\circ$  (1.45 to 0.95 AERO2S) and  $\delta_{te} = 15^\circ$ .



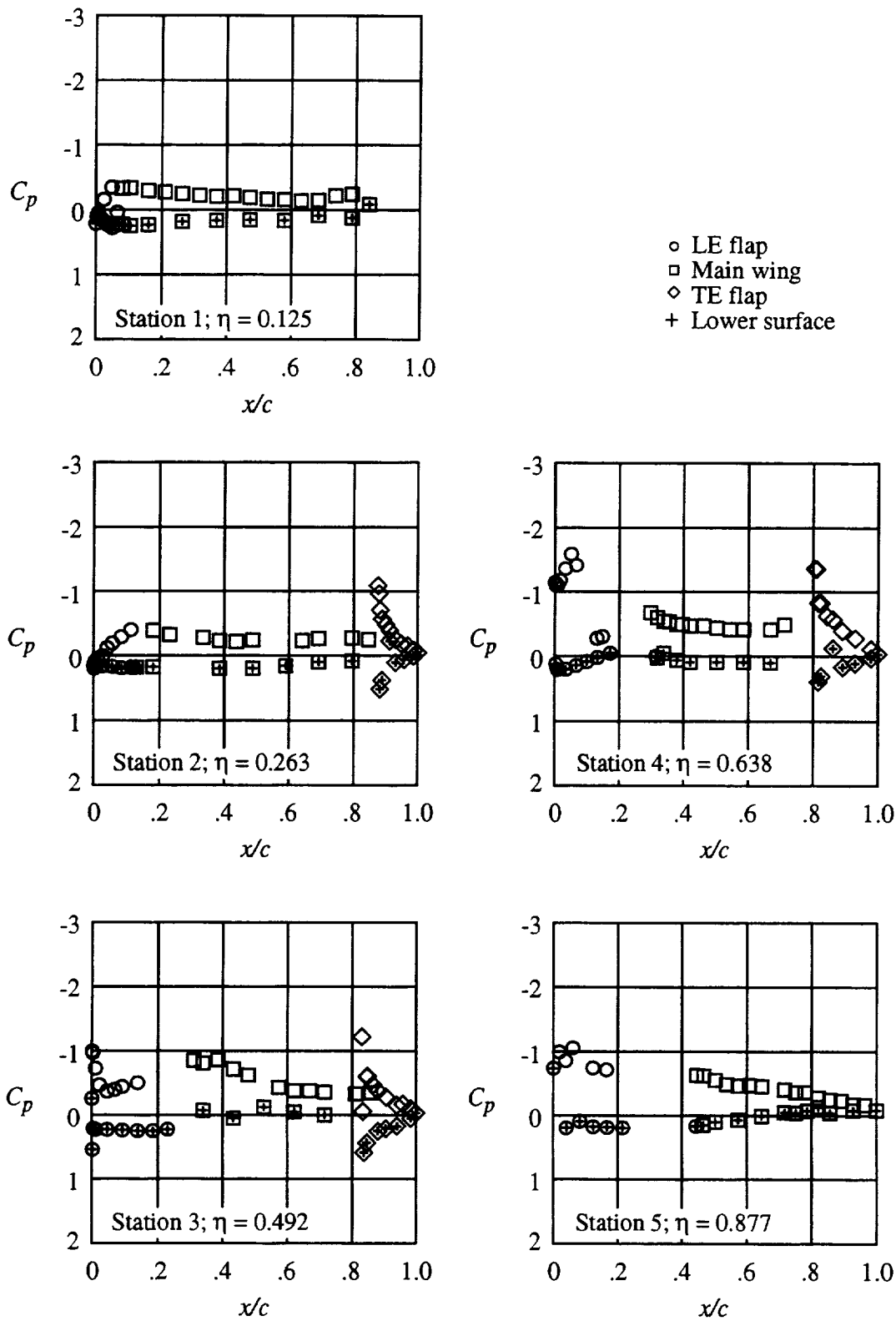
(b)  $C_L = 0.512$ ;  $\alpha = 10.6^\circ$ ;  $S_s = 0.829$ .

Figure 27. Concluded.



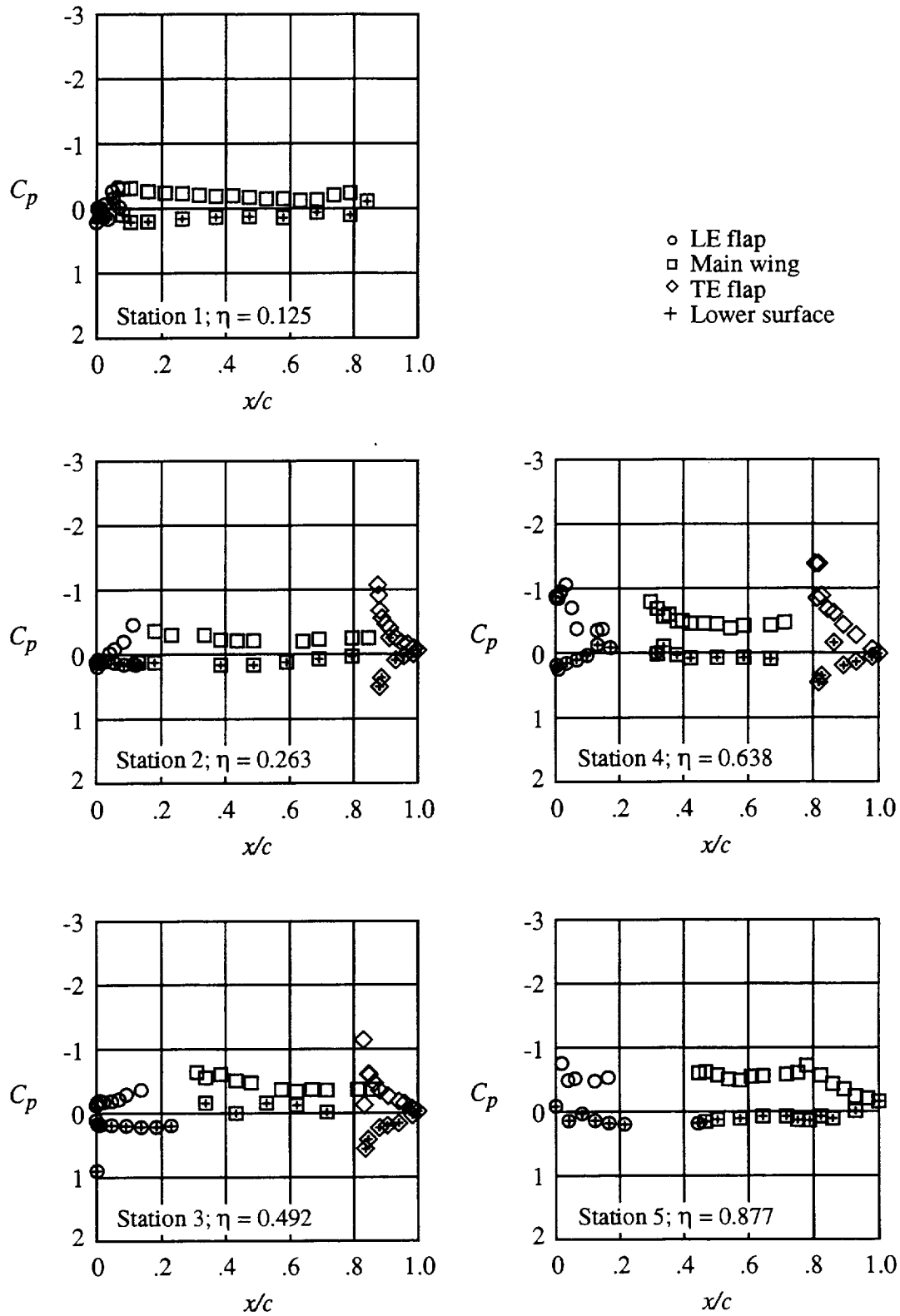
(a)  $C_L = 0.439$ ;  $\alpha = 8.5^\circ$ ;  $S_s = 0.862$ .

Figure 28. Pressure distribution for WBNLEF2 with leading-edge flaps deflected  $36^\circ$ ,  $46^\circ$ ,  $45^\circ$ ,  $43^\circ$ ,  $31^\circ$ , and  $31^\circ$  (1.45 to 0.95 AERO2S), gap between leading-edge flap segments 4 and 5 filled, and  $\delta_{te} = 15^\circ$ .



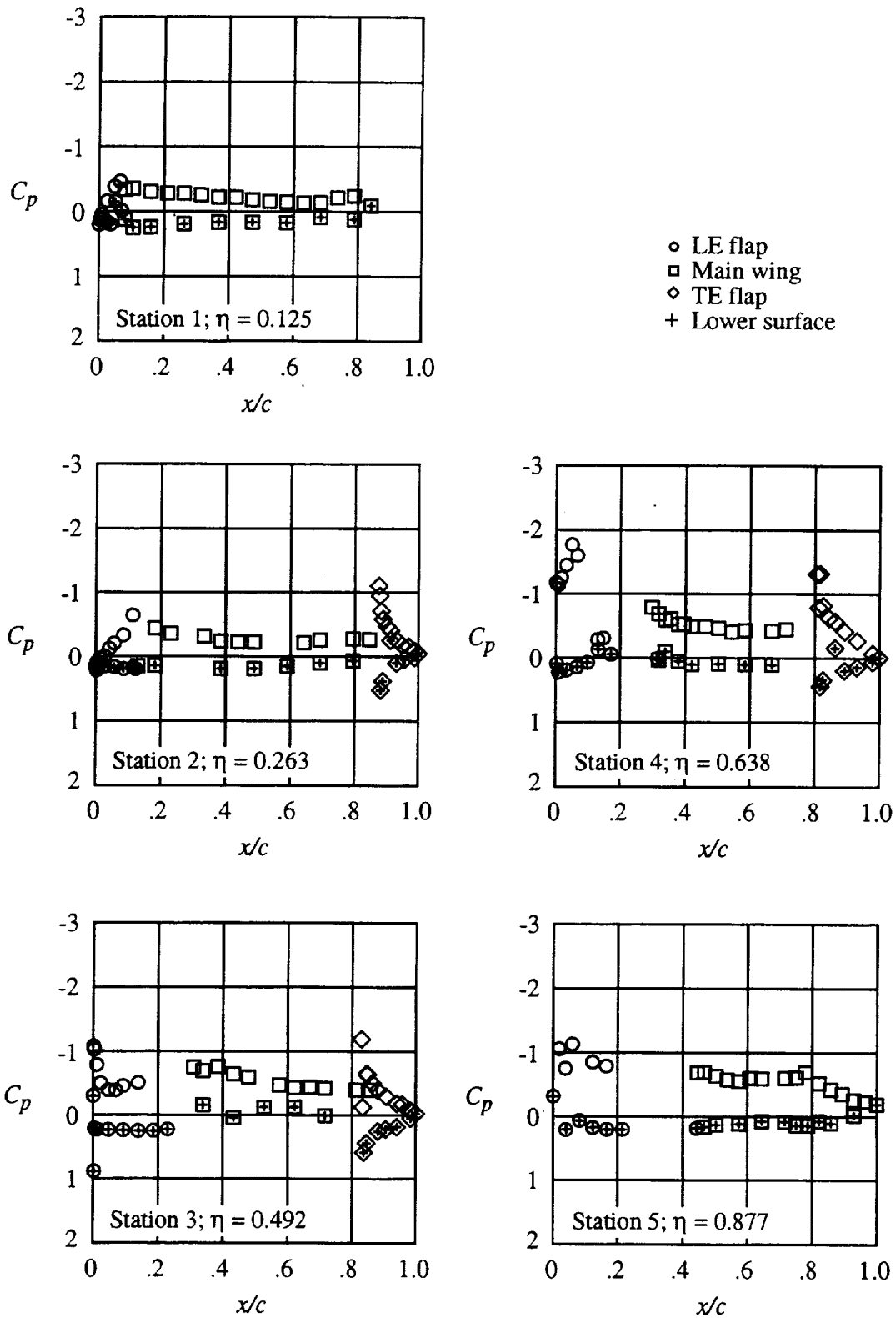
(b)  $C_L = 0.515$ ;  $\alpha = 10.5^\circ$ ;  $S_f = 0.867$ .

Figure 28. Concluded.



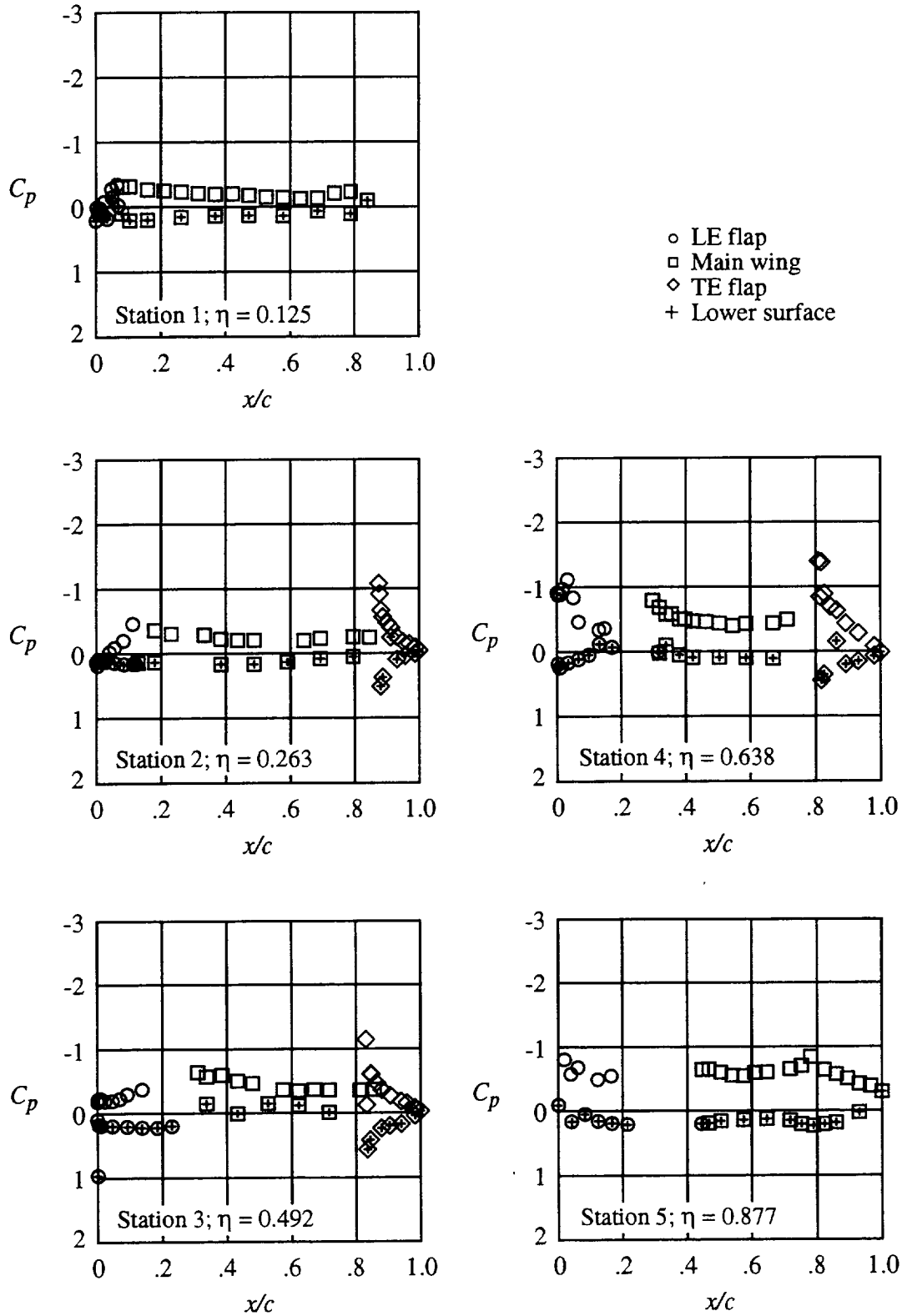
(a)  $C_L = 0.457$ ;  $\alpha = 8.4^\circ$ ;  $S_s = 0.875$ .

Figure 29. Pressure distribution for WBNLEF2 with leading-edge flaps deflected  $36^\circ$ ,  $46^\circ$ ,  $45^\circ$ ,  $43^\circ$ ,  $31^\circ$ , and  $31^\circ$  (1.45 to 0.95 AERO2S), gap between leading-edge flap segments 4 and 5 filled,  $\delta_{te} = 15^\circ$ , and  $\delta_{a,s} = 10^\circ$ .



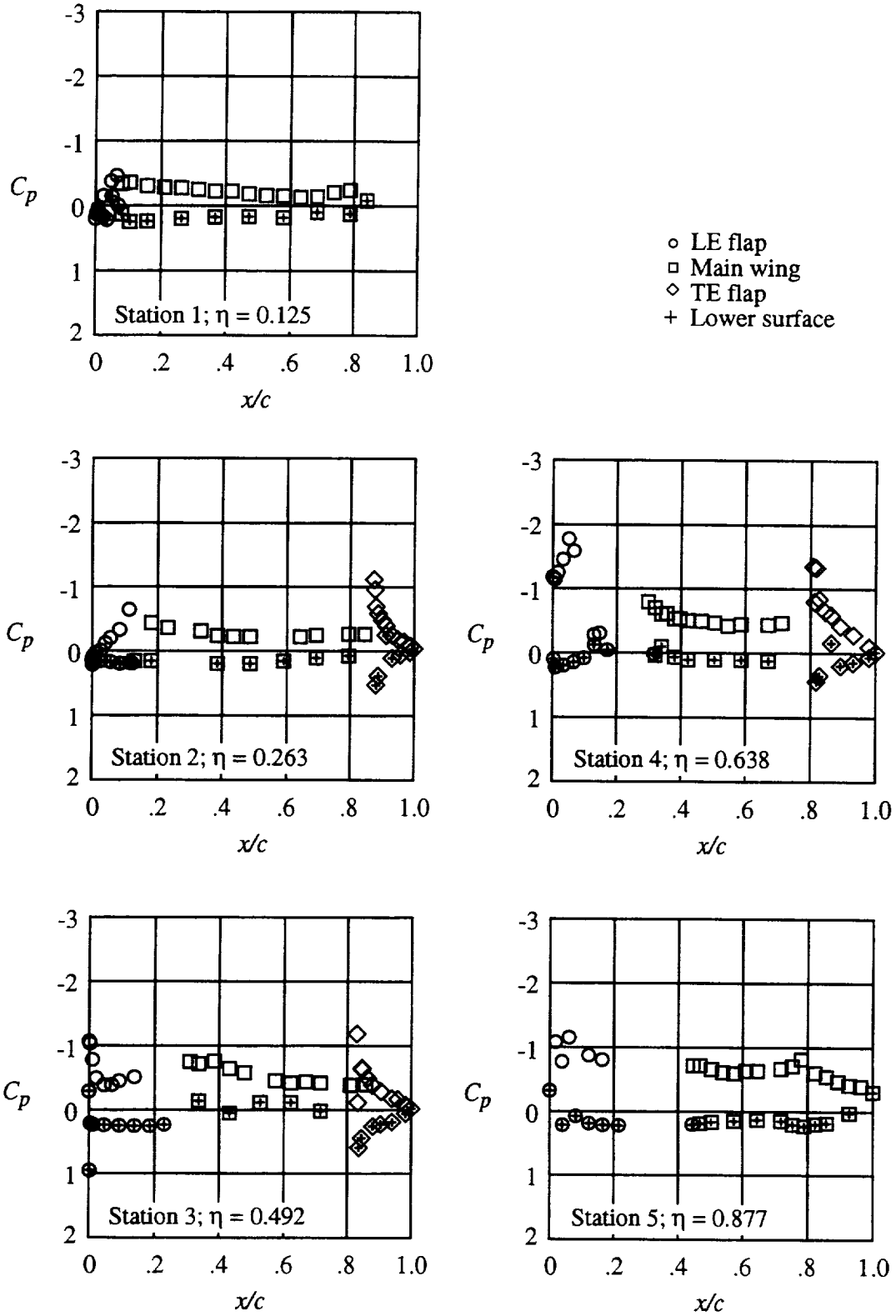
(b)  $C_L = 0.532$ ;  $\alpha = 10.5^\circ$ ;  $S_f = 0.866$ .

Figure 29. Concluded.



(a)  $C_L = 0.482$ ;  $\alpha = 8.5^\circ$ ;  $S_s = 0.877$ .

Figure 30. Pressure distribution for WB NLEF2 with leading-edge flaps deflected  $36^\circ$ ,  $46^\circ$ ,  $45^\circ$ ,  $43^\circ$ ,  $31^\circ$ , and  $31^\circ$  (1.45 to 0.95 AERO2S), gap between leading-edge flap segments 4 and 5 filled,  $\delta_{le} = 15^\circ$ , and  $\delta_{as} = 20^\circ$ .



(b)  $C_L = 0.548$ ;  $\alpha = 10.5^\circ$ ;  $S_s = 0.855$ .

Figure 30. Concluded.

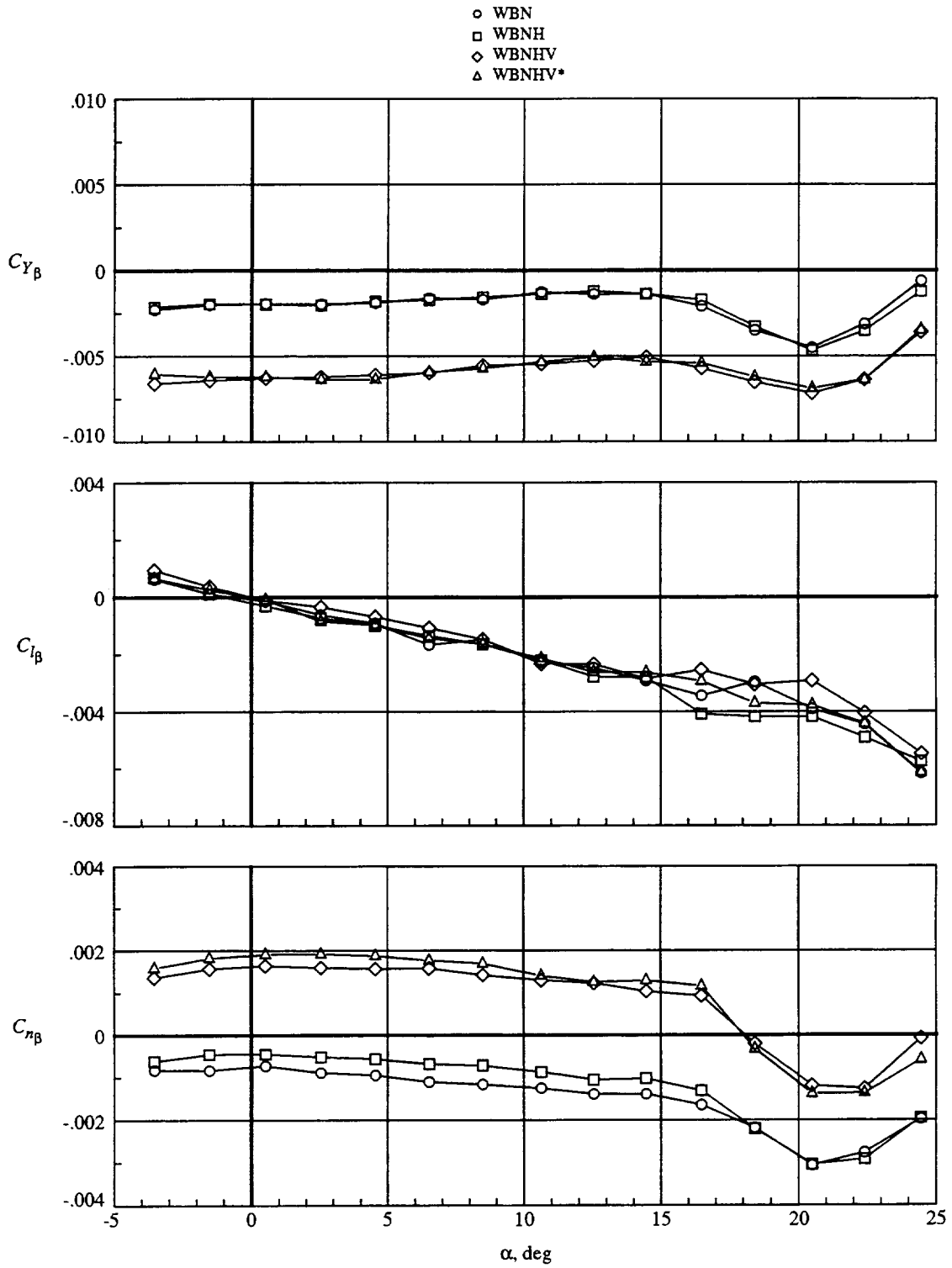


Figure 31. Effect of component buildup on lateral-directional characteristics for LEF1.  $\delta_{le} = \delta_{te} = 0^\circ$ .

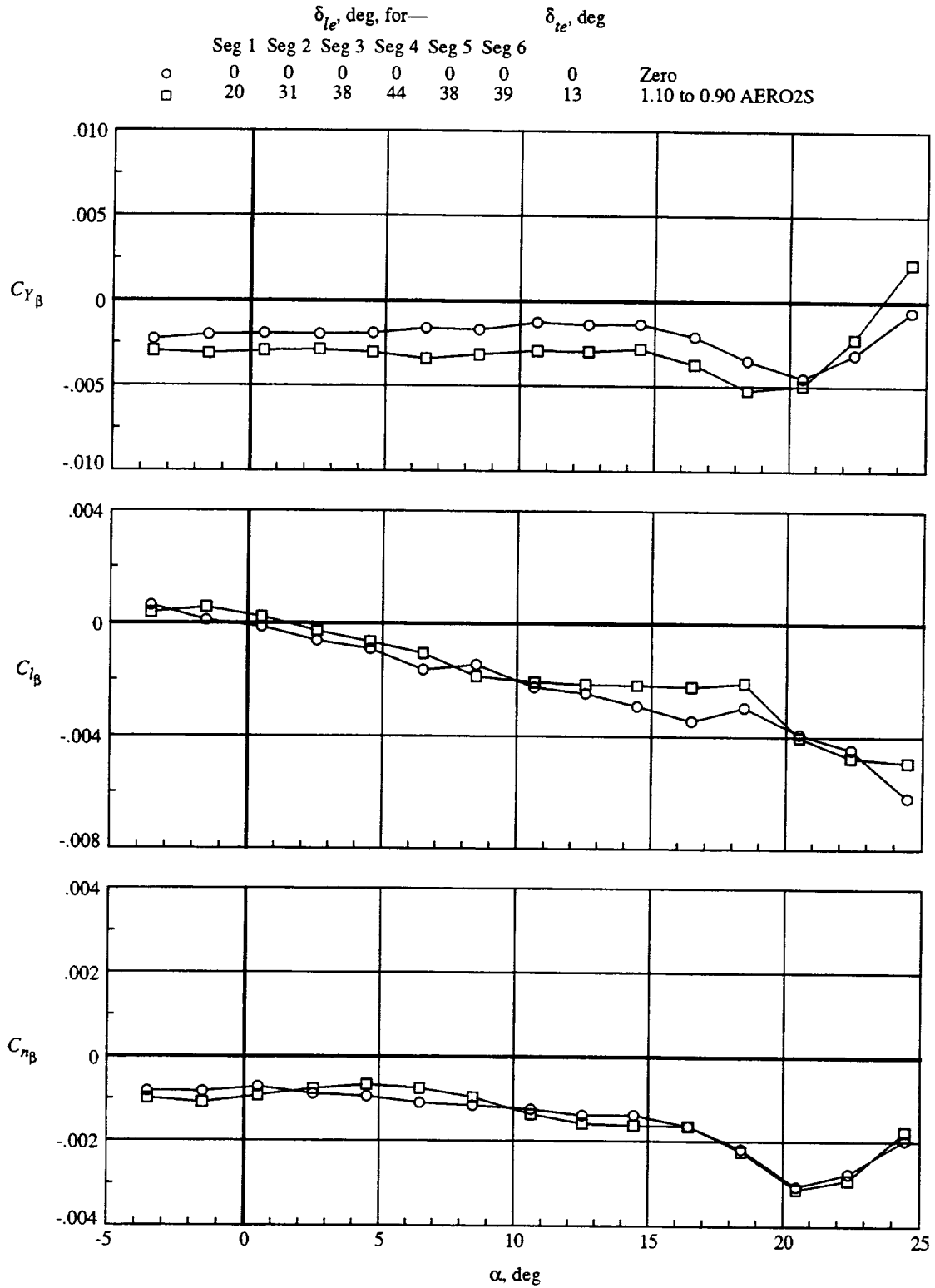
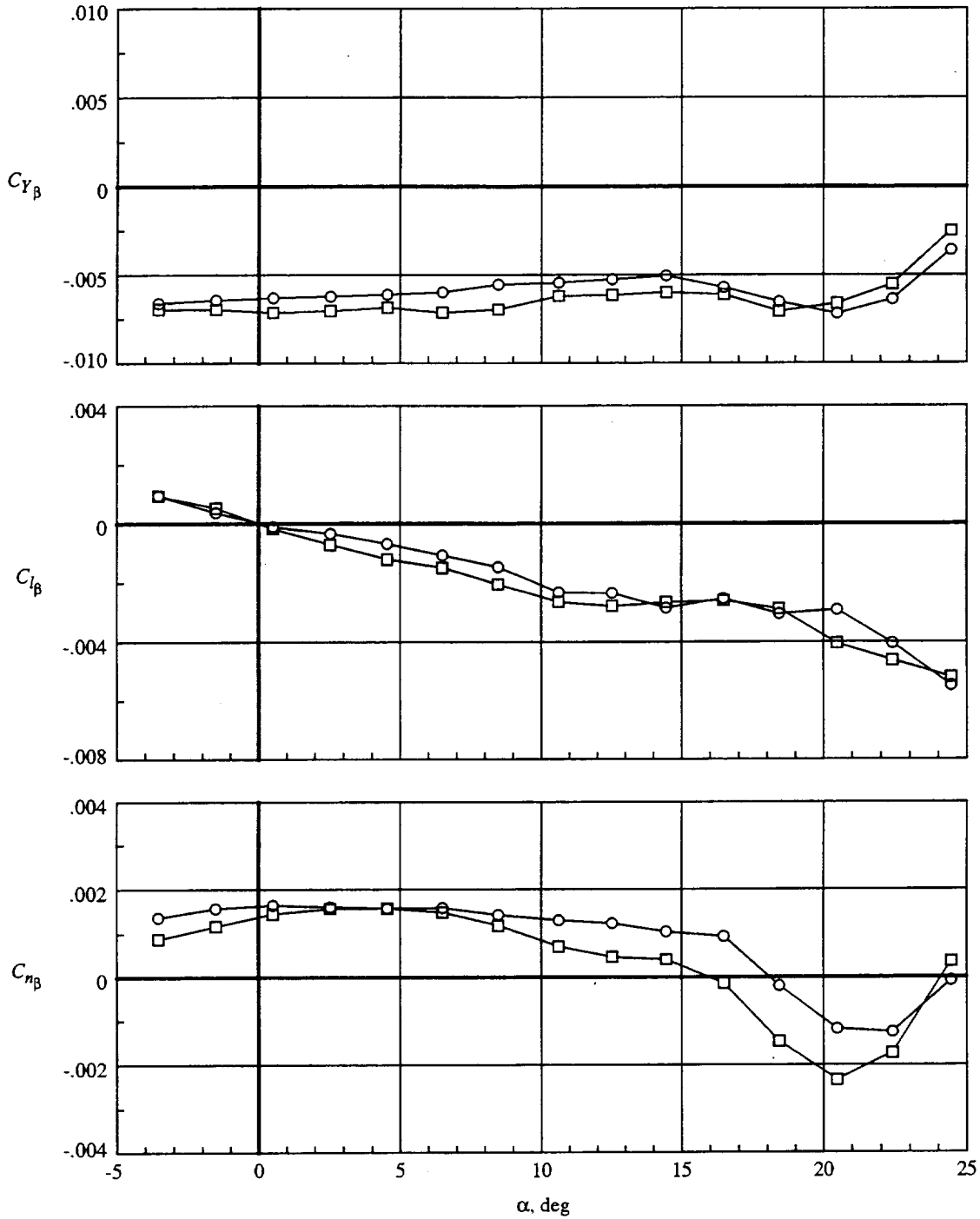


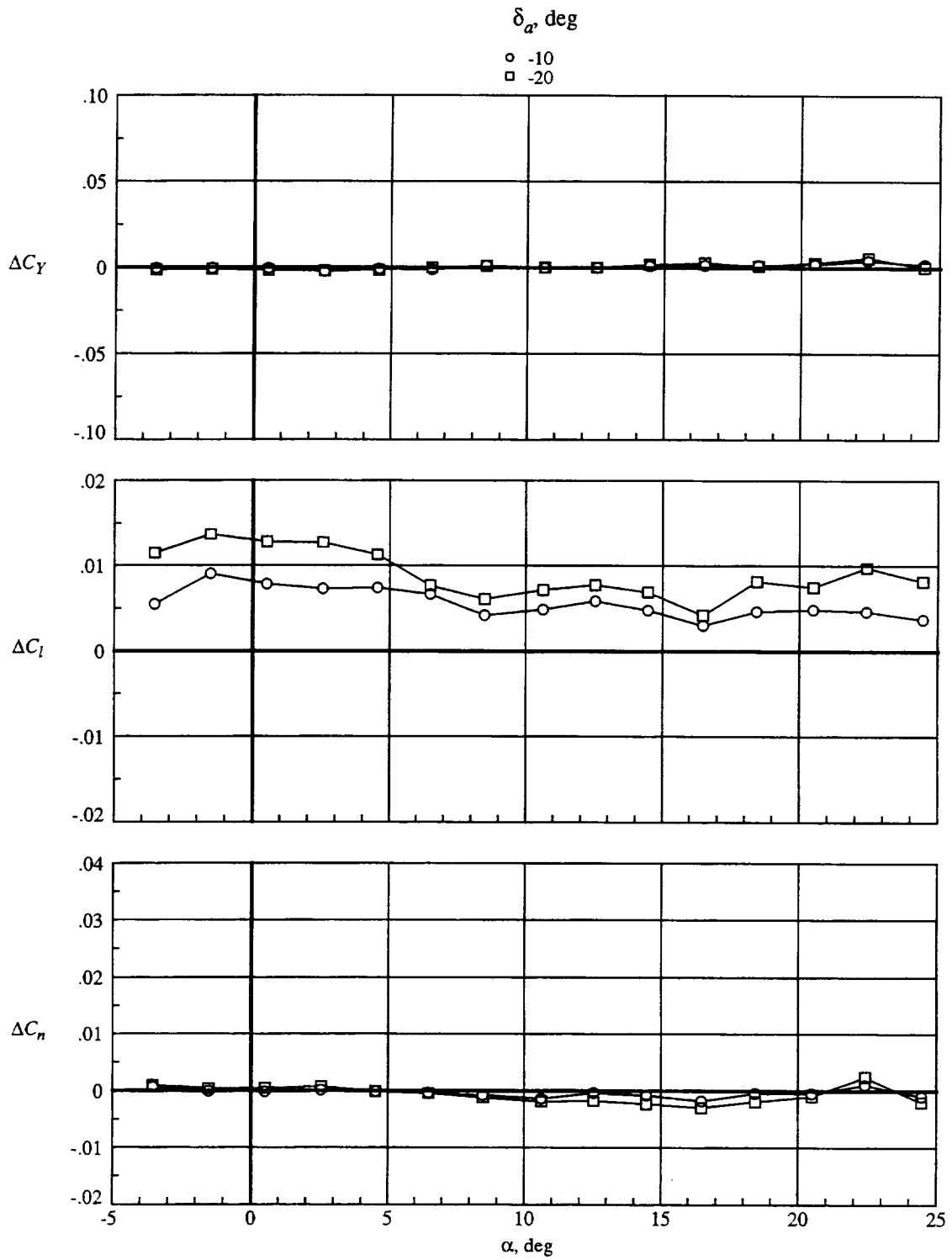
Figure 32. Effect of leading- and trailing-edge flap deflection on lateral-directional characteristics. All control surfaces zero.

	$\delta_{te}$ , deg, for—						$\delta_{te}$ , deg	
	Seg 1	Seg 2	Seg 3	Seg 4	Seg 5	Seg 6	0	Zero
○	0	0	0	0	0	0	0	1.10 to 0.90 AERO2S
□	20	31	38	44	38	39	13	



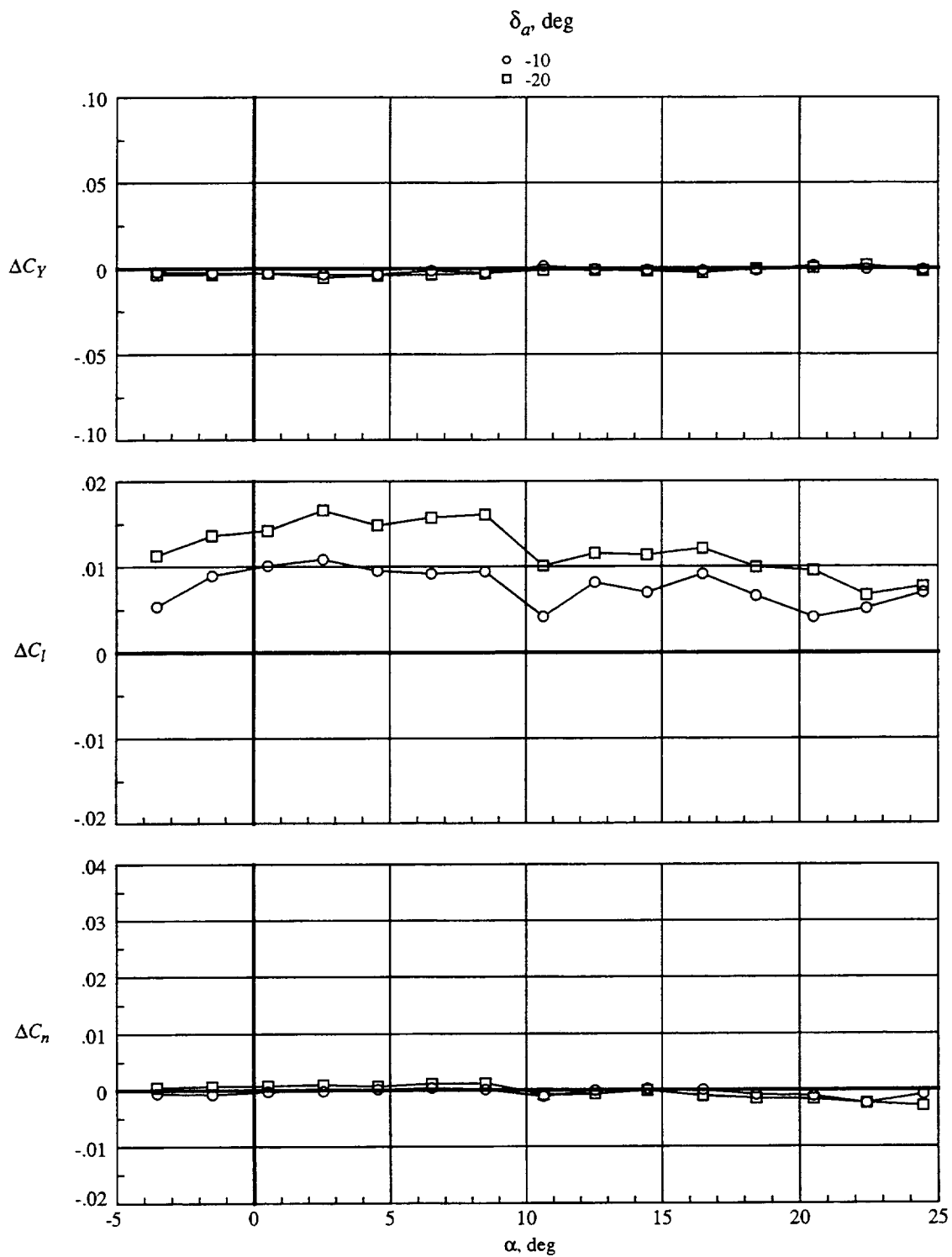
(b) WBNHVLEF1.

Figure 32. Concluded.



(a) Leading- and trailing-edge flaps undeflected.

Figure 33. Effect of differential aileron deflection on lateral-directional characteristics for WBNLEF1.



(b) Leading-edge flaps deflected 20°, 31°, 38°, 44°, 38°, and 39° (1.10 to 0.90 AERO2S);  $\delta_{te} = 13^\circ$ .

Figure 33. Concluded.

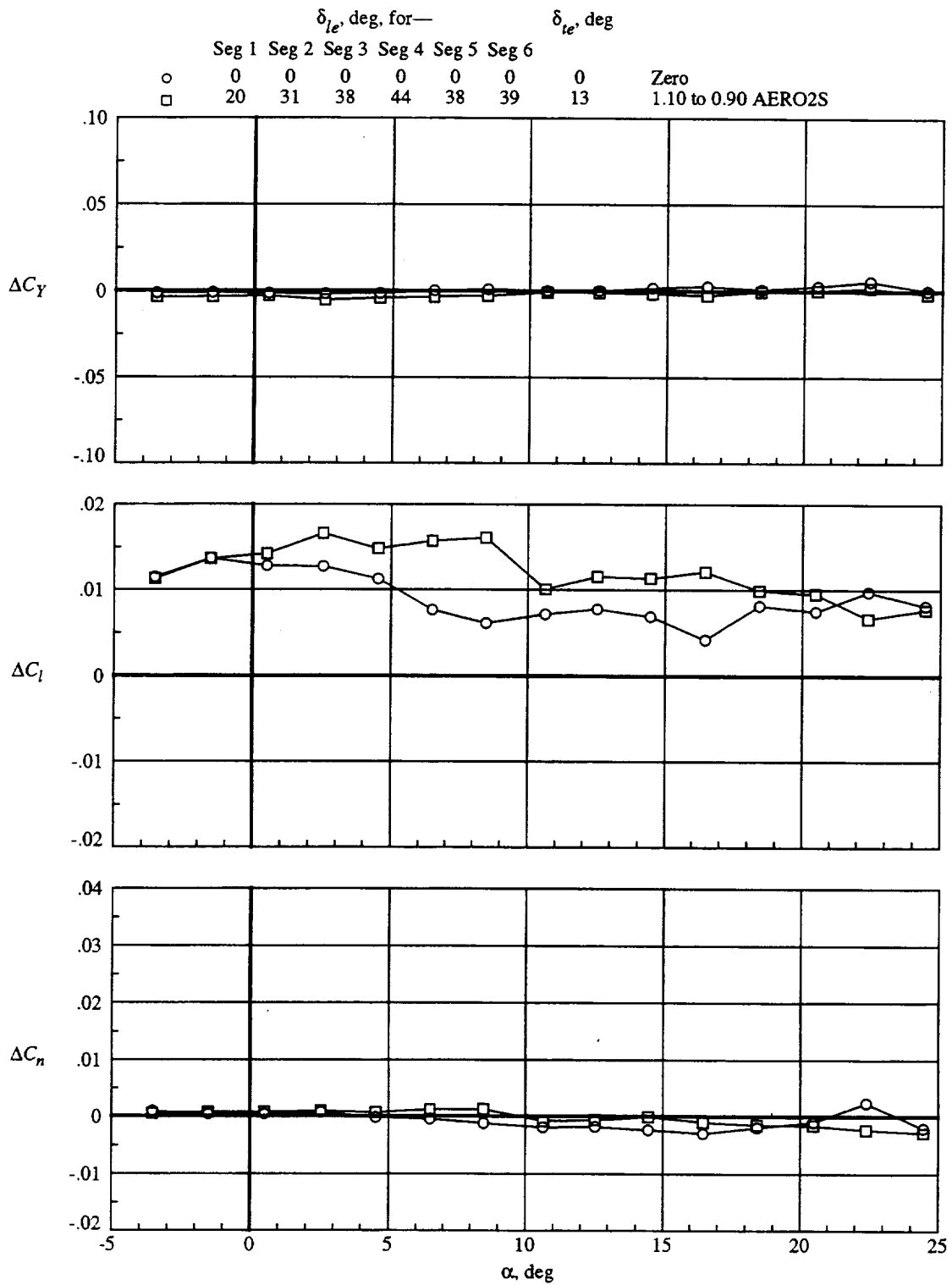
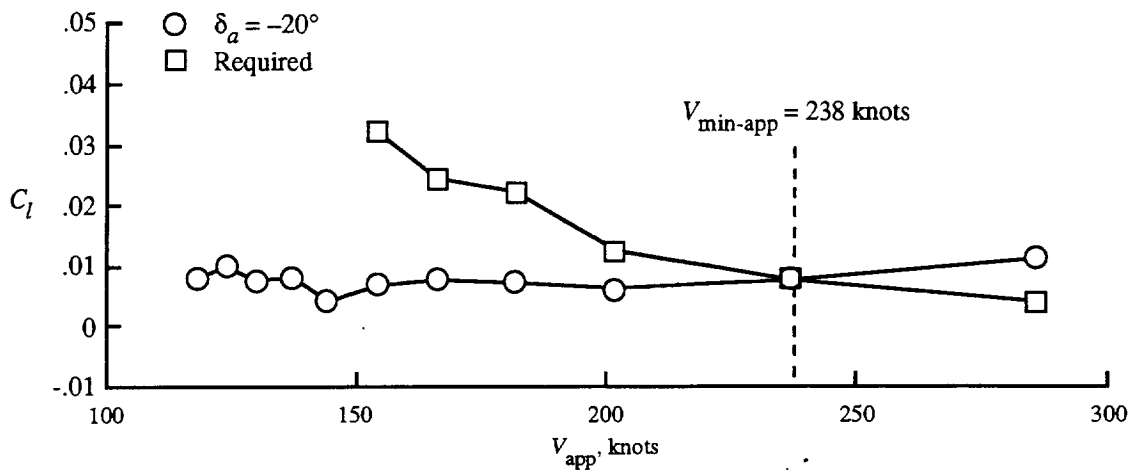
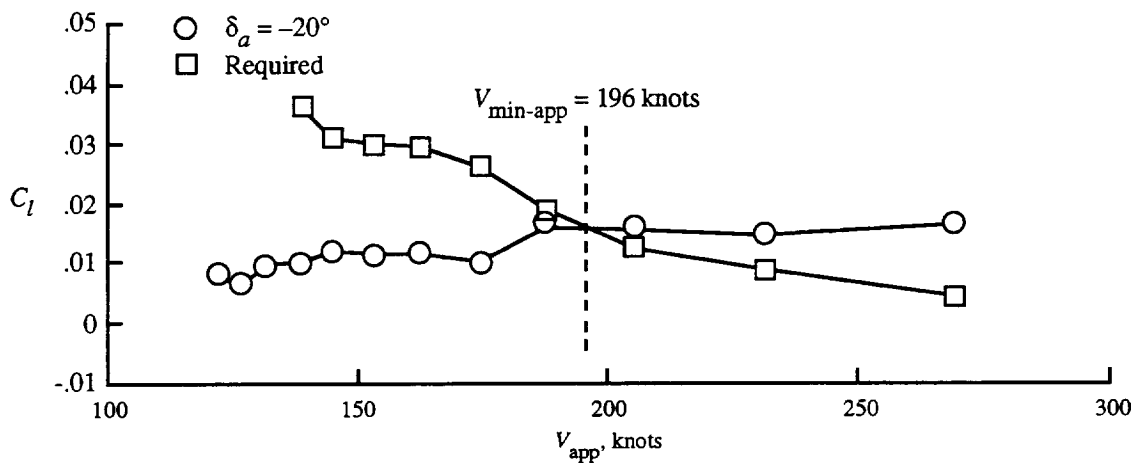


Figure 34. Effect of leading- and trailing-edge flap deflection on aileron control power for WBNLEF1.  $\delta_a = -20^\circ$ .

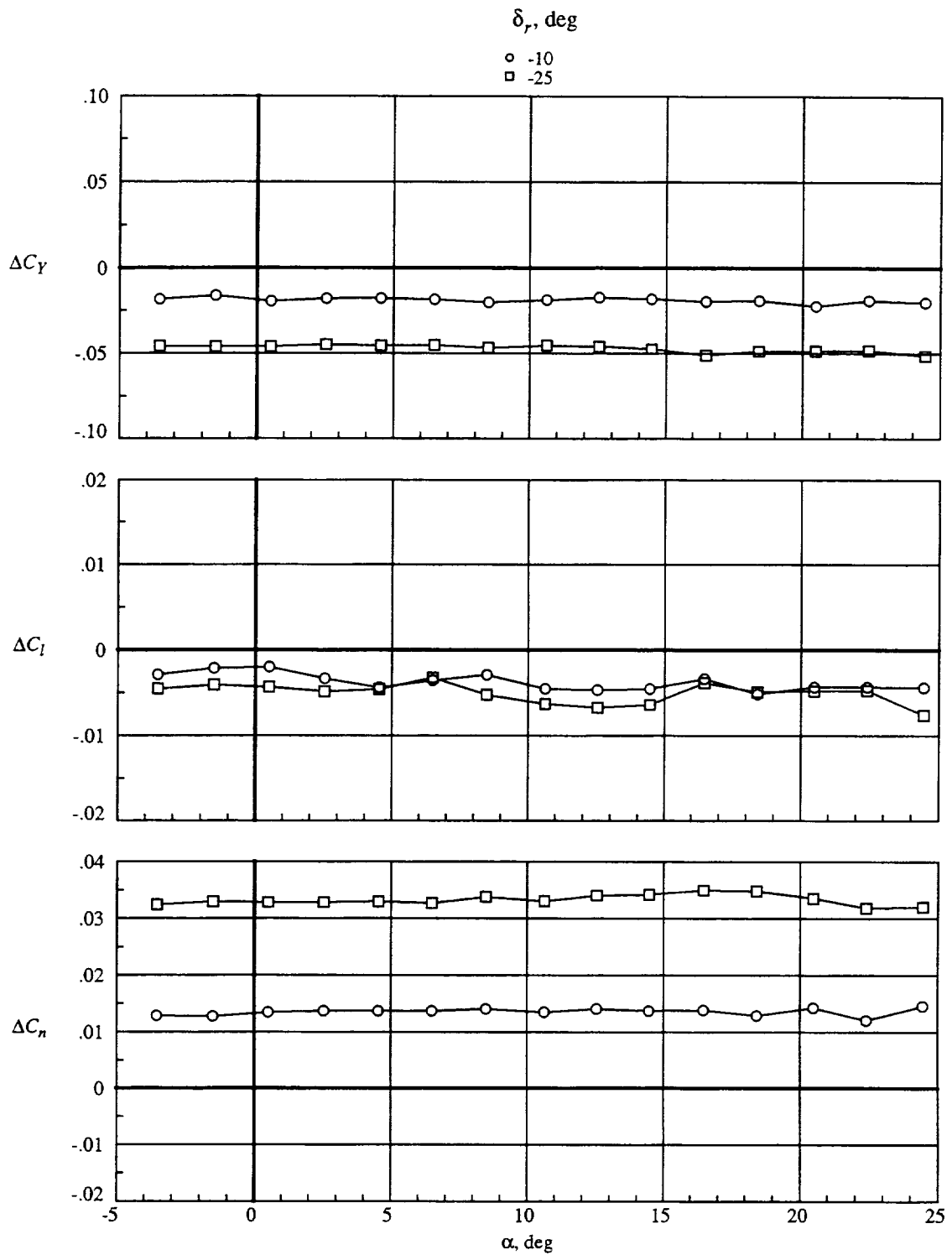


(a) Leading- and trailing-edge flaps undeflected.



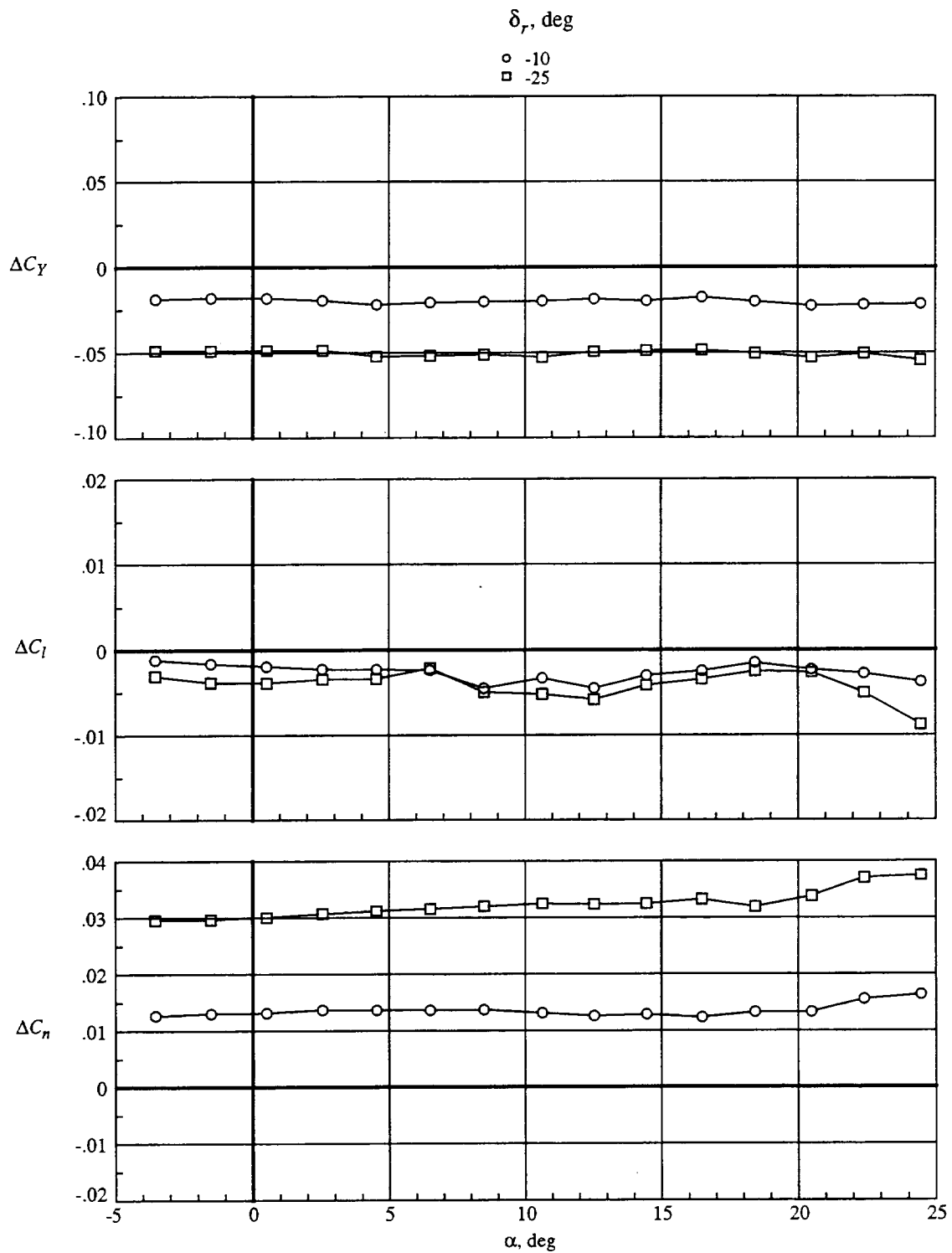
(b) Leading-edge flaps deflected  $20^\circ$ ,  $31^\circ$ ,  $38^\circ$ ,  $44^\circ$ ,  $38^\circ$ , and  $39^\circ$  (1.10 to 0.90 AERO2S);  $\delta_{te} = 13^\circ$ .

Figure 35. Effect of leading- and trailing-edge flap deflection on minimum approach speed for WBNLEF1.



(a) Leading- and trailing-edge flaps undeflected.

Figure 36. Effect of rudder deflection on lateral-directional characteristics for WBNHVLEF1.



(b) Leading-edge flaps deflected 20°, 31°, 38°, 44°, 38°, and 39° (1.10 to 0.90 AERO2S);  $\delta_{te} = 13^\circ$ .

Figure 36. Concluded.

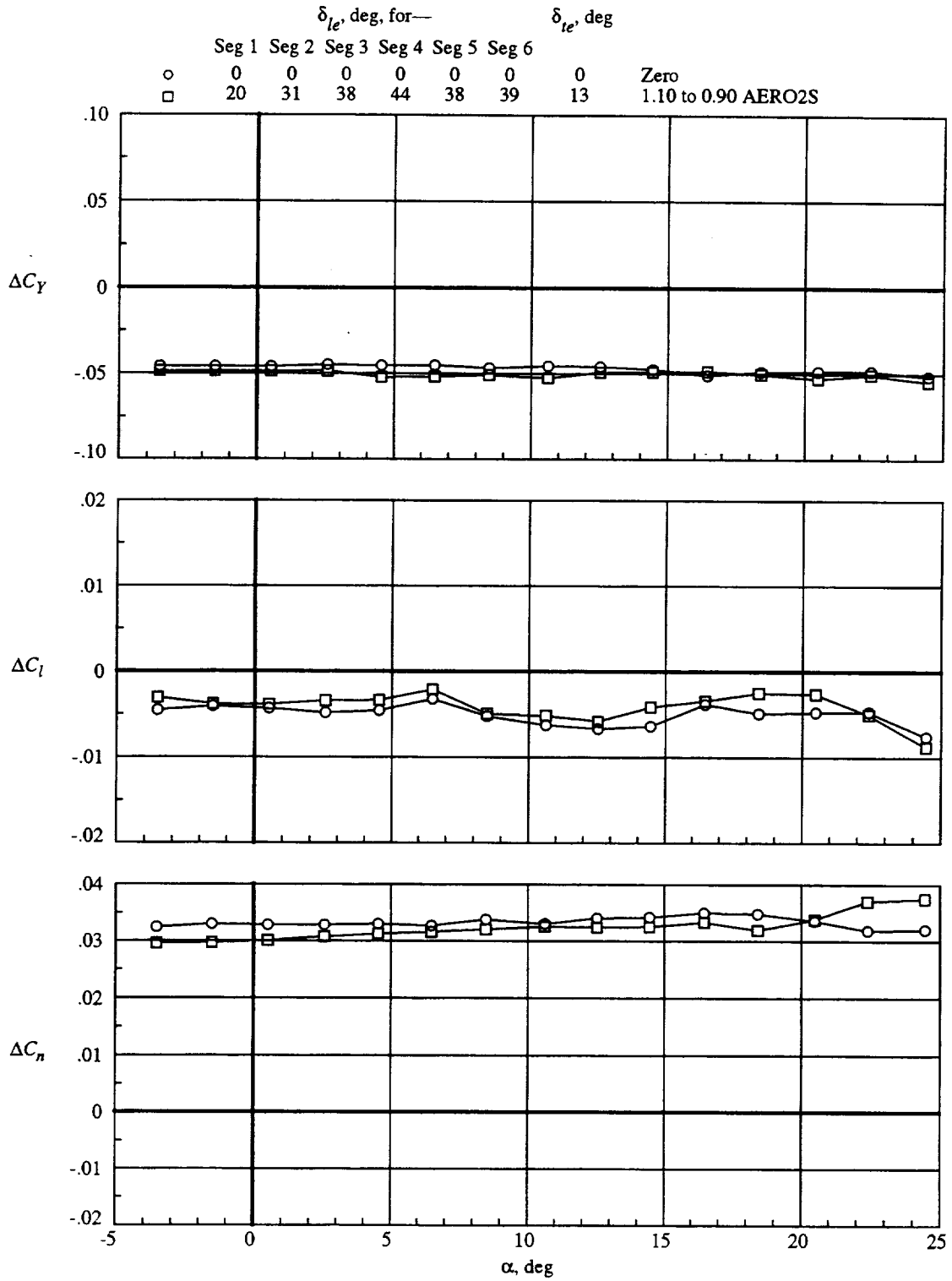


Figure 37. Effect of leading- and trailing-edge flap deflection on rudder control power for WBNHVLEF1.  $\delta_r = -25^\circ$ .

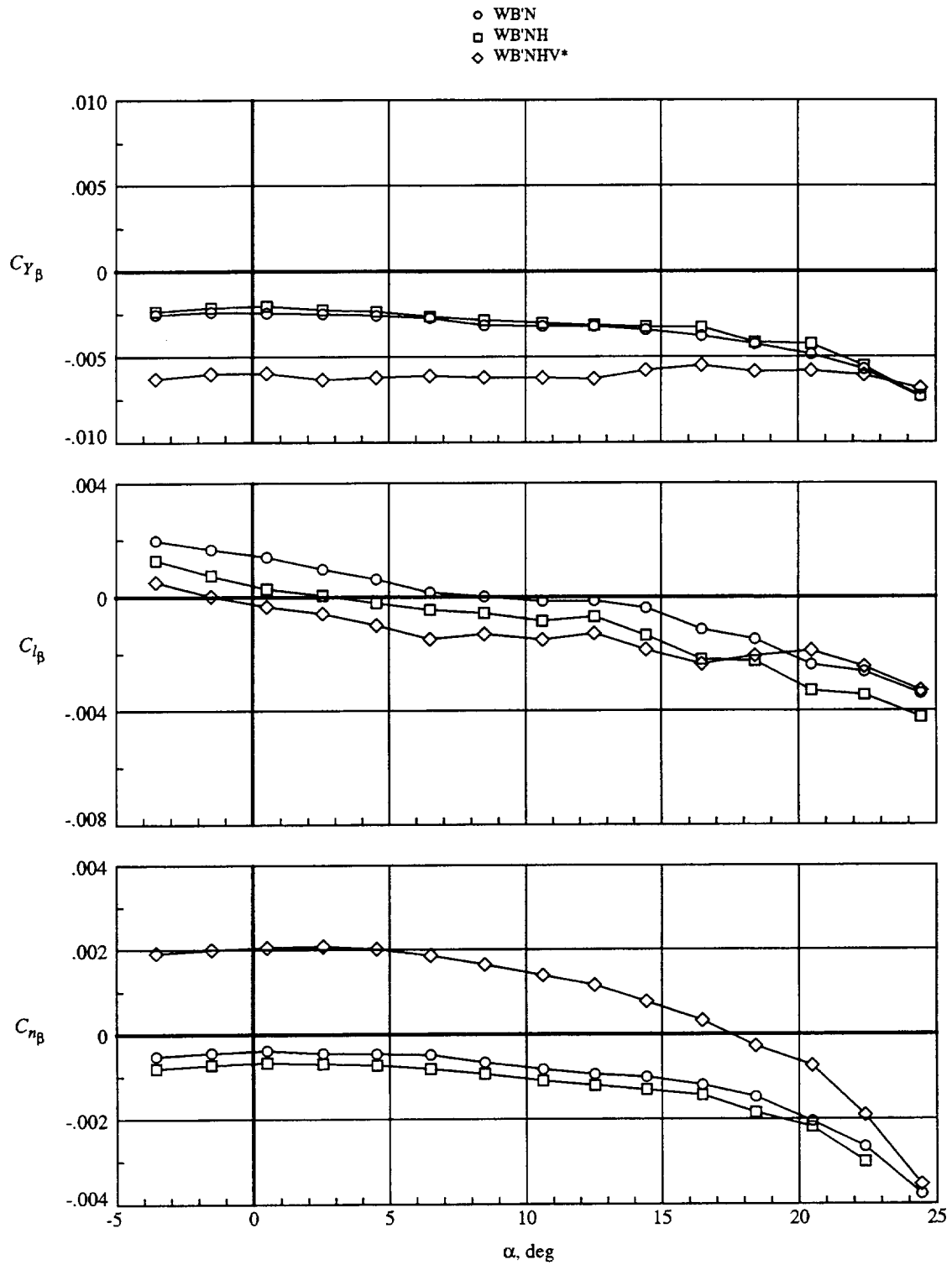


Figure 38. Effect of component buildup on lateral-directional characteristics for LEF2.  $\delta_{le} = \delta_{te} = 0^\circ$ .

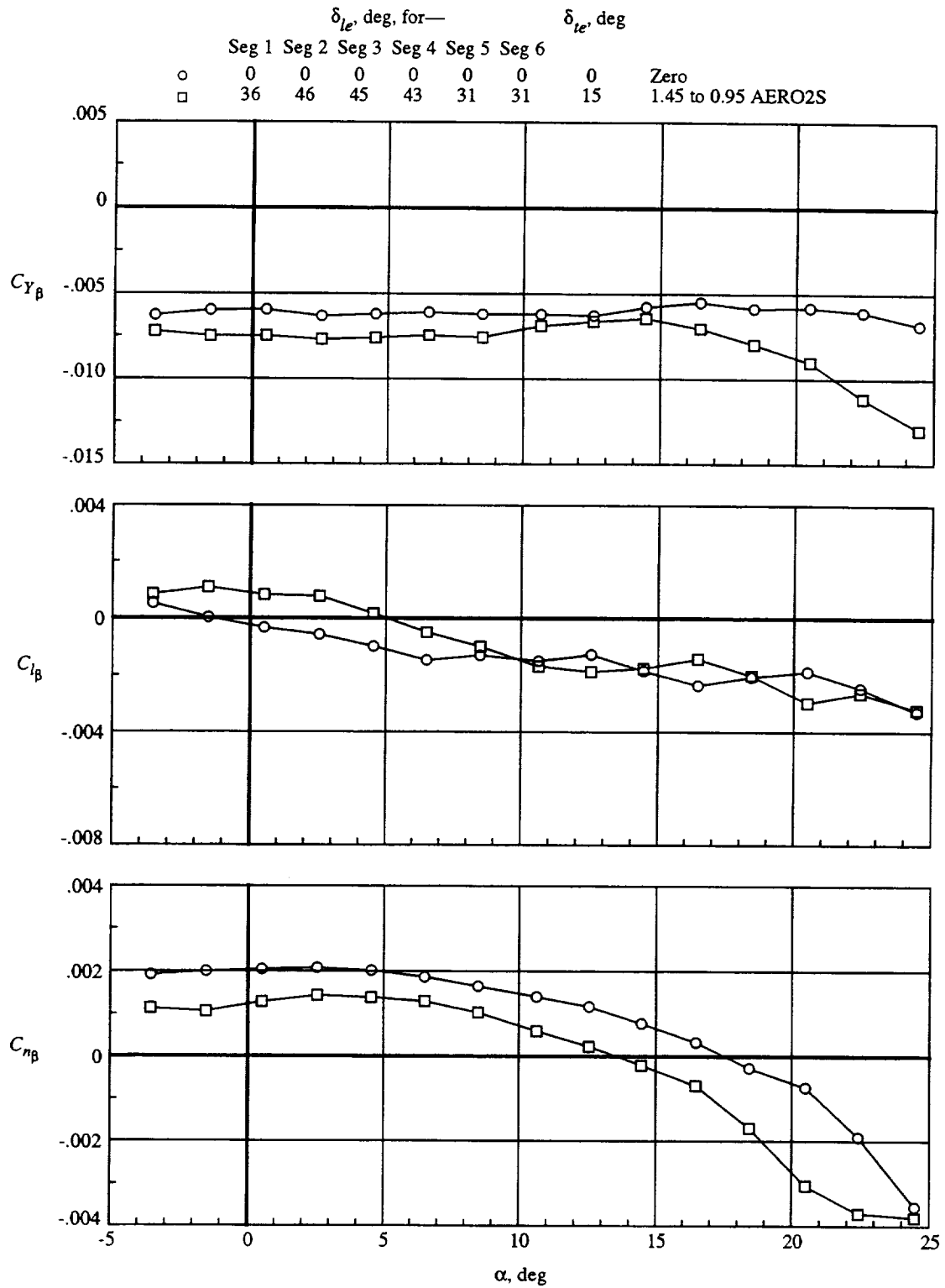


Figure 39. Effect of leading- and trailing-edge deflection on lateral-directional characteristics for WB'NHV\*LEF2. Gap filled between leading-edge flap segments 4 and 5; all control surfaces zero.

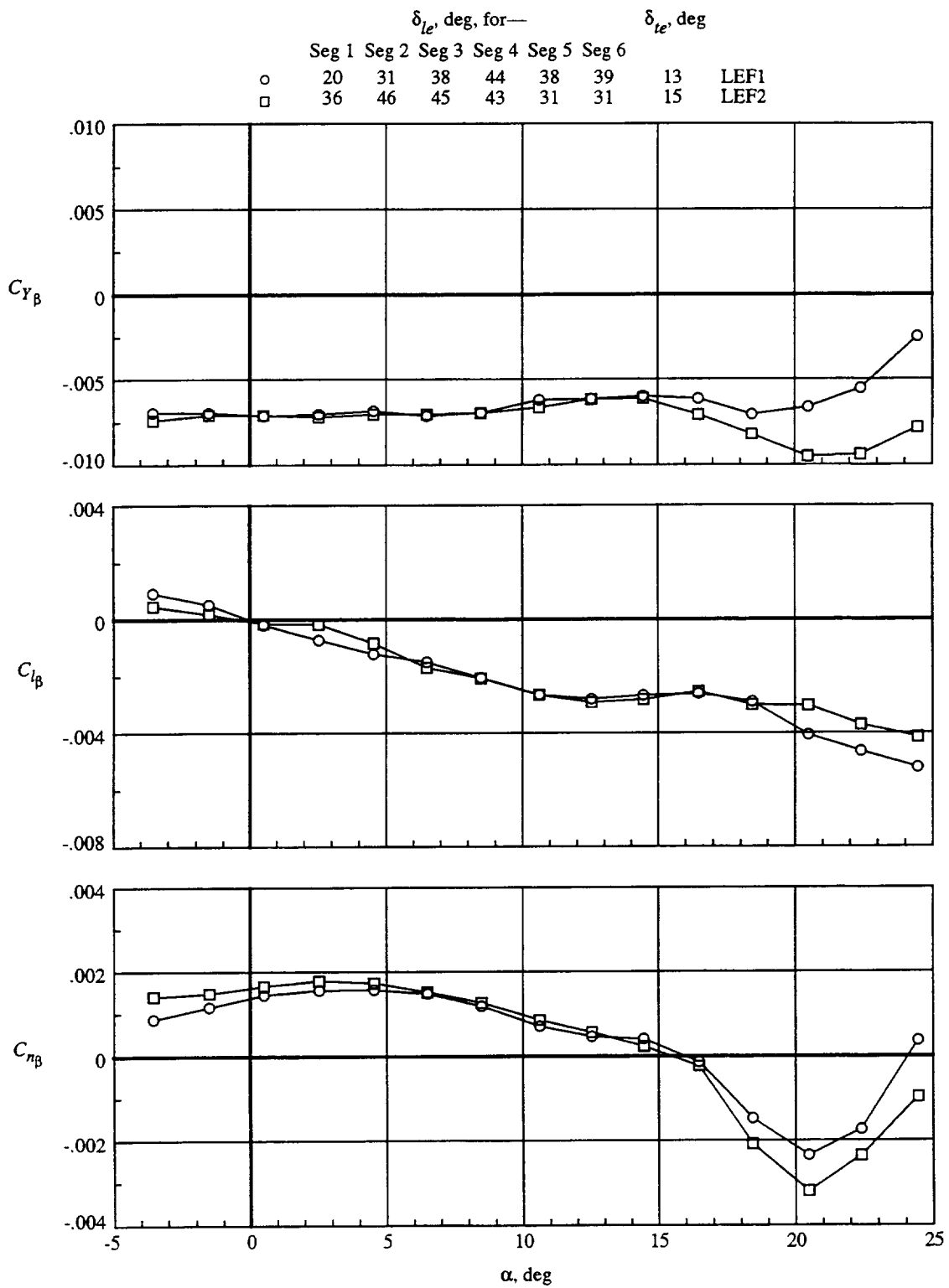


Figure 40. Lateral-directional characteristics of original and modified wing leading-edge configurations. WBNHV.

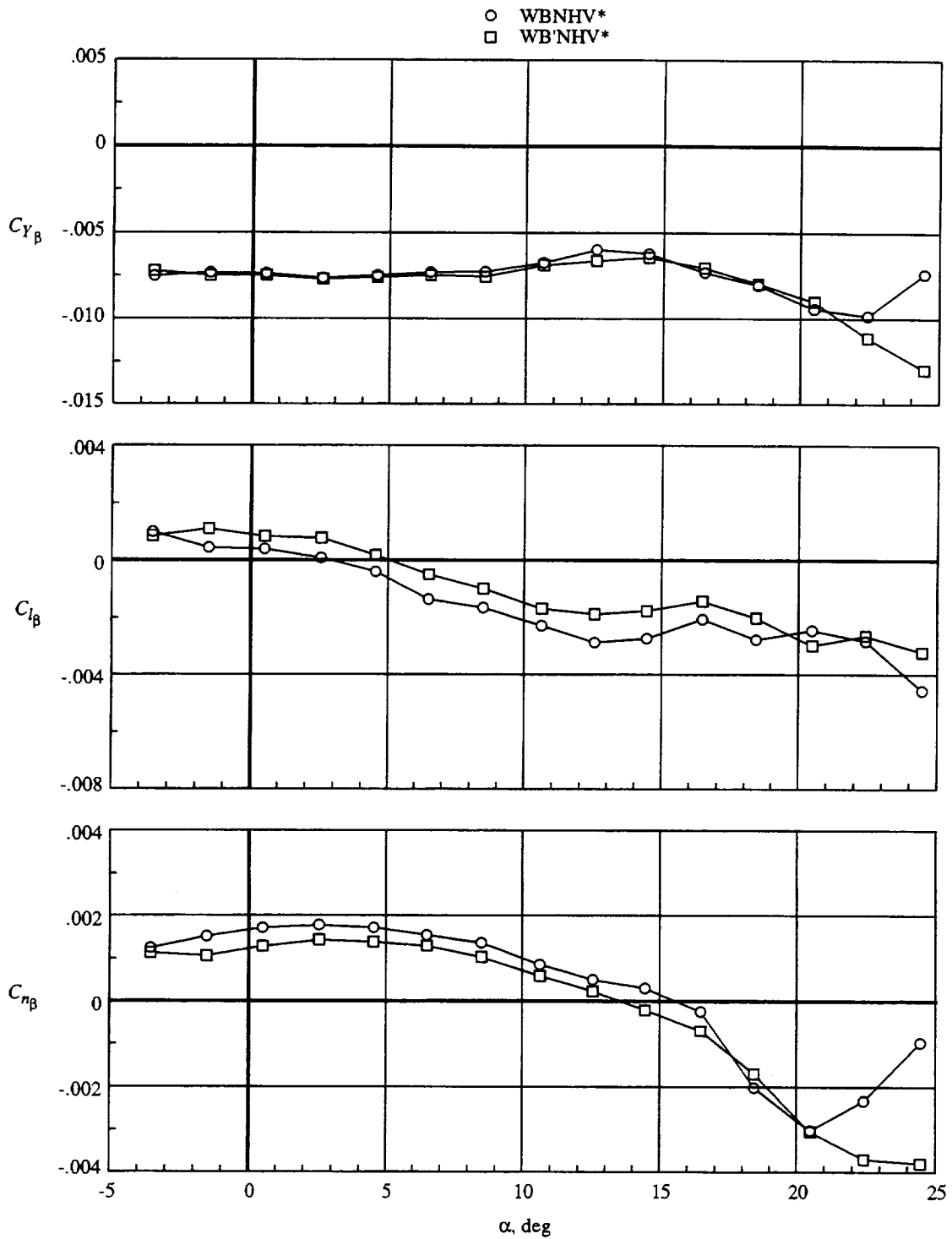
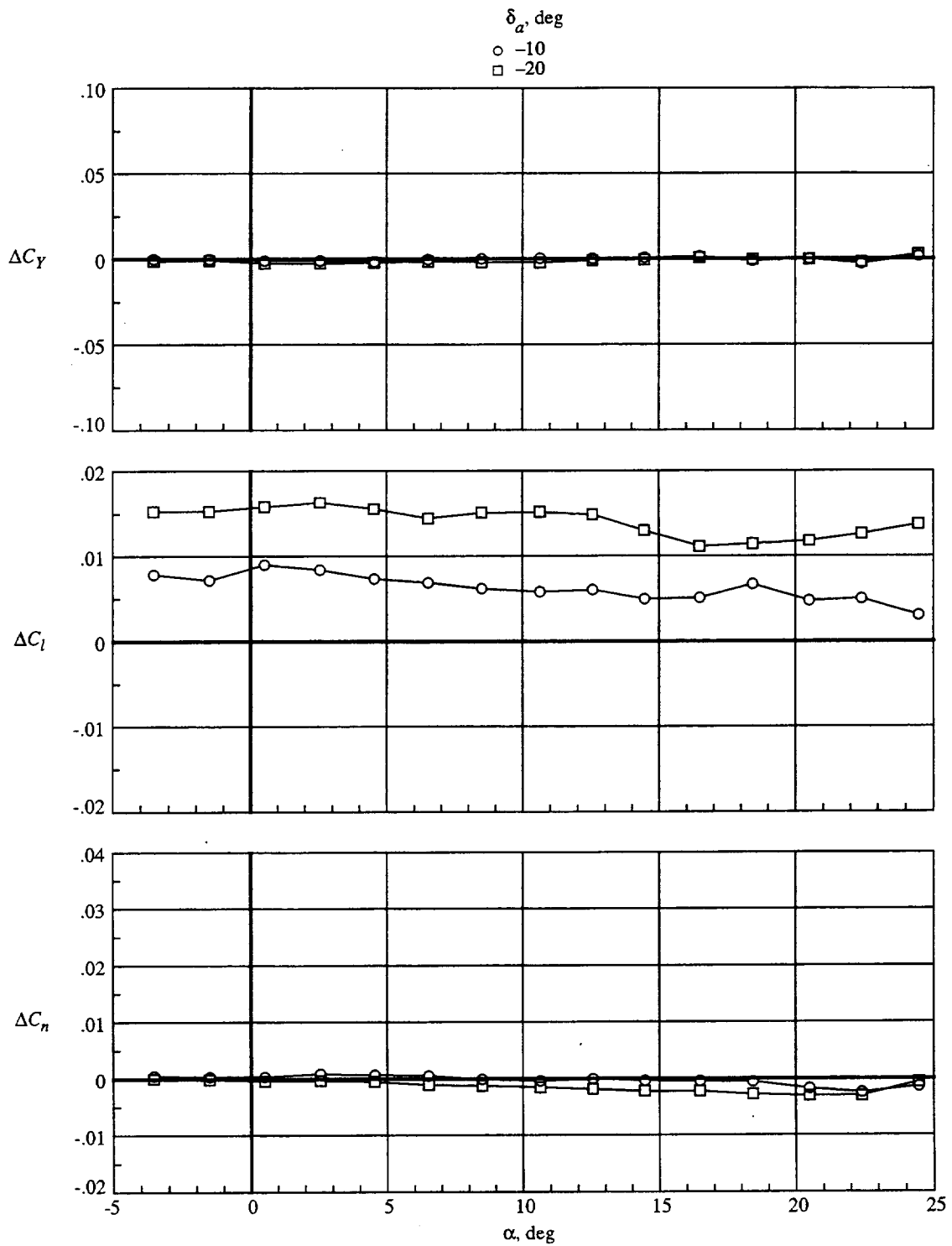
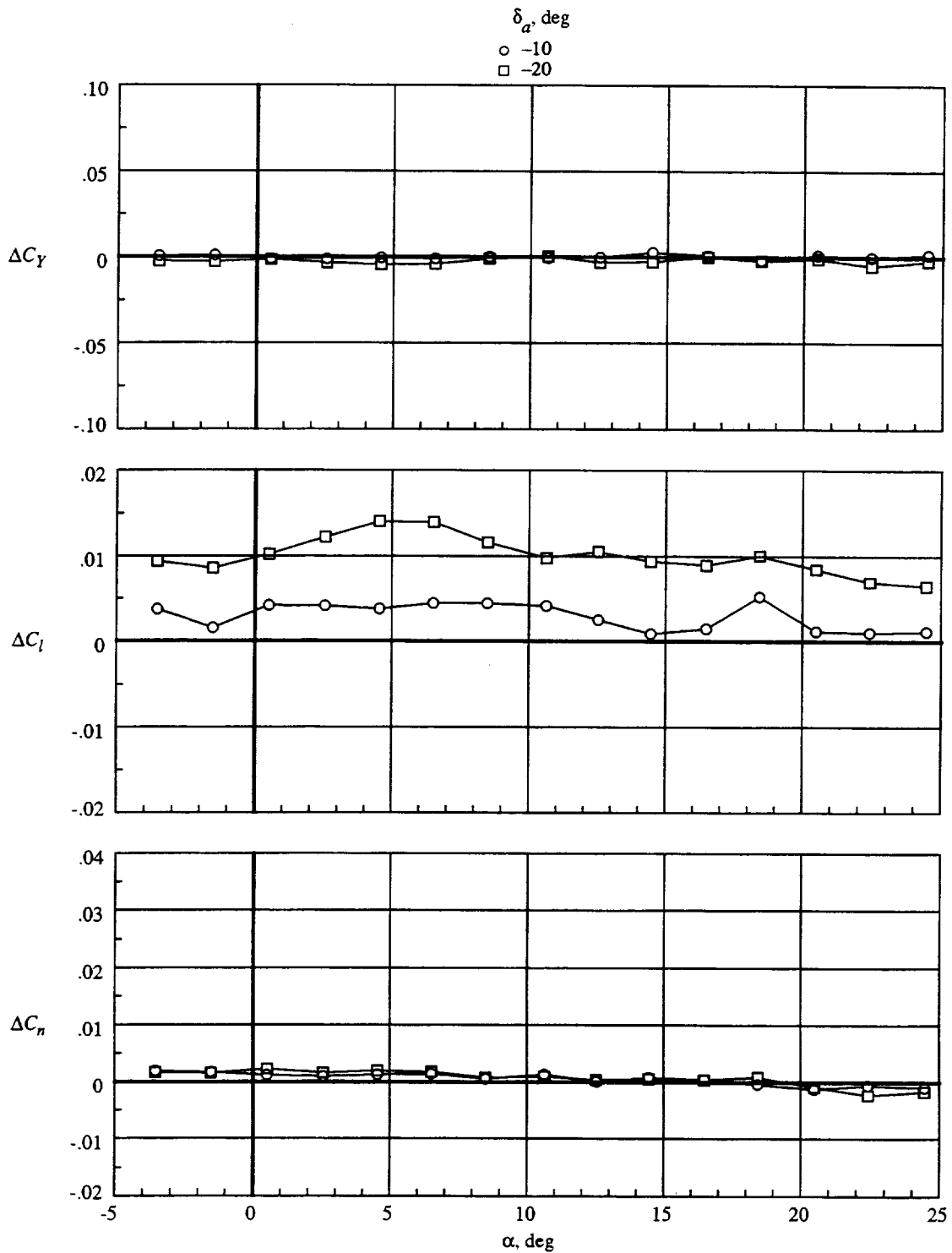


Figure 41. Effect of fuselage forebody on lateral-directional characteristics. Leading-edge flaps deflected 36°, 46°, 45°, 43°, 31°, and 31° (1.45 to 0.95 AERO2S);  $\delta_{te} = 15^\circ$ ; gap filled between leading-edge flap segments 4 and 5; all control surfaces zero.



(a) Leading- and trailing-edge flaps undeflected.

Figure 42. Effect of differential aileron deflection on lateral-directional characteristics for WBNLEF2.



(b) Leading-edge flaps deflected 36°, 46°, 45°, 43°, 31°, and 31° (1.45 to 0.95 AERO2S);  $\delta_{te} = 15^\circ$ ; gap filled between leading-edge flap segments 4 and 5.

Figure 42. Concluded.

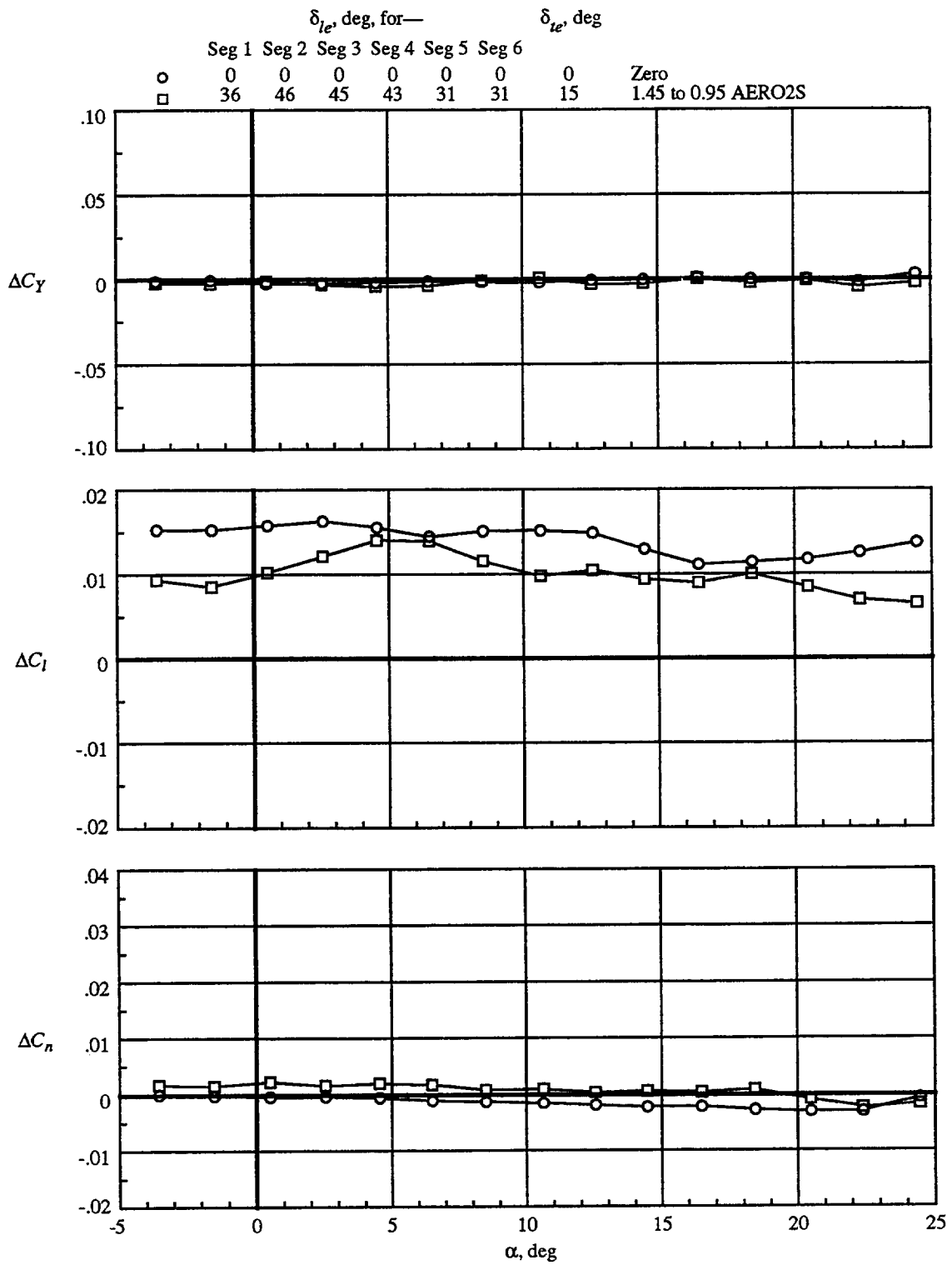


Figure 43. Effect of leading- and trailing-edge flap deflection on aileron control power for WBNLEF2. Gap filled between leading-edge flap segments 4 and 5;  $\delta_a = -20^\circ$ .

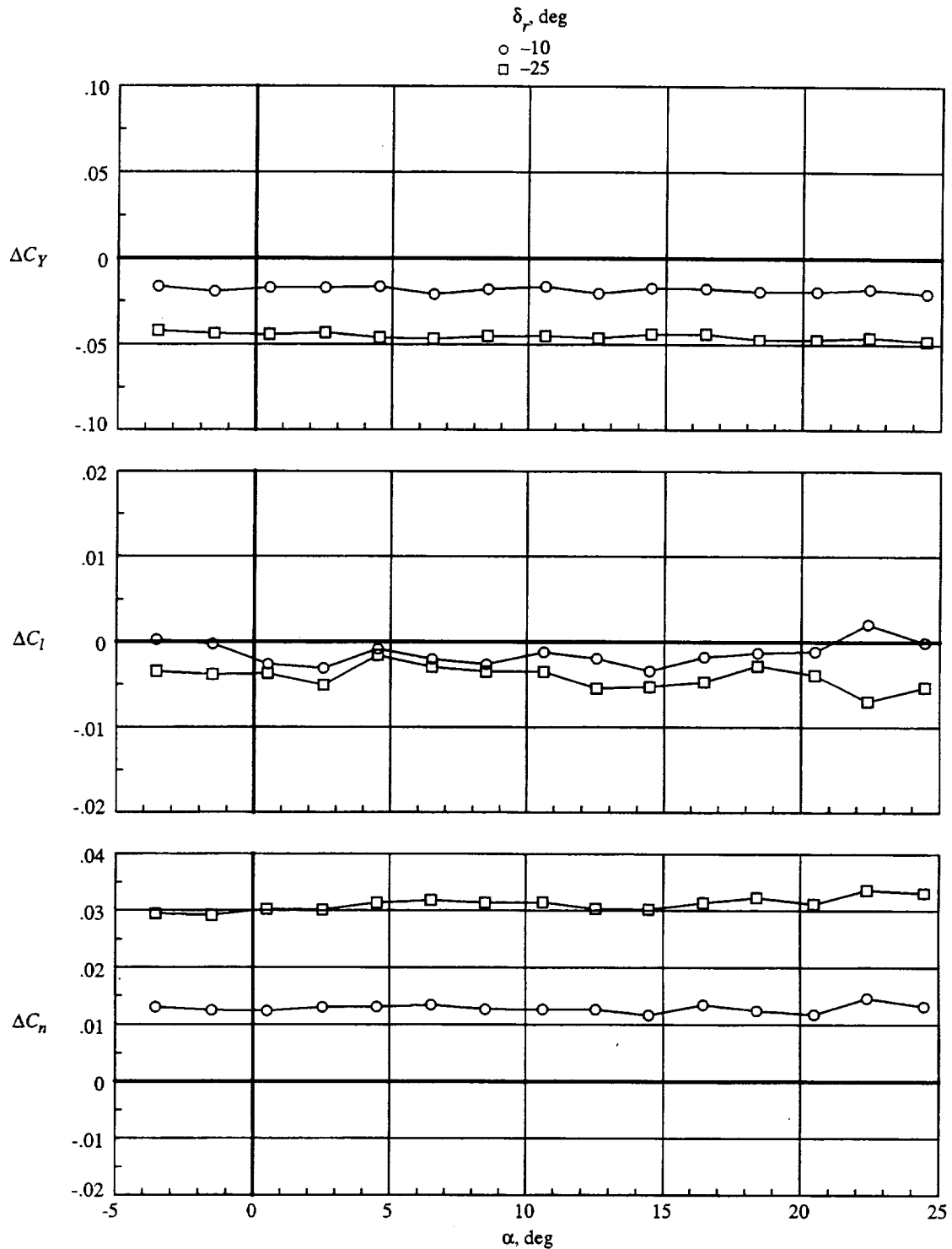
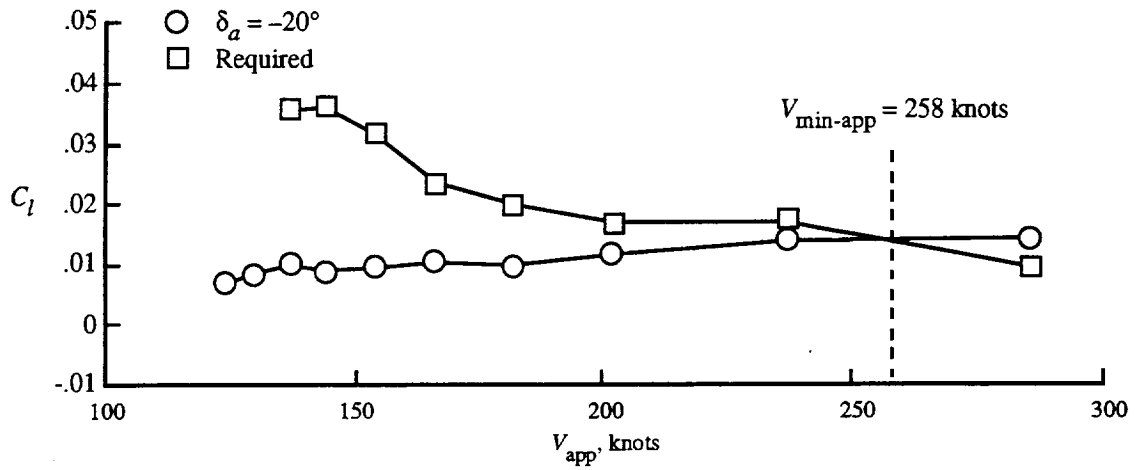
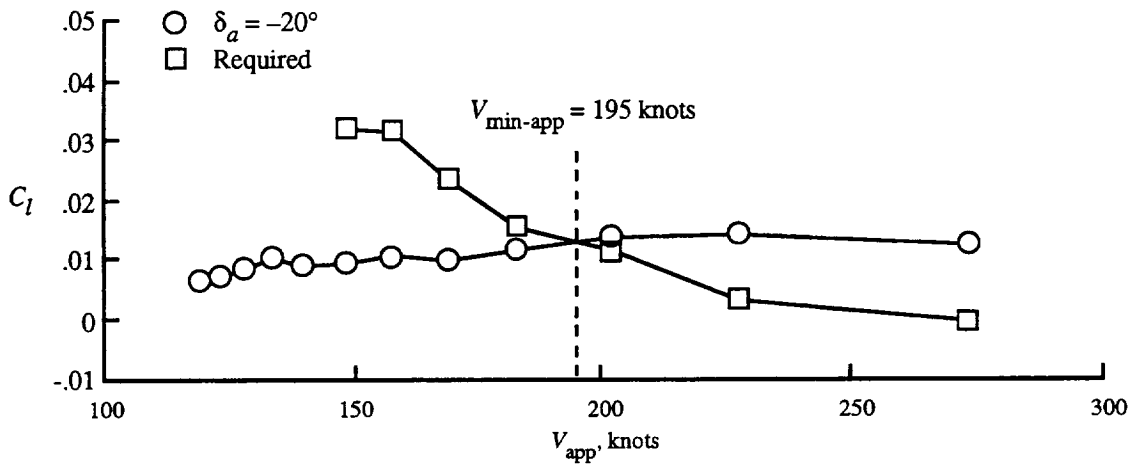


Figure 44. Effect of rudder deflection on lateral-directional characteristics for WBNHVLEF2. Leading-edge flaps deflected 36°, 46°, 45°, 43°, 31°, and 31° (1.45 to 0.95 AERO2S);  $\delta_{te} = 15^\circ$ ; gap filled between leading-edge flap segments 4 and 5.



(a) Leading- and trailing-edge flaps undeflected.



(b) Leading-edge flaps deflected  $36^\circ$ ,  $46^\circ$ ,  $45^\circ$ ,  $43^\circ$ ,  $31^\circ$ , and  $31^\circ$  (1.45 to 0.95 AERO2S);  $\delta_{re} = 15^\circ$ ; gap filled between leading-edge flap segments 4 and 5.

Figure 45. Effect of leading- and trailing-edge flap deflection on minimum approach speed for WBNLEF2.

REPORT DOCUMENTATION PAGE			Form Approved OMB No. 0704-0188	
Public reporting burden for this collection of information is estimated to average 1 hour per response, including the time for reviewing instructions, searching existing data sources, gathering and maintaining the data needed, and completing and reviewing the collection of information. Send comments regarding this burden estimate or any other aspect of this collection of information, including suggestions for reducing this burden, to Washington Headquarters Services, Directorate for Information Operations and Reports, 1215 Jefferson Davis Highway, Suite 1204, Arlington, VA 22202-4302, and to the Office of Management and Budget, Paperwork Reduction Project (0704-0188), Washington, DC 20503.				
1. AGENCY USE ONLY (Leave blank)	2. REPORT DATE December 1999	3. REPORT TYPE AND DATES COVERED Technical Publication		
4. TITLE AND SUBTITLE Experimental and Numerical Optimization of a High-Lift System To Improve Low-Speed Performance, Stability, and Control of an Arrow-Wing Supersonic Transport		5. FUNDING NUMBERS WU 537-03-22-08		
6. AUTHOR(S) David E. Hahne and Louis J. Glaab				
7. PERFORMING ORGANIZATION NAME(S) AND ADDRESS(ES) NASA Langley Research Center Hampton, VA 23681-2199		8. PERFORMING ORGANIZATION REPORT NUMBER L-17537		
9. SPONSORING/MONITORING AGENCY NAME(S) AND ADDRESS(ES) National Aeronautics and Space Administration Washington, DC 20546-0001		10. SPONSORING/MONITORING AGENCY REPORT NUMBER NASA/TP-1999-209539		
11. SUPPLEMENTARY NOTES Hahne: Langley Research Center, Hampton VA; Glaab: Lockheed Martin Engineering & Sciences Co., Hampton, VA.				
12a. DISTRIBUTION/AVAILABILITY STATEMENT Unclassified-Unlimited Subject Category 02 Availability: NASA CASI (301) 621-0390		12b. DISTRIBUTION CODE Distribution: Nonstandard		
13. ABSTRACT (Maximum 200 words) An investigation was performed to evaluate leading- and trailing-edge flap deflections for optimal aerodynamic performance of a High-Speed Civil Transport concept during takeoff and approach-to-landing conditions. The configuration used for this study was designed by the Douglas Aircraft Company during the 1970's. A 0.1-scale model of this configuration was tested in the Langley 30- by 60-Foot Tunnel with both the original leading-edge flap system and a new leading-edge flap system, which was designed with modern computational flow analysis and optimization tools. Leading- and trailing-edge flap deflections were generated for the original and modified leading-edge flap systems with the computational flow analysis and optimization tools. Although wind tunnel data indicated improvements in aerodynamic performance for the analytically derived flap deflections for both leading-edge flap systems, perturbations of the analytically derived leading-edge flap deflections yielded significant additional improvements in aerodynamic performance. In addition to the aerodynamic performance optimization testing, stability and control data were also obtained. An evaluation of the crosswind landing capability of the aircraft configuration revealed that insufficient lateral control existed as a result of high levels of lateral stability. Deflection of the leading- and trailing-edge flaps improved the crosswind landing capability of the vehicle considerably; however, additional improvements are required.				
14. SUBJECT TERMS Low speed; Performance; Stability and control; Supersonic transport; High-lift system design			15. NUMBER OF PAGES 86	16. PRICE CODE A05
17. SECURITY CLASSIFICATION OF REPORT Unclassified	18. SECURITY CLASSIFICATION OF THIS PAGE Unclassified	19. SECURITY CLASSIFICATION OF ABSTRACT Unclassified	20. LIMITATION OF ABSTRACT UL	